UNIVERSITY OF CALIFORNIA SAN DIEGO

Marine Sediment-Derived Actinomycetes: Prolific Sources of New Molecules with the Potential for the Treatment and Prevention of Cancer

A dissertation submitted in partial satisfaction of the

requirements for the degree of Doctor of Philosophy

in

Oceanography

by

Eric David Miller

Committee in charge:

Professor William Fenical, Chair
Professor Lihini Aluwihare
Professor Katherine Barbeau
Professor Joseph O'Connor
Professor Victor Vacquier

2007

The dissertation of Eric David Miller is approved, and is acceptable in quality and form for publication on microfilm:

_____

_____

_____

_____

_____

Chair

University of California, San Diego

2007

To my son Ethan, for reasons that I could never use words to describe

TABLE OF CONTENTS

LIST OF FIGURES

LIST OF TABLES

ACKNOWLEDGEMENTS

I am very happy to be writing this section because within it I am finally able to express my full appreciation to the multitude of people that have made this thesis possible.

First and foremost I must thank Professor William Fenical. If not for Professor Fenical I would simply not be at this point in my academic career. Starting with his championing of my admission to Scripps Institution of Oceanography, Professor Fenical has on numerous occasions gone well beyond his role as mentor to assist with my development as a scientist and as a person. I have always felt lucky that he worked so diligently to obtain the funding so that I may focus intently on research. I will be forever grateful to Bill for the incredible financial investment he has made in me. I am also extremely grateful to Bill for the amount of personal time he has invested in making me into the scientist that I am today. I have always and will always strive to achieve the highest level of scientific excellence so that Bill may feel that his investment in me was worth it. Thank you very much Bill, none of this would have been possible without you.

Secondly, I would like to thank my committee members, Professors Lihini Aluwihare, Katherine Barbeau, Joseph O'Connor and Victor Vacquier for their input, support and scientific advice concerning my thesis research. I sincerely thank you all for your dedication to my development.

Thirdly, I would like to thank Paul Jensen without whom I would not have had access to the incredible chemistry on which this thesis is based. Paul's inspirational

thinking and foresight have provided me with access to organisms the likes of which no chemist has been able to examine before. Thank you very much for all of your hard work Paul. GO CHARGERS!!

Next I would like to express my sincere thanks to Chris Kauffman for his dedication to the fermentations. Chris has on several occasions put in extra time on weekends and holidays to help me get extracts to work with. Chris has also been a great friend throughout my Ph.D. and has many times provided a perspective that helped me focus on what was really important. The Padres will win it all one day Chris, it will happen. Maybe not in our lifetime but it WILL happen.

I would also like to thank Sara Kelly for running all of the in-house HCT-116 *in vitro* assays. None of the work that I have done in the laboratory would have been possible without her help. Thank you very much Sara, I am forever indebted to you. In this regard I would also like to thank Lisa Zeigler and Kelle Freel for running the assays when Sara was away. Thank you both very much.

I would also like to thank Matt Woolery for his tireless dedication to maintaining the laboratory equipment especially the LCMS. Matt's dedication to the maintenance of the LCMS made the "target" based isolation approach possible. Thank you very much Matt and don't give up on your music.

Further, I would like to thank Beth Masek. Beth is an exceptional person and very good friend and her organizational skills are something I aspire to. She has many times provided me with insight and encouragement that were instrumental in getting me through the tough parts and I will always remember her. Thank you very much Beth, you are one of the good ones.

Next, I would like to thank Arnold L. Rheingold and Peter Gantzel for their excellent work in X-Ray crystallography which made determination of the complete stereochemistry of the piperazimycins possible. Also, I must thank the long list of post-docs that have had an incredible influence on my development as a chemist. Specifically, Eliane Garo, Rob Feling and Greg Buchannan for the significant contributions they made to my early development. Next I would like to thank Philip Williams, Hak Cheol Kwon, John MacMillan, Tim Bugni, Ratnakar Asolkar and Chambers Hughes. I would like to first thank Philip for teaching me the benefits of staying up on the literature, helping me to understand the theory behind the chemistry, forcing me to memorize the standard amino acids ("come on there are only 22") and most of all for his inspiration and dedication to the arenicolide project. I would further like to thank Hak Cheol Kwon, a good friend and very talented chemist who taught me the benefits of a purely empirical approach to science. Kwon has structure elucidation skills that are approaching the level of genius and was very supportive in the planar structure elucidation of the piperazimycins. Further, the absolute stereochemical determination of the arenicolides would not have been possible without Kwon's input. Next I would like to thank John MacMillan for his overall dedication to chemistry and for giving me the opportunity to work on the pyridinopyrone project. I was lucky enough to share an office with John and his attention to detail and scientific ethics will stay with me for my entire career. Thank you very much John for being there when the chips were down, I will never forget that. In addition I would like to thank Ratnakar Asolkar for his time spent conversing with me on the various aspects of natural product isolation and his input on various projects most importantly being the

arenicolides. Lastly I would like to thank Chambers Hughes for his input on the piperazimycin project and for proofreading everything I have ever written except for this thesis where he was "forced to draw the line".

In addition I would like to thank all of my fellow graduate students specifically Tracy Mincer, Dong Chan Oh, Sebastian Engel, Ana Paula DM Espindola, Nicole Turkson, Erin Gontang, Alejandra Prieto-Davo, Lauge Farnaes, Wendy Strangman and Chollaratt Boonlarppradab. All of you have in one way or another played a part in my Ph.D., thank you all very much.

In summary, I would like to thank the entire Fenical group as a whole. When I was dealt those devastating cards in my personal life, I often felt that what weighed so heavily on my shoulders was in many was being carried by all of you. I sincerely appreciate all of your support through those days. The fact that you made this environment such a positive one for me during that time was instrumental in the completion of my Ph.D. Coming to work made me feel better and I am very grateful to all of you for that.

Next I would like to thank my friends and family for the incredible amount of support that they have given me not only over the course of my Ph.D. but more importantly, my entire life. Specifically I would like to thank my father for teaching me the power of logic, reason and patience, my mother for instilling in me passion for my work and for making me believe in my intelligence, Judy for teaching me the power of the written word and most of all my sister Jilana whose dedication to academics inspired me to become a scientist. I started all of this because I wanted to be like you J, thanks for being so smart.

I would also like to thank my friends for helping me to keep track of who I am and for standing by my side when my personal life went astray. I owe each and every one of you a great deal of gratitude for believing in me and sticking with me through all of this. The next round is on me.

Lastly, I would like to thank my son Ethan just for being who he is. You are one tough little guy and a constant source of inspiration. I love you very much.

Chapter II, in full, was a reprint of material as it appears in The Journal of Organic Chemistry, 2007 *72*(2), 323-330, Miller, E.D.; Kauffman, C.A..; Jensen, P.R.; Fenical, W. The dissertation author was primary investigator and author of this paper.

Chapter III, in full, was a reprint of material as it appears in The Journal of Organic Chemistry, 2007 *ASAP*, Miller, E.D.; Williams, P.G.; Asolkar, R.N.; Jensen, P.R.; Fenical, W. The dissertation author was primary investigator and author of this paper.

VITA AND PUBLICATIONS

1996	Bachelor of Science, University of California Santa Barbara
1996-2001	Research Chemist, Quidel Corporation, San Diego, California
2007	Doctor of Philosophy, University of California, San Diego

PUBLICATIONS

(i) Miller, E.D.; Williams, P.G.; Asolkar, R.N.; Jensen, P.R.; Fenical, W. Arenicolides A-C, 26-Membered Ring Macrolides from the Marine Actinomycete *Salinispora arenicola*. *J. Org. Chem.* **2007**, *ASAP*

(ii) Miller, E.D.; Kauffman, C.A.; Jensen, P.R.; Fenical, W. Piperazimycins: Cytotoxic Hexadepsipeptides from a Marine-Derived Bacterium of the Genus *Streptomyces.* *J. Org. Chem.* **2007**, *72*(2), **323-330**

ABSTRACT OF THE DISSERTATION

Marine Sediment-Derived Actinomycetes: Prolific Sources of New Molecules with the Potential for the Treatment and Prevention of Cancer

by

Eric David Miller

Doctor of Philosophy

in
Oceanography

University of California, San Diego, 2007

Professor William Fenical, Chair

The following document contains the results of Ph.D. thesis research that was focused toward the isolation and complete structural characterization of new molecules that were effective in the treatment and prevention of cancer. The use of marine sediment-derived actinomycetes as a novel source for the chemical entities led to the isolation of three distinct suites of molecules with unprecedented carbon skeletons each of which displayed some anticancer properties.

In the first project, three potent cancer cell cytotoxins, piperazimycins A-C (**1-3**), were isolated from the fermentation broth of a *Streptomyces* sp., cultivated from marine sediments near the island of Guam.[i] The structures of these cyclic hexadepsipeptides were assigned by a combination of spectral, chemical and crystallographic methods. The piperazimycins were found to be composed of rare amino acids, including hydroxy-acetic acid, α-methyl-serine, γ-hydroxypiperazic acid

and γ-chloropiperazic acid. The novel amino acid residues 2-amino-8-methyl-4,6-nonadienoic acid and 2-amino-8-methyl-4,6-decadienoic acid were found as components of piperazimycins A and C, respectively. When screened in the National Cancer Institute's 60 cancer cell line panel, piperazimycin A exhibited potent *in vitro* cytotoxicity toward multiple tumor cell lines with a mean GI_{50} of 100 nM.

In the second project, chemical evaluation of the saline fermentation broth of several strains of the obligate marine actinomycete *Salinispora arenicola* led to the identification of three new macrolide polyketides designated arenicolides A-C (**1**-**3**).[ii] The planar structures, elucidated via spectroscopic and chemical methods, consisted of 26-membered polyunsaturated macrolactones containing repeating vicinal hydroxyl methoxyl moieties. The relative and absolute stereochemistries of **1**-**3** were assigned by a combination of *J*-based configurational analyses and chemical derivatization. The arenicolides displayed moderate cytotoxicity in an *in vitro* colon adenocarcinoma cell-line (HCT-116) assay and also in the National Cancer Institute's 3 cancer cell line panel. At present, the anticancer properties of the arenicolides are being evaluated in several cancer chemoprevention and anticancer enzyme target based assays. Due to their structural novelty, the NCI has also recently agreed to reevaluate the cytotoxic activity of the arenicolides in the 60 cancer cell line panel.

The final chapter is focused on the isolation and characterization of a novel class of molecules that are likely polyketide derived and exhibit inhibitory activity against the enzyme aromatase. These molecules, the pyridinopyrones, were isolated from a marine sediment-derived *Streptomyces* sp and their chemical structures were solved by various spectral methods. The relatively simple chemical structure of the

pyridinopyrones makes these molecules attractive targets for synthetic modification and structure activity relationship studies directed toward improving their inherent aromatase inhibitory activity.

I

Introduction to the Thesis Research

I.1. Cancer: Statistics and Treatment Modalities

Cancer is a major health problem in the United States and other developed countries. Currently, one in four deaths in the United States is due to cancer and cancer has surpassed heart disease to become the leading cause of death in persons under 85 years of age.[1]

The term cancer defines a class of over 100 diseases that can arise in a variety of tissues and organs. In normal tissue, as a result of the interpretation of a elaborate set of signals that serve as social controls, the cells of multicellular organisms behave in a socially responsible manner, resting, dividing, differentiating, or dying as needed for the good of the organism.[2] The cooperation amongst cells in a multicellular organism does not however exist in opposition to the theory of natural selection. This becomes evident when one realizes that the body as a whole is a clone, and the genome of the somatic cells is the same as that of the germ cells. By self-sacrifice for the sake of the germ cells, the somatic cells help to propagate copies of their own genes. Thus, unlike free-living cells such as bacteria, which compete to survive, the cells of a multicellular organism are committed to collaboration.

Molecular alterations that disturb the cooperative balance between individual cells can cause mutations that if unchecked, may lead to a selective adaptation that allows for a particular cell to divide more vigorously than its neighbors and therfore become the founder of a growing mutant clone. Repeated rounds of mutation, competition and natural selection operating within the population of somatic cells can cause the situation to quickly worsen. These are the hallmarks of cancer: it is a disease in which

individual mutant clones of cells begin by prospering at the expense of their neighbors, but in the end destroy the entire cellular society.[2] In specific, cancer cells and their progeny can be defined by two heritable properties (1) they reproduce in defiance of the normal restraints on cell division and (2) they invade and colonize territories normally reserved for other cells.[2]

So long as the neoplastic cells remain clustered together in a single mass the tumor is said to be benign and complete cure at this stage can usually be achieved by surgical resection of the tumor. A tumor is considered a cancer only if it is malignant, that is, only if its cells have acquired the ability to invade the surrounding tissue. Invasiveness is characterized by the ability for cells to break loose from the primary tumor, enter the bloodstream of lymphatic vessels, and form secondary tumors or metastases, at other sites in the body. The more widely a cancer spreads, the harder it becomes to eradicate.[2]

With certain exceptions, treatment strategies typically consist of one or a combination of the following: surgery, radiation therapy or chemotherapy. With present methods of treatment, one third of patients are cured with local modalities (surgery or radiation therapy), which are quite effective when the tumor has not metastasized by the time of treatment.[3] In these cases chemotherapy can be effective in decreasing tumor volume to allow for surgery or radiation therapy. In the remaining cases where early micrometastasis is a characteristic feature of the neoplasm, a systemic approach such as chemotherapy is required (often along with surgery or radiation) for effective cancer management.[3] At present, about 50% of

patients with cancer can be cured, with chemotherapeutic drugs contributing to cure in 10-15% of patients.[3] Although great progress in the treatment of cancer has been achieved through the administration of chemotherapeutic agents alone or in conjunction with other types of therapy, the need to discover new chemical entities with anticancer properties continues. This becomes evident when one considers that, despite intense effort, mortality rates for many types of cancers are still significant.[1]

I.2. Cancer Chemotherapy: A Historical Perspective

Anticancer chemotherapeutics trace their heritage to synthetic molecules based on the so-called nitrogen mustards that were developed as chemical warfare agents during WWI. The anticancer properties of the first of these agents mechlorethamine (**1**), (Figure I.1), were discovered following an accident at a manufacturing plant that exposed the local population to **1**. Later, it was noted that the white cell counts of exposed individuals had decreased significantly, suggesting that mechlorethamine may provide a possible therapy for Hodgkin's lymphoma. Subsequent clinical use of mechlorethamine to treat Hodgkins lymphoma in the mid-1940s gave rise to field of cancer chemotherapy as it is known today.[4]

Mechlorethamine is a member of a class of anticancer drugs known as "alkylating agents" that exert their anticancer effects by cross-linking guanine residues in DNA double-helix strands. Mechlorethamine induced cross-linking makes the DNA strands unable to uncoil and separate for replication leading eventually to cell death via apoptotic mechanisms. Following the clinical success of mechlorethamine, several other purely synthetic DNA alkylating agents were developed from nitrogen mustards

including cyclophosphamide (**2**),[5] chlorambucil (**3**),[6] busulfan (**4**)[7] and carmustine (**5**),[8] (Figure I.1).

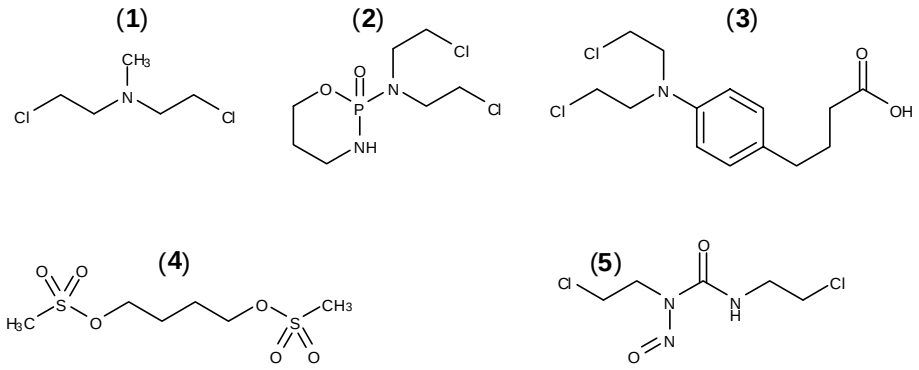

Figure I.1. Synthetic DNA Alkylating Agents Derived from Mustard Gases

I.3. Cancer Chemotherapy: Methods for the Discovery of Anticancer Compounds

In the years that followed the development of the original alkylating agents, anticancer drug discovery was focused on the identification of compounds that were toxic to cancer cells (cytotoxic). Compounds identified by this approach have since made substantial contributions to improving survival and providing clinical benefit for patients with a variety of malignancies.[9] The majority of the compounds discovered in this manner act by inhibiting cell division wherein an acceptable therapeutic index is achieved due to the fact that a relatively higher proportion of cancer cells are proliferating or are in the growth fraction of the cell cycle. However, because cytotoxic molecules typically target or damage DNA (as is the case with the alkylating agents), the majority of the compounds discovered in this fashion are unselective and significant side effects are usually associated with them.

While there is absolutely no doubt that cytotoxic chemotherapy is still making substantial contributions to improving survival and providing clinical benefit for patients with a variety of malignancies, there truly is a new horizon in cancer therapy.[10-14] The emphasis in anticancer drug discovery has shifted from an empirical approach, characterized by high throughput cytotoxicity assays to a more rational and mechanistic, target-based approach. The effect of this new paradigm in anti-cancer drug discovery is realized in the fact that over the last seven years, only one-third of the drugs approved by the FDA for the treatment of cancer can be considered conventional cytotoxic agents.[15] Facilitated by a rapid expansion in our understanding of the specific biologic processes important for growth, survival and metastasis of neoplastic cells, the target-based approach seeks to improve the efficacy and selectivity of anti-cancer drugs by identifying molecules that block the pathogenic mechanisms of cancer. Ideally these agents would interact only with proteins that are specific to tumor cells or that are upregulated during transformation to a malignant phenotype and should therefore, be more selective and less toxic to normal tissue. [16] However, there are significant disadvantages to this approach when compared to the conventional cytotoxic approach. First, compounds discovered by target based methods seek only to correct aberrations in normal cell function and they are likely to be cytostatic rather than cytotoxic.[16] Therefore, in the target based approaches where the tumor cells are never actually killed, active compounds would need to be perennially administered to maintain cancer cell stasis. Further, the fact that agents discovered in this fashion might not cause tumor shrinkage often presents the drug developer with a new challenge to try and document whether or not a potential drug

has clinical activity.[17] Shrinkage of the tumor has long been regarded as a key response variable for activity of a new agent and even a method to obtain an accelerated approval for a that agent.[14,15] Taking the previously mentioned arguments into consideration, the traditional endpoints of Phase I and Phase II clinical trials for conventional cytotoxic drugs (toxicity and response) may not be suitable and therefore clinical trials, by far the most expensive aspect of drug discovery, may need to be conducted for extremely long periods of time to get a true sense of toxicity.[16] Nonetheless, new approaches to treating cancer have been validated that range from attacking the blood vasculature that supplies the tumor to inhibiting tumor cell protein degradation pathways to blocking tumor cell signaling pathways, just to name a few.[16]

Examples of target based drugs currently approved for the treatment of cancer include sorafenib (**6**), (Figure I.2), a small molecule that blocks the recruitment of new vasculature to the tumor (angiogenesis) by inhibiting vascular endothelial growth factor receptor 2 (VEGFR-2). Angiogenesis has been shown to be critical to both tumor growth and metastasis. Pioneering work by Judah Folkman in the 1970s indicated that tumors were unable to grow beyond the size of a pea (2-3 mm) without recruiting new vascular supply.[20] The realization that angiogenesis is required for the growth and metastasis of neoplasms provided excellent rationale for exploring anti-angiogenic therapies in the treatment of cancer.[21]

The biological processes associated with tumor angiogenesis are extremely complex and many targets have been identified that have the potential to disrupt the recruitment of vasculature to growing tumors. Anti-angiogenic drugs in development

can be categorized by mechanisms of action and include: agents that block degradation of extracellular matrix (e.g. matrix metalloproteinase inhibitors), drugs that directly inhibit endothelial cell proliferation and/or migration, agents that inhibit endothelial cell-specific integrin/survival signaling, agents that block promoters of angiogenesis (e.g. anti vascular endothelial growth factor (VEGF) agents) and drugs with unknown mechanisms of action.[21,22] Of all the agents that have been developed that target certain aspects of tumor angiogenesis, those targeting VEGF signaling have shown the most promise to become drugs. Vascular endothelial growth factor receptor 2 (VEGFR-2, KDR in humans) is the major receptor involved in angiogenesis. Activation of VEGFR-2 is important in endothelial cell survival, proliferation, and vascular permeability.[23] The VEGFR-2 inhibitory effects of sorafenib for example have proven to be very effective in treating renal cell carcinoma especially in combination therapy with cytotoxic drugs with only limited side effects being reported.[21]

To continue, inhibition of the mammalian proteasome is emerging as one of the most exciting areas of target based anti-cancer chemotherapy. Proteasomes are large protein complexes responsible for the degradation of transient or damaged proteins through proteolysis (breaking of peptide bonds). The degradation process yields peptides of about seven to eight amino acids long, which can then be further degraded into amino acids and used in synthesizing new proteins.[24] In terms of cancer, inhibition of the proteasome has two main therapeutic outcomes the first being cell cycle arrest and the second being induction of apoptosis (programmed cell death).

Cell-cycle progression in all eukaryotes is driven by cyclin-dependent kinases (CDKs) and their cyclin partners. In vertebrates, the proper and timely duplication of the genome during S-phase of the cell cycle relies on the coordinated activities of positive regulators such as CDK-cyclins and E2F, and negative regulators such as CDK inhibitors of the Cip/Kip and INK4 families.[25] Recent and ongoing work suggests that many important regulators of G_1- and S-phases are targeted for ubiquitination and subsequent degradation by the 26S proteasome. In terms of the G_1-S transition, work in budding yeast has shown that proteasome mediated degradation of Sic1 (Kip1 in vertebrates) is necessary and sufficient for progression into S-phase.[26] Additional studies suggest that the proteasome mediated degradation of cyclin A is essential for the entry into S-phase and also indicate that the destruction of cyclin A in late mitosis to early G_1 helps to ensure that S-phase follows the completion of mitosis (i.e. cells do not divide until the cellular genome has been completely replicated).[27] In total the proteasome mediated degradation of specific proteins has been implicated in the control of the onset of DNA-replication, the order of cell cycle events and the timing or frequency of S-phase. In addition, several mammalian cell types also arrest at the G_1-to-S-phase transition upon treatment with different types of proteasome inhibitors making the proteasome an attractive target for cancer chemotherapy.[28,29]

Proteasome mediated degradation is also important in the control of apoptosis (programmed cell death). Under normal circumstances, nuclear factor NF-κβ is sequestered in the cytoplasm and rendered inactive by the inhibitor protein IκB. In times of cellular stress, IκB is degraded by the proteasome and NF-κB translocates to

the nucleus.[30] NF-κB promotes cell survival by initiating the transcription of genes encoding stress-response enzymes, cell-adhesion molecules, proinflammatory cytokines, and anti-apoptotic proteins such as Bcl-2, cIAP1, and cIAP2.[31-33] In certain malignancies, NFκB is constitutively active and has been shown to promote tumor cell survival and reduce the effectiveness of anticancer therapy.[34]

As indicated above, inhibition of the proteasome has a multi-faceted anticancer effect in that it both stops uncontrolled progression of the cell cycle and induces apoptosis in tumor cells. Bortezomib (**7**), (Figure I.2), a proteasome inhibitor recently approved for the treatment of multiple myeloma exhibited a number of anti-myeloma effects in pre-clinical trials including disruption of the cell cycle and induction of apoptosis.[35]

One of the most interesting and widely exploited anticancer targets is the tyrosine kinase class of enzymes. Tyrosine kinases attach phosphate groups to the amino acid tyrosine and thus control a variety of critical biological processes including cell growth, differentiation and motility. Genetic mutation can cause errant regulation of tyrosine kinase activity leading to a cancerous disease state.[36] Because a comprehensive review of the biology and function of the tyrosine kinase family of enzymes is beyond the scope of this report, this section will instead focus of one particular tyrosine kinase, epidermal growth factor receptor (EGFR).

Epidermal growth factor receptor exists on the cell surface and is activated by binding of specific ligands including epidermal growth factor and transforming growth factor alpha. Once bound by its activating ligands, EGFR undergoes a transition from

an inactive monomer to an active homodimer. Dimerization of EGFR stimulates its intracellular protein-kinase activity resulting in the autophosphorylation of five tyrosine residues in the C-terminal domain of EGFR. This autophosphorylation elicits downstream activation and signaling by several other proteins initiating a signal transduction cascade that leads to DNA synthesis and cell proliferation. Mutations of EGFR leading to constant activation have been identified in several types of cancer.[37] One very potent and FDA approved inhibitor of EGFR, erlotinib (**8**), has been shown to be very effective in treating both lung and pancreatic cancer. Erlotinib specifically targets EGFR by binding in a reversible fashion to the ATP binding site of the receptor.[38] Inhibition of the ATP binding site prevents autophosphorylation of the EGFR homodimer thus stopping the signal transduction cascade and inhibiting uncontrolled cell proliferation.

Another exciting approach to cancer chemotherapy is that which seeks to control cancer by inhibiting protein targets that are regulators of gene expression. Epigenetic modifications are increasingly recognized as having a substantial role to play in both normal cellular physiology and disease processes, particularly in cancer where inappropriate gene expression has long been known to play a fundamental role in the aetiology of the disease.[39] Histone deacetylase (HDAC) inhibitors comprise a new class of relatively specific anticancer drugs, which were originally identified due to their ability to reverse the cancerous phenotype in transformed cells.[40] Subsequent studies have shown that HDAC inhibitors are able to induce growth arrest, activate differentiation and also induce apoptosis in tumour cells. The mechanism by which

HDAC inhibitors induce their anticancerous effect is a topic of much debate that is currently receiving a great deal of attention.[41] HDAC inhibitors have recently been used as chemotherapeutic compounds and their antineoplastic activity was observed in cell lines originating from different types of human cancers, including neuroblastoma,[42] breast cancer,[43] prostate cancer,[44] and lung cancer.[45] Most importantly, in both *in vitro* and *in vivo* experiments, HDAC inhibitors have been shown to have a deleterious affect on cancer cells while leaving normal cell comparatively unharmed.[44,46] The clinical efficacy of HDAC inhibitors has been documented by several Phase I trials in patients with solid tumours or leukaemias[47,48] and many have been found to exhibit favorable toxicity profiles in phase II clinical trials.[49] An example of a HDAC inhibitor that was recently approved by the FDA for clinical use is vorinostat (**9**), (Figure I.2) which has proven to be very effective against cutaneous T-cell lymphoma in patients that have tried and failed other treatment options.

Another emerging field in the arena of cancer treatment is that of chemoprevention. While chemotherapy manages established disease, chemoprevention seeks to block cancer from occurring in the first place or to delay the onset of cancer beyond a normal human lifespan. Traditionally, cancer chemoprevention has been defined by the use of pharmacologic or natural agents that inhibit the development of invasive cancer either by blocking the DNA damage that initiates carcinogenesis "blocking agents" or by arresting or reversing the progression of premalignant cells in which such damage has already occurred "suppressing agents". [50]

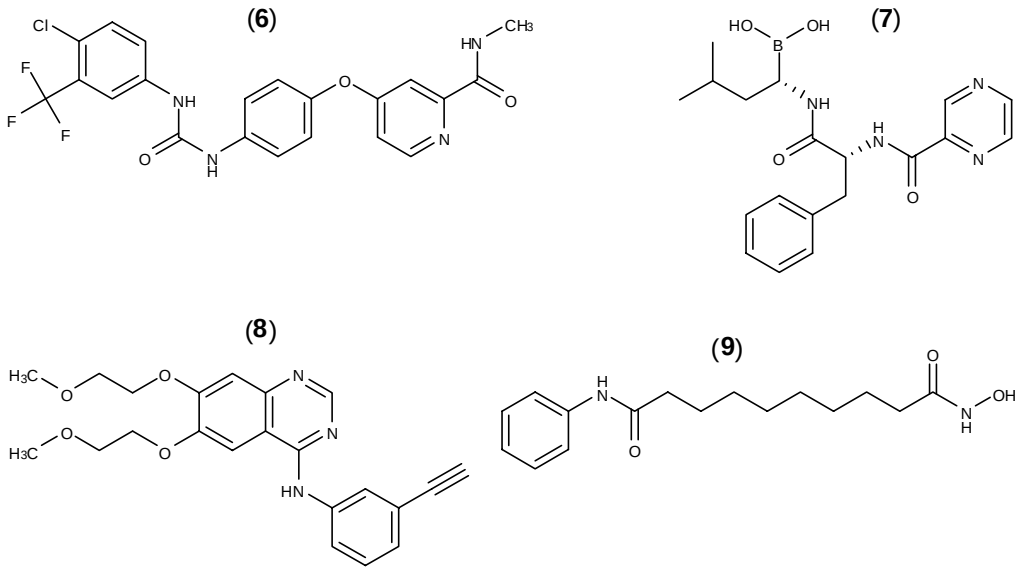

Figure I.2. Anti-Cancer Drugs Discovered by Target Based Screening

One of the most important cancer chemoprevention targets is ornithine decarboxylase (ODC). In humans, the enzyme ornithine decarboxylase (ODC) is a homodimer of 461 amino acids that catalyzes the decarboxylation of ornithine resulting in the production of the diamine putrescine. Putrescine is the simplest member of a class of molecules known as the polyamines, organic compounds having two or more primary amino groups that are required for cell division in eukaryotes. Conversion of ornithine to putrescine via ODC is the first and the rate limiting step for the production of polyamines and is a hallmark of rapidly proliferating cells.[51] It has also been shown that if the production of putrescine is inhibited, premalignant tumor cell growth is arrested or profoundly slowed.[51] A number of animal models have

shown that various types of cancers, e.g. skin, breast, colon, urinary, bladder and intestinal can be inhibited, dramatically in some cases, by inhibition of ODC activitiy.[52] Therefore, the inhibition of ODC and subsequent reduction of the production of putrescine constitutes an attractive target for the discovery of chemopreventative "suppressing agents". An example of an FDA approved drug that exhibits ODC inhibitory activity is eflornithine (**10**), (Figure I.3).

An additional cancer chemoprevention target is the enzyme aromatase. The development of aromatase inhibitors and inactivators for breast cancer treatment is one of the most successful contemporary achievements in cancer therapy.[53] Epidemiological data have for some time indicated a hormonally mediated basis for breast cancer and i*n vitro* and *in vivo* evidence indicated that estrogen played a central role in the promotion of breast cancer and possibly in its initiation as well.[54] The development of the estrogen receptor inhibitor tamoxifen (**11**), (Figure I.3) has been an extremely important occurrence especially when one considers that breast cancer is by far the most common cancer in women.[1] Tamoxifen has demonstrated efficacy in the prevention of estrogen-receptor positive breast cancer recurrence following resection of the primary tumor, exhibiting a one-third reduction in mortality 15 years from diagnosis in women receiving 5 years of postoperative therapy.[55] However, tamoxifen also has significant side effects arising from the fact that it often acts as an estrogen agonist. The severe side effects associated with tamoxifen (initiation of endometrial carcinoma and thromboembolic episodes) has led to the development of

second generation breast cancer chemotherapeutics including those that inhibit the enzyme aromatase.

Aromatase (estrogen synthetase) is the main enzyme involved in the production of estrogen in post-menopausal women (See: Chapter IV for a more detailed discussion). Aromatase acts by catalyzing the conversion of testosterone to estradiol and inhibition of aromatase activity has proven very successful in the treatment and prevention of estrogen receptor positive breast cancer.[54] Aromatase inhibitors including anastrozole (**12**), (Figure I.3) have recently been shown to be superior to tamoxifen in terms of both efficacy and toxicity in the treatment and prevention of breast cancer. Although the long term therapeutic action and toxicities of aromatase inhibitors have yet to be fully evaluated, these types of inhibitors a show a great deal of promise and are proving to be a logical alternative to tamoxifen for the treatment and prevention of breast cancer.

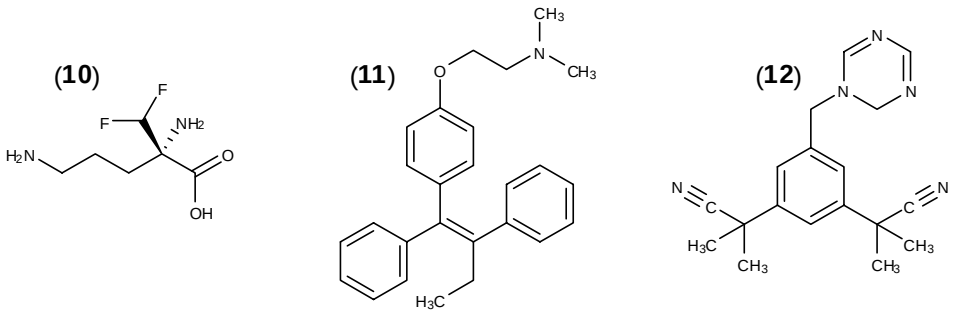

Figure I.3. Cancer Chemopreventative Agents

I.4. Cancer Chemotherapy: The Source of New Anticancer Compounds

Currently, there are two main sources for small molecule drugs in the field of cancer chemotherapy, those being: (1) molecules produced synthetically in a laboratory setting and (2) those produced in nature by biological organisms. In either case, the desired outcome is the identification of a large number of chemically diverse, biologically active lead molecules to examine the drug-like potential of in animal models and human clinical trials.

Traditionally, agents derived from nature (natural products) have supplied the majority of the molecules used as anticancer drugs. Medicine and drugs derived from nature (natural products) have been closely linked for many thousands of years through the use of traditional medicines and natural poisons.[56] However, over the past few decades, many of the large pharmaceutical companies have either terminated or considerably scaled down their natural product operations in favor of synthetic chemical libraries produced by combinatorial chemistry methodologies.[57] This transformation was due in large part to the technological revolution in the pharmaceutical industry that occurred in the 1980s. When automation, robotics, and personal computers were introduced into the field, chemistry became the rate-limiting step in drug discovery programs. The situation worsened in the early 1990s, with high-throughput screening, fast personal computers, and the extremely fast pace at which molecular biology was identifying new biological targets. Natural products methodologies were unable to supply the huge numbers of compounds required by the target based screens that by this time were taking months instead of years to complete.[58] Further, combinatorial methods produced molecules with much less

chemical complexity when compared to natural products. On average, natural products have higher molecular weights; incorporate fewer nitrogen, halogen, or sulfur atoms but more oxygen atoms; and are sterically more complex, with more bridgehead tetrahedral carbon atoms, rings, and chiral centers.[58] In this regard, synthetic molecules were also more attractive as the issue of supply could be easily overcome due to the fact that chemically simple molecules required less investment of both time and resources to produce.

Although the contribution that combinatorial chemistry will have on drug discovery has yet to be truly determined as simply not enough time has passed to allow for an unbiased evaluation, the role that secondary metabolites derived from natural sources have played in anticancer chemotherapy cannot be overstated. This becomes evident when one realizes that 61% of the 877 small-molecule new chemical entities introduced as drugs worldwide during 1981–2002 can be traced to or were inspired by natural products. These include natural products (6%), natural product derivatives (27%), synthetic compounds with natural-product-derived pharmacophores (5%), and synthetic compounds designed on the basis of knowledge gained from a natural product (that is, a natural product mimic; 23%). In certain therapeutic areas, the productivity is higher: 78% of antibacterials and 74% of anticancer compounds are natural products or have been derived from, or inspired by, a natural product. [59]

Anecdotal evidence had long implicated terrestrial plants as producers of bioactive metabolites and subsequent investigation into the biomedical potential of terrestrial plants yielded many important compounds including morphine (**13**),[60] quinine (**14**)[61] and aspirin (**15**)[62] (Figure I.4). Terrestrial plants have also been prolific producers of

anticancer compounds such as taxol (**16**)[63] and the Vinca alkaloids vinblastine (**17**)[64] and vincristine (**18**)[65] (Figure I.5).

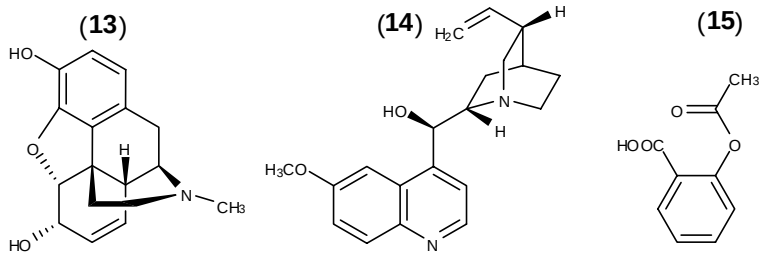

Figure I.4. Important Bioactive Molecules Derived from Terrestrial Plants

Taxol, vinblastine and vincristine were extremely important molecules in the field of anticancer drug discovery because although identified through traditional cytotoxic methods, these molecules exhibited their effects through DNA independent mechanisms. Taxol has been shown to interfere with the function of microtubules by stabilizing their structure thus arresting the cells in metaphase.[66] Specifically, taxol binds to the β subunit of tubulin which is a building block of microtubules. The resulting association between taxol and tubulin prevents microtubules from disassembling which effectively arrests dividing cells in the metaphase stage of mitosis, triggering apoptosis and cell death.[67] Interestingly, vinblastine and vincristine also act upon microtubules by binding tubulin. However, in opposition to the mechanism of action of taxol, vinblastine and vincristine act by binding free tubulin thus preventing the assembly of microtubules which ultimately leads to arrest in the metaphase stage of mitosis.[68]

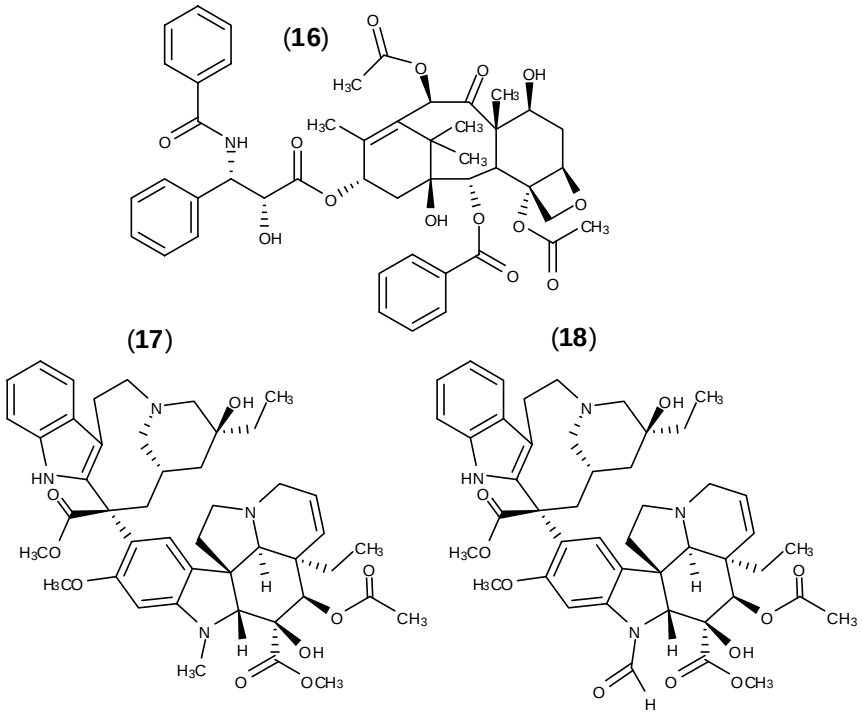

Figure I.5. Anticancer Drugs Derived from Terrestrial Plants

Following the landmark discovery of penicillin by Alexander Fleming in the 1920s, the microbial realm was also recognized as an extremely important resource for drugs.[69] After Fleming's discovery, an exhaustive examination of the secondary metabolites produced by soil based microbes ensued that yielded a multitude of agents important to human healthcare. The structural diversity of the chemicals produced by microorganisms kept discovery pipelines full for nearly 70 years forming the basis of the pharmaceutical industry as we know it today. During this time, a specific order of Gram-positive bacteria known as the *Actinomycetales* (commonly called actinomycetes) emerged as arguably the most important producer of bioactive compounds from nature. Both antibiotic [e.g. erythromycin (**19**),[70] streptomycin

(**20**)[71] and vancomycin (**21**),[72] (Figure I.6)] and anticancer [e.g. actinomycin D (**22**),[73] bleomycin (**23**),[74] doxorubicin (**24**),[75] and mitomycin C (**25**)[76] (Figure I.7)] drugs were isolated from various genera within the actinomycete order. In general, the role that actinomycetes play as a source of useful pharmaceuticals is highlighted by the remarkable fact that, as of 1988, actinomycetes accounted for approximately two-thirds of the naturally derived antibiotics discovered and from 1940-2002 were responsible for 17% of new anticancer drugs approved for clinical use. [77,78]

It is especially exciting to consider that the oceans, which cover greater than 70% of the surface of the earth, have been completely overlooked as a resource for new bioactive compounds. In terms of microbial density, the terrestrial environment pales in comparison to that of the oceans with estimates from the marine environment reaching one-million bacterial cells per milliliter of sea water and one-billion bacterial cells per milliliter of sediment. [79,80] In addition, the Fenical group at Scripps Institution of Oceanography has isolated multiple strains of filamentous bacteria belonging to a novel genus of marine actinomycetes designated the *Salinispora*.[81] These organisms require seawater for growth and are both widespread and persistent in marine sediments.[81] The biomedical potential of the *Salinispora* has also been realized following the isolation of an extremely potent cytotoxin, salinosporamide A (**26**), (Figure I.8), produced by *S. tropica*.[82] Salinosporamide has been shown to be an irreversible inhibitor of the mammalian proteasome and is currently in phase I clinical trials for the treatment of multiple myeloma.[83]

The overall goal of the research presented within this thesis was to use marine sediment-derived actinomycetes as a source to discover molecules with novel carbon

skeletons that were potentially effective in the treatment and/or prevention of cancer. In order to accomplish this goal, several hundred strains of sediment-derived actinomycetes were cultured and their fermentation extracts were screened in various cancer relevant assays. In chapter II, the isolation, structure elucidation and biological activities of the piperazimycins, potently cytotoxic depsipeptides produced by a marine-derived isolate of the genus *Streptomyces* are covered. Chapter III deals with the isolation and structure elucidation of the arenicolides, cytotoxic polyketides from a strain of *Salinispora arenicola* the complete biological activities of which are currently under investigation. Finally, Chapter IV covers the isolation and structure elucidation of the pyridiopyrones, pyridine containing molecules of likely polyketide origin that have been isolated from another marine-derived bacterium of the genus *Streptomyces*. The pyridinopyrones exhibit cancer chemopreventative activities the details of which are also under investigation.

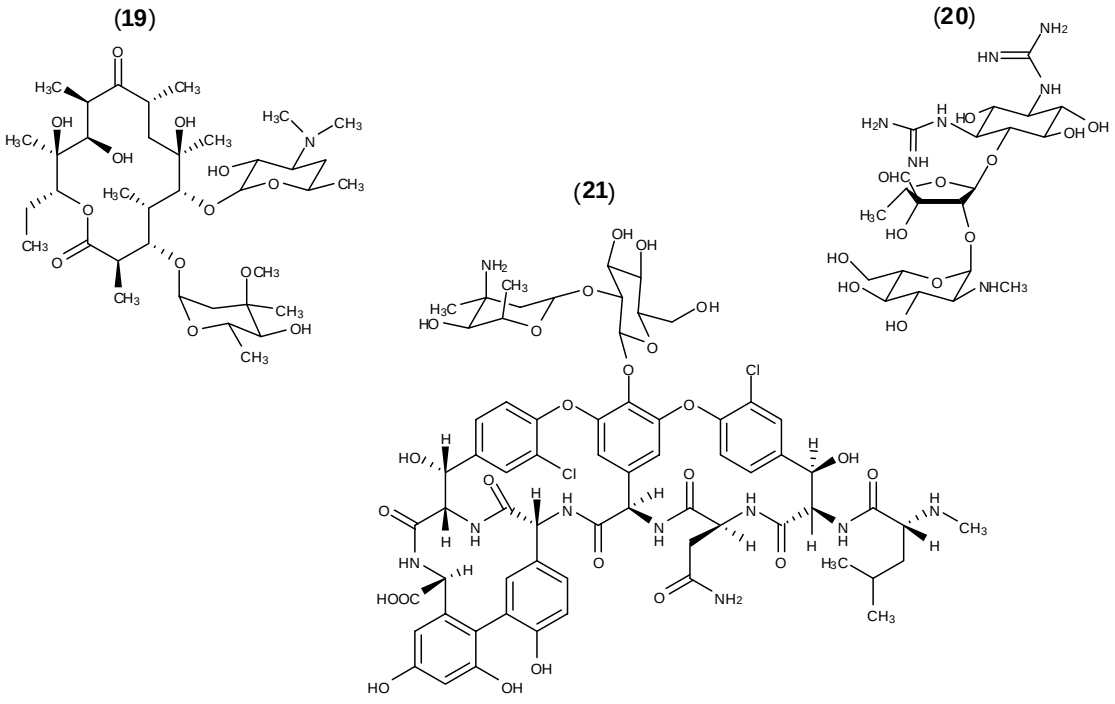

Figure I.6. Antibiotic Drugs Isolated From Terrestrial Actinomycetes

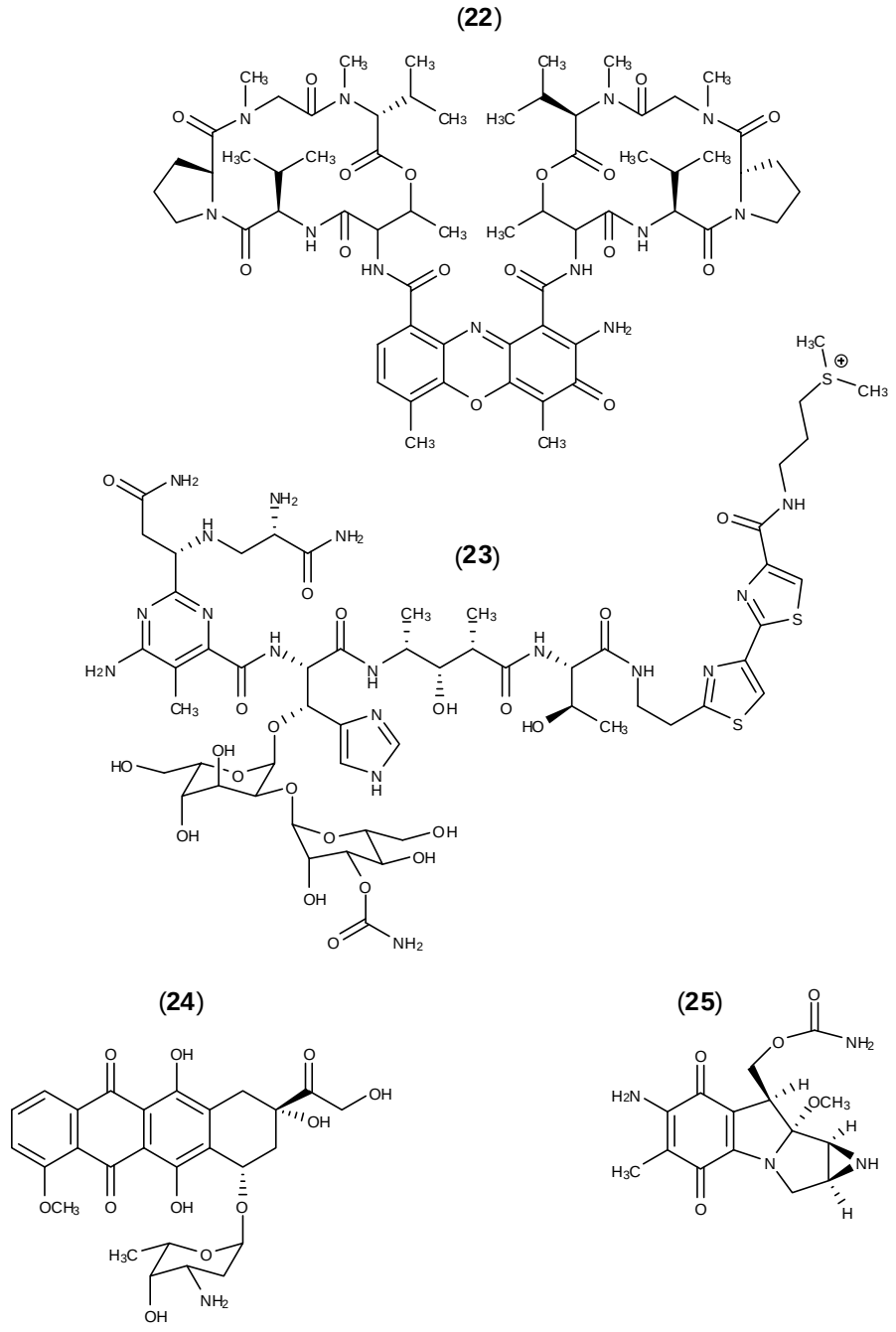

Figure I.7. Anticancer Drugs Isolated from Terrestrial Actinomycetes

(**26**)

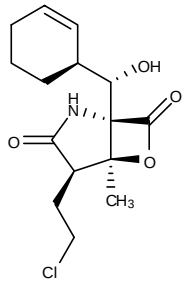

Figure I.8. Salinosporamide A from *Salinispora tropica*

References

(1) Gansler, T.; Eyre, H. *CA. Cancer J. Clin*. **2006**, *56*, 1

(2) Alberts, B.; Bray, D.; Lewis, J.; Raff, M.; Roberts, K.; Watson, J. (eds), Molecular Biology of the Cell. Garland Publishing Inc., New York: **1994**, 1255-1291, 1313-1361

(3) Chu, E.; et al. *Cancer Chemotherapy*. In: Katzung, B.(ed), Basic and Clinical Pharmacology. McGraw-Hill Companies Inc., New York: **2004**, 898-930

(4) Anslow, W.; Karnovsky, D.A.; Val Jager, B.; Smith, H. *Journal of Pharmacology and Experimental Therapeutics*. **1947**, *91*, 224-235

(5) Fraiser, L.H.; Kanekal, S.; Kehrer, J.P. *Drugs*. **1991**, *42*, 781-795

(6) Van Putten, L. M.; Lelieveld, P. *European Journal of Cancer*. **1971**, *7*, 11-16

(7) Tariq, M.; Al-Badr, A. *Analytical Profiles of Drug Substances*. **1987**, *16*, 53-83

(8) Marsh, J.C.; DeConti, R.C.; Hubbard, S.P. *Cancer Chemotherapy Reports Part 1*. **1971**, *55*, 599-606

(9) Von Hoff, D.D. *Horizons for Cancer Chemotherapy (and NonChemotherapy*). In: The Process of New Drug Discovery and Development. Smith, C.G.; O'Donnell, J.T. (eds), **2006**, 445-455, New York, NY.

(10) Goldberg, R.M.; Sargent, D.J.; Morton, R.F.; Fuchs, C.S.; Ramanathan, R.K.; Williamson, S.K.; Findlay, B.P.; Pitot, H.C.; Alberts, S.R. *J. Clin. Oncol.* **2004**, *22*, 23-20

(11) Giacchetti, S.; Perpoint, B.; Zidani, R.; Le Bail, N.; Faggiuolo, R.; Focan, C.; Chollet, P.; Llory, J.F.; Letourneau, Y.; Coudert, B.; Bertheaut-Cvitkovic, F.; Larregain-Fournier, D.; Le Rol, A.; Walter, S.; Adam, R.; Misset, J.L.; Lévi, F. *J. Clin. Oncol*. **2000**, *18*, 136-147

(12) Andre, T.; Boni, C.; Mounedji-Boudiaf, L.; Navarro, M.; Tabernero, J.; Hickish, T.; Topham, C.; Zaninelli, M.; Clingan, P.; Bridgewater, J.; Tabah-Fisch, I.; de Gramont, A. *N. Engl. J. Med*. **2004**, *350*, 2343-2351

(13) Vogelzang, N.J.; Rusthoven, J.J.; Symanowski, J.; Denham, C.; Kaukel, E.; Ruffie, P.; Gatzemeier, U.; Boyer, M.; Emri, S.; Manegold, C.; Niyikiza, C.; Paoletti, P. *J. Clin. Oncol*. **2003**, *21*, 2636-2644

(14) Hanna, N.; Shepherd, F.A.; Fossella, F.V.; Pereira, J.R.; De Marinis, F.; Von Pawel, J.; Gatzemeier, U.; Chang Yao Tsao, T.; Pless, M.; Muller, T.; Lim, H-L.; Desch, C.; Szondy, K.; Gervais, R.; Shaharyar, Manegold, C.; Paul, S.; Paoletti, P.; Einhorn, L.; Bunn, P.A. *J. Clin. Oncol*. **2004**, *22*, 1589-1597

(15) www.accessdata.fda.gov/scripts/cder/onctools/druglist.cfm

(16) Fox, E.; Curt, G.A.; Balis, F.M. *The Oncolcogist*. **2002**, *7*, 401-409

(17) Cunningham, D.; Pyrhonen, S.; James, R. D.; Punt, C. J.; Hickish, T. F.; Heikkila, R.; Johannesen, T. B.; Starkhammar, H.; Topham, C.A.; Awad, L.; Jacques, C.; Herait, P. *The Lancet*. **1998**, *352*, 1413-1418

(18) O'Shaughnessy, J.A.; Wittes, R.E.; Burke, G.; Friedman, M.A.; Johnson, J.R.; Niederhuber, J.E.; Rothenberg, M.L.; Woodcock, J.; Chabner, B.A.; Temple, R. *J. Clin. Oncol*. **1991**, *9*, 2225-2232

(19) Dagher, R.; Johnson, J.; Williams, G.; Keegan, P.; Pazdur, R. *J. Natl. Cancer Inst*. **2004**, *96*, 1500-1509

(20) Folkman J. *N. Engl. J. Med*. **1971**, *285*, 1182-1186

(21) Akarija, A. Soff, G. *Current Opinion in Oncology*, **2005**, *17*, 578-583

(22) Rak, J.; Kerbel, R.S. *Prospects and progress in the development of anti-angiogenic agents.* In: Principles & Practice of Biologic Therapy of Cancer, 3rd edition. Rosenberg S.A.(ed) **2002**, Philadelphia, PA

(23) Ferrara, N.; Gerber, H-P.; LeCouter, J. *Nat. Med*. **2003,** *9*, 669-676

(24) Hochstrasser, M. *Cell*. **1996**, *84*, 813-815

(25) Yew, P.R. *J. Cell. Phys*. **2001**, *187*, 1-10

(26) Verma, R.; Annan, R.S.; Huddleston, M.J.; Carr, S.A.; Reynard, G.; Deshaies, R. J. *Science*. **1997**, *278*, 455-460

(27) Hershko, A. *Curr*. *Opin*. *Cell Biol*. **1997**, *9*, 788-799

(28) Sherwood, S.W.; Kung, A.L.; Roitelman, J.; Simoni, R.D.; Schimke, R.T. *PNAS*. **1993**, *90*, 3353-3357

(29) Machiels, B.M.; Henfling, M.E.; Gerards, W.L.; Broers, J.L.; Bloemendal, H.; Ramaekers, F.C.; Schutte, B. *Cytometry*. **1997**, *28*, 243-252

(30) Adams, J. *Current Opinion in Oncology*. **2002**, *14*, 628-634

(31) Chen, C.; Eldstein, L.C.; Gelinas, C. *Mol*. *Cell*. *Biol*. **2000**, *20*, 2687-2695

(32) Wang, C.Y.; Mayo, M.W.; Korneluk, R.G.; Goeddel, A.S.; Baldwin, A.S. *Science*. **1998**, *281*, 1680-1683

(33) Wang, C.Y.; Guttridge, D.C.; Mayo, M.W.; Baldwin, A.S. *Mol*. *Cell*. *Biol*. **1999**, *19*, 5923-5929

(34) Zong, W.X.; Edelstein, L.C.; Chen, C.; Bash, J.; Gelinas, C. *Genes Dev*. **1999**, *13*, 382-387

(35) Field-Smith, A.; Morgan, G.J.; Davies, F.E. *Therapeutics and Clinical Risk Management*. **2006**, *2*, 271-279

(36) Lynch, T.J.; Bell, D.W.; Sordella, R.; Gurubhagavatula, S; Okimoto, R.A.; Brannigan, B.W.; Harris, P.L.; M.S., Haserlat, S.M.; B.A., Supko, J.G.; Haluska, F.G.; Louis, D.N.; Christiani, D.C.; Settleman, J.; Haber, D.A. *N. Engl. J. Med.* **2004**, *350*, 2129-39

(37) Paez, J.G.; Jänne, A.p.; Lee, J.C.; Tracy, S.; Greulich, H.; Gabriel, S.; Herman, P.; Kaye, F.J.; Lindeman, N.; Boggon, T.J.; Naoki, K.; Sasaki, H.; Fujii, Y.; Eck, M.J.; Sellers, W.R.; Johnson, B.E.; Meyerson, M. *Science*. **2004,** *304*, 1497-500

(38) Petra, M. *Cancer Control*. **2006**, *13*, 129-140

(39) Pienta, K.J.; Smith, D. C. *CA. Cancer J. Clin*. **2005**, *55*, 300-318

(40) Marks, P.A.; Rifkind, R.A.; Richon, V.M.; Breslow, R.; Miller, T.; Kelly, W.K. *Nat. Rev. Cancer*. **2001**, *1*, 194–202

(41) Johnstone, R.W. *Nat. Rev. Drug. Discov*. **2002**, *1*, 287–299

(42) Glick, R.D.; Swendeman, S.L.; Coffey, D.C.; Rifkind, R.A.; Marks, P.A.; Richon, V.M.; La Quaglia, M.P. *Cancer Res*. **1999**, *59*, 4392–4399

(43) Schmidt, K.; Gust, R.; Jung, M. *Arch. Pharm. (Weinheim)*. **1999**, *332*, 353–357

(44) Butler, L.M.; Agus, D.B.; Scher, H.I.; Higgins, B.; Rose, A.; Cordon-Cardo, C.; Thaler, H.T.; Rifkind, R.A.; Marks, P.A.; Richon, V.M. *Cancer Res*. **2000**, *60*, 5165–5170

(45) Zhu, W.G.; Lakshmanan, R.R.; Beal, M.D.; Otterson, G.A. *Cancer Res*. **2001**, *61*, 1327–1333

(46) He, L.Z.; Tolentino, T.; Grayson, P.; Zhong, S.; Warrell, R.P.; Rifkind, R.A.; Marks, P.A.; Richon, V.M.; Pandolfi, P.P. *J. Clin. Invest*. **2001**, *108*, 1321–1330

(47) Gilbert, J.; Baker, S.D.; Bowling, M.K.; Grochow, L.; Figg, W.D.; Zabelina, Y.; Donehower, R.C.; Carducci, M.A. *Clin. Cancer Res*. **2001**, *7*, 2292–2300

(48) Piekarz, R.L.; Robey, R.; Sandor, V.; Bakke, S.; Wilson, W.H.; Dahmoush, L.; Kingma, D.M.; Turner, M.L.; Altemus, R.; Bates, S.E. *Blood*. **2001**, *98*, 2865–2868

(49) Inche, A.G.; La Thangue, N.B. *Drug Discovery Today*. **2006**, *11*, 97-109

(50) Hong, W.K.; Sporn, M.B. *Science*. **1997,** *278*, 1073-1077

(51) McCann, P.; Pegg, A.E. *Pharmacol. Ther*. **1996**, *54*, 195-215

(52) Thompson, H.J.; Herbst, E .J.; Meeker, L.D. *J. Nat. Cancer Inst*. **1986**, *77*, 595-598

(53) Geisler, J.; Lonning, P.E. *Clin. Cancer. Res*. **2005,** *11*, 2809-2821

(54) Goss, P.E.; Strasser-Weippl, K. *Clin. Cancer Res*. **2004**, *Suppl(10)*, 372s-379s

(55) Collaborative Group Listed at the end of the Publication. *The Lancet*. **1998**, *351*, 1451-1467

(56) Newman, D.J.; Cragg, G.M.; Snader, K.M. *Nat*. *Prod*. *Rep*. **2000**, *17*, 215-324

(57) Butler, M.S. *J*. *Nat*. *Prod*. **2004**, *67*, 2141-2158

(58) Rouhi, A.M. *CENEAR*, **2003**, *81*, 77-78, 82-83, 86, 88-91

(59) Newman, D.J.; Cragg, G.M.; Snader, K.M. *J*. *Nat*. *Prod*. **2003**, *66*, 1022-1037

(60) Muhtadi, F. J. *Analytical Profiles of Drug Substances*. **1988**, *17*, 259-366

(61) Kremsner, P.G.; Winkler, S.; Brandts, C.; Neifer, S.; Bienzle, U.; Graninger, W. *The Journal of Infectious Diseases*. **1994**, *169*, 467-470

(62) Florey, K. *Analytical Profiles of Drug Substances*. **1979**, *8*, 1-46

(63) Suffness, M. *Annual Reports in Medicinal Chemistry*. **1993**, *28*, 305-314

(64) Muhtadi, F. *Analytical Profiles of Drug Substances*. **1992**, *21*, 611-658

(65) Armstron, J. *Cancer Chemotherapy Reports*. **1968**, *52*, 527-535

(66) De Brabander, M.; Geuens, G.; Nuydens, R.; Willebrords, R.; De Mey, J. *PNAS*, **1981**, *78*, 5608-612

(67) De Brabander, M.; De Mey, J.; Geuens, G.; Nuydens, R.; Willebrords, R. *Journal of Submicroscopic Cytology*, **1984**, *16*, 1-2

(68) Tannock, I. F. *Experimental Cell Research*, **1967**, *47*, 345-56

(69) Fleming, A. *British J. Exp. Pathol*. **1929**, *10*, 226-236

(70) Perun, T. *Drug Action Drug Resist. Bact*. **1971**, *1*, 123-152

(71) Mossa, J. *Analytical Profiles of Drug Substances*. **1987**, *16*, 507-609

(72) Griffith, R. *Journal of Antimicrobial Chemotherapy*. **1984**, *Suppl (14)*, 1-5

(73) Hirayama, N. *Gendai Kagaku*. **2001**, *366*, 51-53

(74) Crooke, S. *Cancer Chemother*. **1981**, *3*, 343-350

(75) Blum, R. *Ann. Int. Med*. **1974**, *80*, 249-259

(76) Beijnen, J.; et al. J*ournal of Pharmaceutical and Biomedical Analysis*. **1986**, *4*, 275-295

(77) Okami,Y.; et al. *Search and Discovery of New Antibiotics*. In: Goodfellow M, Williams ST, Mordarski M (eds), *Actinomycetes in Biotechnology*. Academic, New York: **1988**, 33-67

(78) Newman D.; et al. *The discovery of Anticancer Drugs from Natural Sources*. In: Zhang L, Demain, A (eds), *Natural Products Drug Discovery and Therapeutic Medicine*. Humana Press, New Jersey: **2005**, 129-168

(79) Azam, F. *Science*. **1998**, *280*, 694-696

(80) Torsvik, V.; Øvreås, L.; Thingstad, T.F. *Science*. **2002**, *296*, 1064-1066

(81) Mincer, T.J.; Jensen, P.R.; Kauffman, C.A.; Fenical, W. *Appl. Env. Microbiol*. **2002**, *68*, 5005-5011

(82) Feling, R.H.; Buchanan, G.O.; Mincer, T.J.; Kauffman, C.A.; Jensen, P.R.; Fenical, W. *Angew. Chem. Int. Ed*. **2003**, *42*, 355-357

(83) Groll, M.; Huber, R.; Potts, B.C.M. *Journal of the American Chemical Society*. **2006**, *128*, 5136-5141

II

Piperazimycins: Cytotoxic Hexadepsipeptides from a Marine-Derived Bacterium of the Genus *Streptomyces*

II.1. Introduction

A major portion of the thesis research was devoted toward the discovery of cytotoxic compounds using a colon adenocarcinoma whole cell assay. This discovery platform was chosen for three main reasons. First, the cytotoxicity approach has a proven track record in that a multitude of clinically successful anticancer drugs have been identified using this methodology (See: Section I.3). Second, many of the enzymes that are validated as anticancer targets have been discovered when a newly discovered compound exhibits a cytotoxic effect in a whole cell system by a previously unknown mechanism. The colon adenocarcinoma cell line HCT-116 was specifically chosen due to the fact that cells of this type are typically very resistant to chemotherapy and therefore, any potential drugs discovered in this assay should be potently cytotoxic toward a multitude other types of cancers.

The cytotoxic activity of test samples toward HCT-116 colon adenocarcinoma cells was determined using a *in vitro* assay that quantified cell viability via bio-reduction of (3-(4,5-dimethylthiazol-2-yl)-5-(3-carboxymethoxyphenyl)-2-(4-sulfophenyl)-2H-tetrazolium (MTS), (**27**) to formazan (**28**) in the presence of the electron coupling reagent phenazine methyl sulfate (PMS), (**29**). Cell mediated reduction of tetrazolium salts in the presence or absence of intermediate electron carriers is commonly used as a convenient test for animal or bacterial cell viability (Figure II.1).[84-88] Although dehydrogenase enzymes are suspected to be the driving force behind the bio-reduction, the mechanisms and subcellular localization of reducing systems or species in viable or intact cells have not been fully elucidated.[84] Nonetheless, these reactions

are widely used as indicators of metabolic activity,[89-91] and have also been shown to be excellent indicators of *in vivo* inhibitory activity.[82,83] In the MTS assay system, the quantity of formazan product in the cell supernatant as measured by the absorbance at 490nm is directly proportional to the number of living cells in culture and by serial dilution, the GI_{50} of a test compounds can be determined.

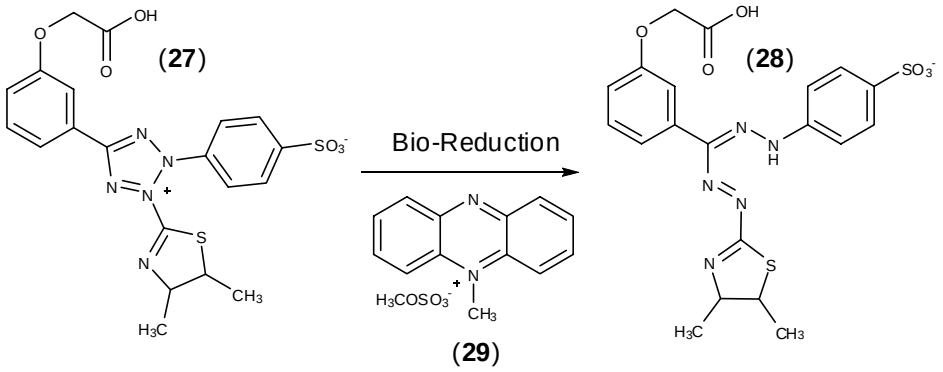

Figure II.1. Bioreduction of MTS to Formazan in the Presence of PMS by Metabolically Active Cells

As part of the effort to discover new cytotoxic molecules from marine sediment-derived bacteria, a crude extract produced by an isolate of the genus *Streptomyces*, was identified as being potently cytotoxic (GI_{50} = 76 ng/mL) toward HCT-116 cells. Bioassay-guided fractionation led to the isolation of three cyclic peptides, piperazimycins A-C (**30**-**32**), (Figure II.2), which were responsible for the overall cytotoxicity of the extract.

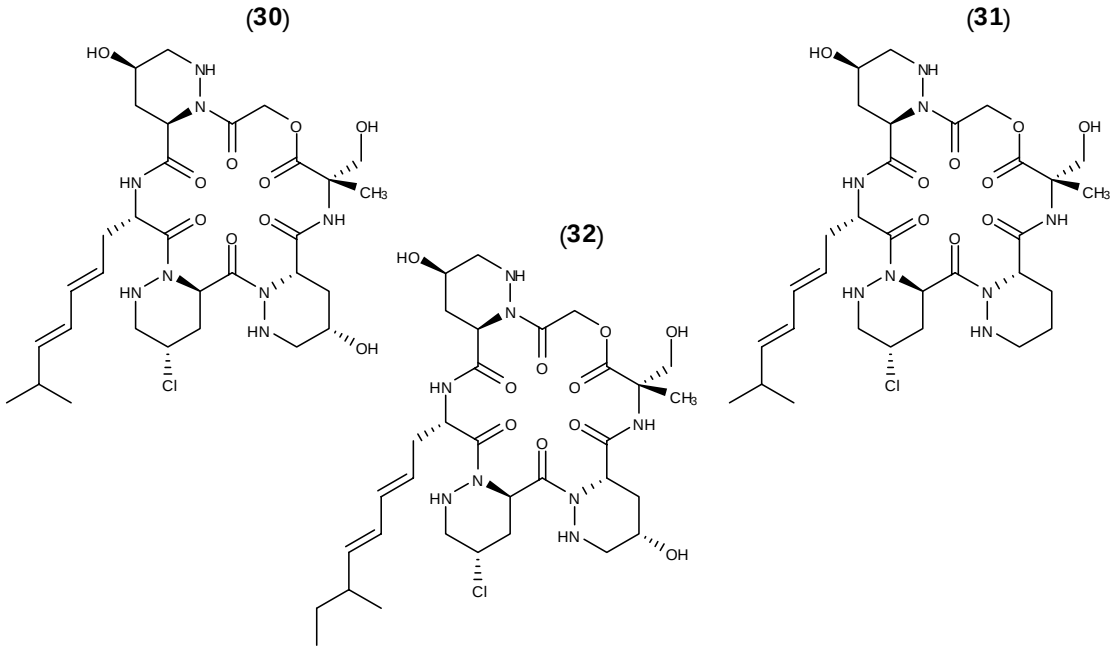

Figure II.2. Piperazimycins A (30), B (31) and C (32)

II.2. Isolation and Planar Structure Elucidation of Piperazimycins A-C (30-32)

Piperazimycin A (**30**) was isolated and purified by EtOAc extraction of the whole microbial culture broth, followed by bioassay-guided fractionation via flash, C_{18} reversed phase column chromatography and C_{18} reversed phase HPLC (57% CH_3CN:H_2O). In the purified form, **30** was obtained as a white powder that analyzed for the molecular formula $C_{31}H_{47}N_8O_{10}{}^{35}Cl$ by HRFABMS $[M+H]^+$ m/z = 727.3186 and NMR spectral data. Interpretation of HSQC and DEPT NMR spectral data enabled the assignment of all protons to their respective carbons, with the exception of eight exchangeable ^1H NMR signals that were assumed to be attached to heteroatoms. The chemical shifts of these ^1H NMR signals suggested, although did not confirm, the

presence of three alcohols, two amides and three secondary amines (Table II.1). This information, in combination with the ^{13}C NMR spectra, which revealed six carbonyl carbons within the amide/ester range, suggested **30** was composed of six amino acids. The possibility that **30** was a depsipeptide (also possessed an ester linkage) was inferred by these data, but not rigorously indicated until additional NMR data were obtained. Subsequent analysis of HSQC, COSY and HMBC NMR spectral data allowed five amino acids and one hydroxy acid to be assembled, accounting for all of the atoms in **30**. The specific assignments made from analysis of the 1D and 2D NMR spectra of **30** are as follows:

A hydroxy-acetic acid (HAA) residue was assigned following the observation of a pair of oxygenated methylene ^1H NMR signals (H_2-31) that exhibited exclusively geminal coupling [d, J = 15.5 Hz]. COSY NMR correlations were observed only within the H_2-31 geminal pair and the only HMBC NMR correlations observed from H_2-31 were to carbonyl carbons at positions C-1 and C-30 (Table II.1). An α-methyl-serine residue was then assigned following the observation of COSY NMR correlations originating from another set of oxygenated methylene ^1H NMR signals (H_2-3) to an unassigned ^1H NMR signal (OH-1), indicating that a hydroxyl group was attached to C-3 [δ_C 64.2]. HMBC NMR correlations observed from both H_2-3 and a secondary amide proton signal (NH-1 [δ_H 7.57 (s)]), to a carbonyl carbon (C-1) and a quaternary carbon (C-2) implied the presence of a modified serine residue. Further HMBC NMR correlations from H_2-3 and NH-1 to a methyl singlet (H_3-4), coupled

with HMBC NMR correlations from H_3-4 to C-1, C-2 and C-3, indicated methylation of C-2 and confirmed this residue as α-methyl-serine (αMeSer).

The 2-amino-8-methyl-4,6-nonadienoic acid (AMNA) residue in **30** was assigned following analysis of ^{13}C and ^{1}H NMR chemical shifts, ^{1}H multiplicity, *J* values and interpretation of correlations observed in COSY and HMBC NMR spectral data (Table II.1). A gem-dimethyl configuration for the C-23 and C-24 terminal methyl groups was proposed based on COSY NMR correlations from the overlapping methyl doublets H_3-23 [δ_H 0.97 (d, J = 7.0 Hz)] and H_3-24 [δ_H 0.97 (d, J = 7.0 Hz)] to the methine proton signal, H-22. Interpretation of a network of COSY and HMBC NMR correlations originating from H-22 established the connectivity to C-16 and the presence of a conjugated diene with unsaturation at C-20 and C-18. HMBC NMR correlations observed from the amide proton, NH-4 [δ_H 7.60 (d, J = 6.0 Hz)], to C-16 and the carbonyl carbon C-15, coupled with the observation of HMBC NMR correlations from H-16 and H_2-17 to C-15 established the novel AMNA residue.

Combined spectral analyses allowed three substituted piperazic acids in **30** to be defined. The first, a rare, but known γ-hydroxypiperazic acid (γOHPip1) residue, was identified following interpretation of COSY and HMBC NMR correlations originating from the methine proton signal H-6, which established connectivity from the carbonyl carbon C-5 to the secondary ε-amine (NH-2) (Table II.1). COSY NMR correlations from H-8 to an unassigned proton signal (OH-2) indicated that an alcohol was attached to C-8 [δ_C 58.9]. The observation of an HMBC NMR correlation from NH-2 to C-6, that could only be rationalized if the residue was cyclic, at first, suggested a γ-

hydroxyproline residue. Closer examination of the COSY NMR data revealed that H-6 was not coupled to NH-2 as would be expected in this amino acid. On this basis, and based on the proportionally larger number of nitrogen atoms present in **30**, this group was assigned as a γ–hydroxypiperazic acid (γOHPip1) moiety. Comparison of the ^{13}C and ^{1}H NMR chemical shift values found in this study to those of previously reported for γOHPip amino acids supported this structural assignment.[92,93] The structures of two other modified piperazic acid units, another γ-hydroxypiperazic acid (γOHPip2) residue and one γ-chloropiperazic acid (γClPip) were subsequently proposed following analysis of ^{1}H and ^{13}C NMR chemical shift values and comparison to those observed in γOHPip1 (Table II.1).

The sequence of amino acids in **30** was initially determined by interpretation of key correlations observed in the HMBC NMR spectra (Figure II.3). Specifically, HMBC NMR correlations observed from the αMeSer amide proton (NH-1) to the γOHPip carbonyl carbon (C-5) established the connectivity of those two residues. Additional HMBC NMR correlations from the γOHPip1 alpha proton (H-6) and secondary amine (NH-2) to the γClPip carbonyl carbon (C-10) allowed these two residues to be connected. Additional HMBC NMR correlations from the γClPip alpha proton (H-11) and secondary amine (NH-3) to the AMNA carbonyl carbon (C-15) indicated that the AMNA residue was attached to the γClPip moiety. Further HMBC NMR correlations from the AMNA alpha proton (H-16) to the γOHPip2 carbonyl carbon (C-25) and from the AMNA amide proton (NH-4) to the γOHPip2 alpha carbon (C-26) established the position of the γOHPip2 residue in **30**. HMBC NMR correlations from

Table II.1. NMR Spectral Data for 30 Recorded in $CDCl_3$ (500 MHz) 25 ºC

Unit	Position	δ_H mult (*J* in Hz)	δ_C, DEPT	HMBC	COSY
αMeSer C=O	1		173.6, C		
α	2		63.0, C		
β	3a	[a]4.04 dd(11.5,4.0)	64.2, CH_2	C1,C2,C4	H3b,OH-1
	3b	[a]4.14 dd(11.5,11.5)		C1,C2,C4	H3a,OH-1
αMe	4	1.57 s	18.3, CH_3	C1,C2,C3	
NH-1		7.57 s		C1,C2,C3,C4,C5,C6	
OH-1		[a]3.24 dd(11.5,4.0)			H3ab
γOHPip1 C=O	5		172.4, C		
α	6	5.15 dd(7.0,2.0)	51.2, CH	C5,C7,C8,C10	H7ab
β	7a	[b]2.01 m	28.5, CH_2	C5,C6,C8,C9	H6,H7b,H8
	7b	[b]2.26 m		C8,C9	H6,H7a,H8
γ	8	[b]3.75 bs	58.9, CH	C6,C7,C9	H7ab,H9ab,OH-2
δ	9a	2.86 ddd(14.5,13.0,2.0)	53.8, CH_2	C7,C8	H8,H9b,NH-2
	9b	3.05 dd(14.5,3.0)		C7,C8	H8,H9a,NH-2
NH-2		4.59 dd(13.0,3.0)		C8,C10	H9ab
OH-2		6.27 d(7.0)		C7,C8	H8
γClPip C=O	10		174.4, C		
α	11	5.81 dd(7.0,2.5)	51.0, CH	C10,C12,C13,C15	H12ab
β	12a	[b]2.00 m	35.7, CH_2	C10,C11,C13,C14	H11,H12b,H13
	12b	2.40 ddd(10.0,4.0,3.0)		C11,C13,C14	H11,H12a,H13
γ	13	3.92	51.3, CH	C11,C12,C14	H12ab,H14ab
δ	14a	2.78 td(13.5,10.5)	53.9, CH_2	C12,C13	H13,H14b,NH-3
	14b	3.30 ddd(10.5,4.0,3.0)		C12,C13	H13,H14a,NH-3
NH-3		5.20 dd(13.5,3.0)		C11,C13,C14,C15	H14ab
AMNA C=O	15		172.2, C		
α	16	5.28 ddd(6.0,6.0,4.0)	50.4, CH	C15,C17,C18,C25	H17ab,NH-3
β	17a	2.48 ddd(14.5,7.0,4.0)	36.2, CH_2	C15,C16,C18,C20	H16,H17b,H18
	17b	2.52 ddd(14.5,8.5,6.0)		C15,C16,C20	H16,H17a,H18
γ	18	5.37 ddd(15.5,8.5,7.0)	124.8, CH	C16,C17,C21	H17ab,H19
δ	19	[b]5.94 m	141.5, CH	C17,C20,C21,C22	H18,H20
ε	20	[b]5.92 m	134.3, CH	C17,C18,C19,C21,C22	H19,H21
Z	21	5.57 dd(14.5,6.5)	126.7, CH	C20,C22,C23,C24	H20,H22
H	22	[b]2.28 m	31.0, CH	C19,C21,C23,C24	H21,H23,H24
Θ	23	0.97 d(7.0)	22.2, CH_3	C19,C22,C24	H22
H-Me	24	0.97 d(7.0)	22.3, CH_3	C19,C22,C23	H22
NH-4		7.60 d(6.0)		C15,C16,C25,C26	H16
γOHPip2 C=O	25		169.5, C		
α	26	4.93 dd(7.0,2.0)	51.0, CH	C25,C27,C28	H27ab
β	27a	[b]2.01 m	28.5, CH_2	C25,C26,C28,C29	H26,H27b,H28
	27b	2.16 ddd(15.0,4.5,2.5)		C25,C26,C28,C29	H26,H27a,H28
γ	28	3.75 bs	58.6, CH	C26,C27,C29	H27ab,H29ab,OH-3
δ	29a	2.81 ddd(14.5,13.0,2.0)	53.5, CH_2	C28	H28,H29b,NH-5
	29b	2.99 dd(14.5,2.5)		C27,C28	H28,H29a,NH-5
NH-5		4.37 dd(13.0,2.5)		C26,C28,C29,C30	H29ab
OH-3		6.47 d(7.0)		C27,C28	H28
HAAC C=O	30		169.1, C		
	31a	4.40 d(15.5)	63.0, CH_2	C1,C30	H31b
	31b	5.49 d(15.5)		C1,C30	H31a

All multiplicity obtained by interpretation of *J*-resolved NMR spectral data unless otherwise noted.
[a] Multiplicity determined from ^1H NMR in $CDCl_3$ (500 MHz) 25 ºC
[b] Unresolved in homonuclear 2D*J* analyses

Table II.2. NMR Spectral Data for 31 Recorded in $CDCl_3$ (500 MHz) 25 ºC

Unit	Position	δ_H mult (*J*,Hz)	δ_C, DEPT	HMBC	COSY
αMeSer C=O	1		173.6, C		
α	2		62.6, C		
β	3a	3.99 m	64.6, CH_2	C1,C2	H3a
	3b	4.10 m		C1,C2,C4	H3b
αMe	4	1.60 s	18.7, CH_3	C1,C2,C3	
NH-1		7.16 s		C1,C2,C4,C5	
OH-1		3.22 bd(9.0)			
Pip C=O	5		170.0, C		
α	6	4.98 bd(5.5)	50.9, CH	C5,C7,C8,C10	H7ab
β	7a	1.68 m	22.8, CH_2	C5,C6,C8,C9	H6,H7b,H8
	7b	2.18 m		C6,C9	H6,H7a,H8
γ	8a	1.50 bd(14.0)	20.6, CH_2	C7,C9	H7ab,H9ab
	8b	1.50 bd(14.0)		C7,C9	H7ab,H9ab
δ	9a	2.76 m	47.3, CH_2	C8	H8,H9b,NH-2
	9b	3.12 bd(13.0)		C7,C8	H8,H9a,NH-2
NH-2		4.11 m		C8	H9ab
γClPip C=O	10		174.2, C		
α	11	5.89 m	50.3, CH	C10,C12,C13,C15	H12ab
β	12a	2.00 m	36.0, CH_2	C10,C11,C13,C14	H11,H12b,H13
	12b	2.39 bd(13.5)		C11,C13,C14	H11,H12a,H13
γ	13	4.02 m	51.4, CH	C14	H12ab,H14ab
δ	14a	2.78 td(13.5,10.5)	54.1, CH_2	C12,C13	H13,H14b,NH-3
	14b	3.32 bd(14.0)		C12,C13	H13,H14a,NH-3
NH-3		5.29 bd(12.5)		C13,C14,C15	H14ab
AMNA C=O	15		171.8, C		
α	16	5.25 m	50.6, CH	C15,C17,C18,C25	H17ab,NH-3
β	17a	2.48 m	36.1, CH_2	C15,C16,C18,C20	H16,H17b,H18
	17b	2.53 m		C15,C16,C18,C20	H16,H17a,H18
γ	18	5.37 dt(15.0,7.5)	124.7, CH	C16,C17,C19	H17ab,H19
δ	19	5.92 m	134.1, CH	C17,C18,C20,C21,C22	H18,H20
ε	20	5.90 m	126.7, CH	C18,C19,C22	H19,H21
ζ	21	5.56 dd(14.5,6.5)	141.3, CH	C20,C22,C23,C24	H20,H22
η	22	2.29 dqq(8.0,7.0,7.0)	31.0, CH	C19,C21,C23,C24	H21,H23,H24
θ	23	0.97 d(7.0)	22.3, CH_3	C21,C22,C24	H22
η-Me	24	0.97 d(7.0)	22.3, CH_3	C21,C22,C23	H22
NH-4		7.60 d(6.5)		C15,C25	H16
γOHPip C=O	25		169.4, C		
α	26	4.95 bd(7.5)	51.0, CH	C25,C27,C28,C30	H27ab
β	27a	2.01 m	28.5, CH_2	C26	H26,H27b,H28
	27b	2.14 m		C28,C29	H26,H27a,H28
γ	28	3.75 bs	58.6, CH	C26,C29	H27ab,H29ab,OH-2
δ	29a	2.80 m	53.6, CH_2	C28	H28,H29b,NH-5
	29b	2.98 d(13.0)		C27,C28	H28,H29a,NH-5
NH-5		4.35 d(13.0)		C28,C29	H29ab
OH-2		6.49 d(7.5)		C27,C28	H28
HAAC C=O	30		169.1, C		
	31a	4.40 d(16.0)	63.0, CH_2	C1,C30	H31b
	31b	5.44 d(16.0)		C1,C30	H31a

All ^1H multiplicities and $^3J_{HCCH}$ values determined from 1H NMR in $CDCl_3$ (500MHz) 25ºC

Table II.3. NMR Spectral Data for 32 Recorded in $CDCl_3$ (500 MHz) 25 ºC

Unit	Position	δ_H mult (*J*,Hz)	δ_C, DEPT	HMBC	COSY
αMeSer C=O	1		173.6, C		
α	2		63.0, C		
β	3a	4.04 d(11.5)	64.2, CH_2	C1	H3b
	3b	4.15 d(11.5)		C1,C2	H3a
αMe	4	1.58 m	18.3, CH_3	C1,C2,C3	
NH-1		7.57		C1,C5	
OH-1		3.24			
γOHPip1 C=O	5		172.3, C		
α	6	5.15 bd(6.5)	51.2, CH	C5,C7,C8	H7ab
β	7a	2.03 m	28.5, CH_2	C6	H6,H7b
	7b	2.30 bd(8.5)			H7a,H9b
γ	8	3.75 bs	58.8, CH		H7a,H9b,OH
δ	9a	2.85 m	53.8, CH_2	C8	H9b,NH-2
	9b	3.05 bd(13.5)			H7b,H9a,NH-2
NH-2		4.58 bd(12.5)			H9ab
OH-2		6.27			H8
γClPip C=O	10		174.3, C		
α	11	5.81 bd(6.5)	51.0, CH	C10,C12,C13	H12a
β	12a	2.05 m	35.7, CH_2	C10,C13	H11, H12b,H13
	12b	2.42 bd(10.5)		C15	H12a,H13
γ	13	3.91 m	51.3, CH		H12ab,H14ab
δ	14a	2.78 m	54.0, CH_2		H13,NH-3
	14b	3.31 bd(13.5)			H13
NH-3		5.19 bd(13.5)		C5	H14a
AMDA C=O	15		172.2, C		
α	16	5.28 m	50.4, CH	C15,C17,C18,C26	H17ab,NH-4
β	17a	2.48 m	36.2, CH_2	C15,C16,C18,C20	H16,H18
	17b	2.53 m		C15,C16,C18,C20	H16,H18
γ	18	5.38 m	124.6, CH	C21	H17ab,H19,H21
δ	19	5.94 m	140.3, CH		H18,H20
ε	20	5.90 m	134.3, CH		H19,H21
ζ	21	5.50 m	127.9, CH	C20,C22,C24	H18,H19,H20,H22
η	22	2.02 m	38.2, CH	C19,C21,C23,C24,C32	H21,H24
θ	23a	1.30 m	29.6, CH_2	C19,C22,C24,C32	H22,H24,H32
	23b	1.30 m		C19,C22,C24,C32	H22,H24,H32
θ-Me	32	0.83 t(7.5)	11.8, CH_3	C22,C23	H23ab,H24
η-Me	24	0.96 d(7.0)	19.8, CH_3	C19,C22,C23	H22,H23ab,H32
NH-4		7.60		C15,C25	H16
γOHPip2 C=O	25		169.5, C		
α	26	4.93 bd(7.5)	50.9, CH	C25,C27,C28	H27a
β	27a	2.03 m	28.5, CH_2	C26	H26,H27b
	27b	2.17 bd(15.0)			H27a,H29b
γ	28	3.75 bs	58.6, CH		H27ab,OH-3
δ	29a	2.81 m	53.5, CH_2	C28	NH-5
	29b	2.99 bd(13.5)			NH-5
NH-5		4.36 bd(12.5)		C30	H29ab
OH-3		6.47			
HAAC C=O	30		169.1, C		
	31a	4.40 d(15.5)	63.0, CH_2	C1,C30	H31b
	31b	5.48 d(15.5)		C1,C30	H31a

All ^1H multiplicities and $^3J_{HCCH}$ values determined from 1H NMR in $CDCl_3$ (500MHz) 25ºC

the γOHPip2 alpha proton (H-26) and secondary amine (NH-5) protons to the HAA carbonyl carbon (C-30) were then used to establish the connectivity of the γOHPip2 and HAA residues. Using this approach, all partial structures in **30** could be accounted for. Observation of an HMBC NMR correlation from the oxygenated methylene at position H_2-31 to the αMeSer ester carbonyl carbon (C-1) suggested the cyclic lactone nature of **30**, thus accounting for the single remaining degree of unsaturation inherent in the molecular formula.

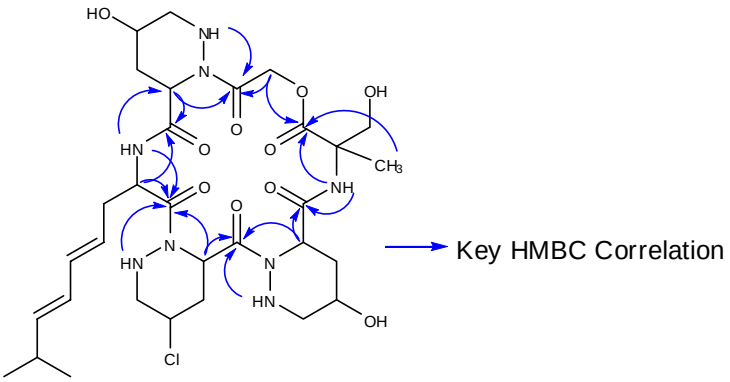

Figure II.3. Key HMBC Correlations Used to Establish the Amino Acid Sequence of Piperazimycin A (30)

Support for the initially hypothesized depsipeptide structure was also obtained by a characteristic IR absorption (1737cm^{-1}) indicative of an ester functionality. The ester linkage in **30** was then confirmed by sodium methoxide methanolysis to yield the methyl ester (**33**), (LRESIMS $[M+Na]^+$ *m/z* 781.4). Subsequent analysis of 1D and

2D NMR spectra showed the presence of a new methoxyl substituent [δ_H 3.75 (s); δ_C 53.6] in the ^{1}H NMR spectrum of **33**. HMBC NMR correlations from the methoxyl group protons to the αMeSer carbonyl carbon (C-1) indicated the presence of a methyl ester, as would be expected following methanolysis of the ester linkage in **30**. Further support was obtained by the observation of an additional hydroxyl group (OH-4) in the ^{1}H NMR spectra of **33.** COSY NMR correlations observed from H_2-31 to OH-4 indicated that the alcohol was attached to C-31, hence confirming that this is the site of lactonization in **30.**

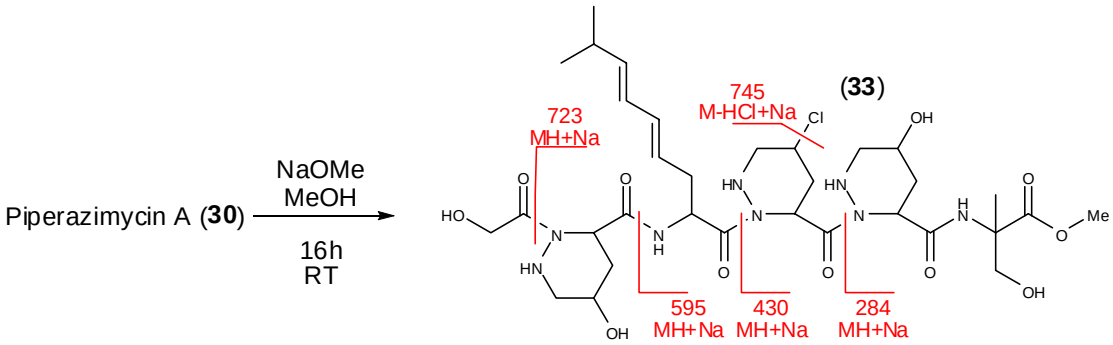

Figure II.4. MS/MS Fragmentation Pattern of the Methanolysis Product of 30 (33)

The amino acid sequence of **30**, assigned on the basis of HMBC correlations (Figure II.3), was fully supported by the ESI-MS/MS fragmentation pattern of **33** (Figure II.4). Key fragmentations include *m/z* 745 which indicated cleavage of chlorine from γClPip and fragment ions at *m/z* 723, 595, 430 and 284, which resulted

from successive cleavage of amide bonds between HAA/γOHPip2, γOHPip2/AMNA, AMNA/γClPip, and γClPip/γOHPip1, respectively.

Piperazimycin B (**31**) was isolated as a white powder that analyzed for the molecular formula $C_{31}H_{47}N_8O_9{}^{35}Cl$ by HRFABMS ($[M+H]^+$ *m/z* 711.3231) and comprehensive analysis of NMR data. The ^1H and ^{13}C NMR spectra of **31** (Table II.2) were highly analogous to those of **30** and consistent with a cyclic hexadepsipeptide, however, major differences were observed in the γOHPip1 region. The most notable difference appeared at the γ-position of the residue where the oxygenated methine of **30** (H-8) had been replaced by a methylene group (H_2-8) thus forming an unsubstituted piperazic acid (Pip) unit in **31**. NMR analyses utilizing a combination of ^{13}C NMR, ^1H NMR, DEPT, HSQC, COSY and HMBC experiments, coupled with examination of the molecular formula, allowed **31** to be assigned as the γOHPip1 desoxy congener of **30**.

Piperazimycin C (**32**) was isolated as a white powder that analyzed for the molecular formula $C_{32}H_{49}N_8O_{10}{}^{35}Cl$ by HRFABMS $[M+H]^+$ *m/z* 741.3337) and comprehensive analysis of NMR data. The ^1H and ^{13}C NMR spectra of **32** (Table II.3) were highly analogous to those of **30** and consistent with a cyclic hexadepsipeptide, however, major differences were observed in the AMNA region. The most notable difference appeared at the θ-position of the AMNA residue where the methyl group in **30** (H_3-23) had been replaced by an ethyl group in **32**, thus forming 2-amino-8-methyl-4,6 decadienoic acid (AMDA), a novel amino acid residue. Analyses utilizing a combination of ^{13}C, ^1H, DEPT, HSQC, COSY and HMBC NMR experiments,

coupled with examination of the molecular formula, allowed **32** to be assigned as the AMDA congener of **30**.

II.3. Relative Stereochemical Determination of Piperazimycin A (30)

Following assignment of planar structures for **30**-**32** efforts were focused on the determination of the relative stereochemistry of **30**. The conjugated diene of the AMNA residue was determined to be 18*E,* 20*E* by ^{1}H NMR selective decoupling experiments and interpretation of *J* values. Decoupling the ^{1}H NMR signal at H_2-17 converted the ^{1}H NMR signal at H-18 from a doublet of doublets of doublets (*J* = 15.5, 8.5, 7.0 Hz) to a broad doublet (*J* = 15.5 Hz) indicating the *E* configuration of the C-18, C-19 olefin. Likewise, decoupling the H-22 multiplet converted the ^{1}H NMR signal for H-21 from a doublet of doublets (*J* = 14.5, 6.5 Hz) to a doublet (*J* = 14.5 Hz), indicating that the C-20, C-21 olefin was also *E*.

The relative stereochemistry and chair conformation of the γOHPip1, γOHPip2 and γClPip1 rings were established through 1D NOESY NMR experiments (Figure II.5). Specific 1D NOESY NMR correlations observed between the γOHPip1 α-methine proton (H-6) and both protons at position H_2-7 indicated H-6 was equatorial. An additional NOESY correlation observed from H-7a to H-9a indicated a 1, 3-diaxial interaction suggesting a chair conformation for the γOHPip1 ring. NOESY correlations from H-8 to H-7ab and H-9ab illustrated that H-8 was equatorial and the C-8 hydroxyl group axial. The secondary amine proton (NH-2) exhibited a NOESY correlation to only H-9b indicating the proton at position NH-2 was also axial. The

γOHPip2 residue was assigned the same conformation as γOHPip1 after identical NOESY NMR correlations were observed between the respective γOHPip2 protons. The γClPip residue was also assigned the same overall conformation as the γOHPip1 and γOHPip2 residues however an important exception in the configuration at the γ position was noted after NOESY NMR correlations were observed from H-13 to only H-12b and NH-3 indicating that H-13 was in an axial position and the C-13 chlorine in an equatorial position.

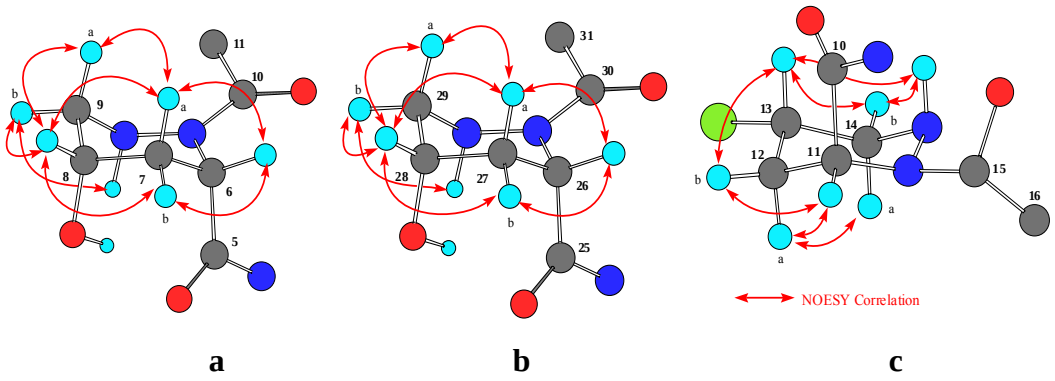

a **b** **c**

Figure II.5. Key NOESY Correlations Used to Establish the Relative Stereochemistries of the γOHPip1 (a), γOHPip2 (b) and γClPip (c) Residues of Piperazimycin A (30)

II.4. Absolute Stereochemical Determination of Piperazimycin A (30)

The absolute stereochemistry of **30** was determined by a combination of spectral and chemical methods. Initially the Marfey method,[94, 95] a commonly used method to determine the stereochemistry of standard amino acids in peptides was employed.

Following detailed analyses, only partial success was achieved with the absolute configurations of the αMeSer and AMNA residues being described (see: section II.4.1). However, none of the substituted piperazic acid residue stereochemistry could be determined by this method. Subsequent analyses employed the Mosher method, a method commonly used to determine the absolute configuration of secondary alcohols (see: section II.4.2). However, these attempts were also unsuccessful in ascertaining the configurations of either of the two secondary alcohol containing piperazic acid residues. After multiple attempts at crystallization, a suitable crystal was obtained (see: section II.4.3) and X-ray data was collected. The X-ray structure allowed for the relative stereochemistry of the entire molecule to be ascertained but due to poor crystal quality, the absolute configuration of **30** could not be determined from the X-ray data alone. However, when the X-ray data was analyzed in conjunction with the stereochemical information obtained by the Marfey analysis, the absolute configurations of all of the stereocenters in **30** to could be determined.

II.4.1. Determination of the Absolute Configurations of the αMeSer and AMNA Residues in 30 by Application of the Marfey Method

The Marfey method utilizes chemical derivatization and HPLC to discern between amino acid enantiomers thus allowing for the absolute configurations of the alpha centers of the amino acids to be determined. In the course of the Marfey analysis, amino acids of unknown configuration are typically liberated from their parent peptide via acid hydrolysis. The amino acids are subsequently derivatized with specific chiral

derivatizing reagents (CDRs), of known configurations thus forming diastereomers that can be separated by HPLC. The most commonly used CDR is 1-fluoro-2,4-dinitrophenyl-5-L or D-alaninamide (FDAA) which has the advantage of possessing both a readily identifiable chromophore and an easily derivatizable functional group (Figure II.6). With the configuration of the alpha center of the CDR known, the configuration of the amino acid alpha carbon can be determined by comparison of retention time on reversed phase HPLC to standards of known configuration (Marfey method), or in the case of non-standard amino acids, by analysis of the relative hydrophobicity of the diastereomer (advanced Marfey method). The mechanism for chromatographic separation of the resulting diastereomers has been proposed to arise due to intramolecular hydrogen bonding between the two nitro groups in the benzene ring and the amino groups of the amino acid in question and the L or D-alaninamide (Figure II.6). This hydrogen bonding essentially forms a planar three ring system analogous to anthracene with the functional groups of the amino acid and the alaninamide moiety oriented perpendicular to the plane of the three ring system. The resolution betwen L and D amino acid derivatives is proposed to be due to differences in hydrophobicity derived from the cis or trans-type arrangement of the hydrophobic substituents at both alpha carbons of the amino acid and the alanamide (Figure II.6). The FDAA derivatives of the cis-type arrangement, as would be the case for a *S*-amino acid derivatized with *D*-FDAA, interact more strongly with reversed phase C_{18} resin and thus have longer retention times than those of the trans-type arrangement (*S*-amino acid derivatized with *L*-FDAA, (Figure II.6).

In the case of **30** the αMeSer residue was determined as *S* by acid hydrolysis and application of Marfey's method using standards of known configuration (Table II.4). As previously noted, the absolute configurations of the γOHPip1, γOHPip2 and γClPip residues could not be determined from any hydrolysate by the Marfey method even after multiple variations to both the hydrolysis and derivatization conditions. This same result has been reported in subsequent publications by other researchers.[96] Previous studies have shown that reductive cleavage of piperazic acid to ornithine was possible via catalytic hydrogenation and that the absolute configuration of ornithine could be determined by Marfey's analysis.[97,98] Consequently, reductive cleavage of the various γOHPip and γClPip N-N bonds by catalytic hydrogenation was attempted. Despite significant effort utilizing both $Pt(IV)O_2$ and Pd/C as catalysts no reduced γOHPip or γClPip residues could be identified following derivatization with Marfey reagent. In a separate experiment, acid hydrolysis of **30**, followed by $Pt(IV)O_2$ catalyzed hydrogenation, derivatization with FDAA and application of the advanced Marfey method led to the assignment of the absolute stereochemistry at C-16 of the reduced AMNA residue as *S* (Table II.4).[99,100] It should be noted that in studies subsequent to this report, other research groups have successfully reduced piperazic acids to ornithine using more rigorous reductive conditions.[101] However, these studies were conducted using piperazic acids as substrates and the applicability of those methods to γ-substituted piperazic acids was not demonstrated.

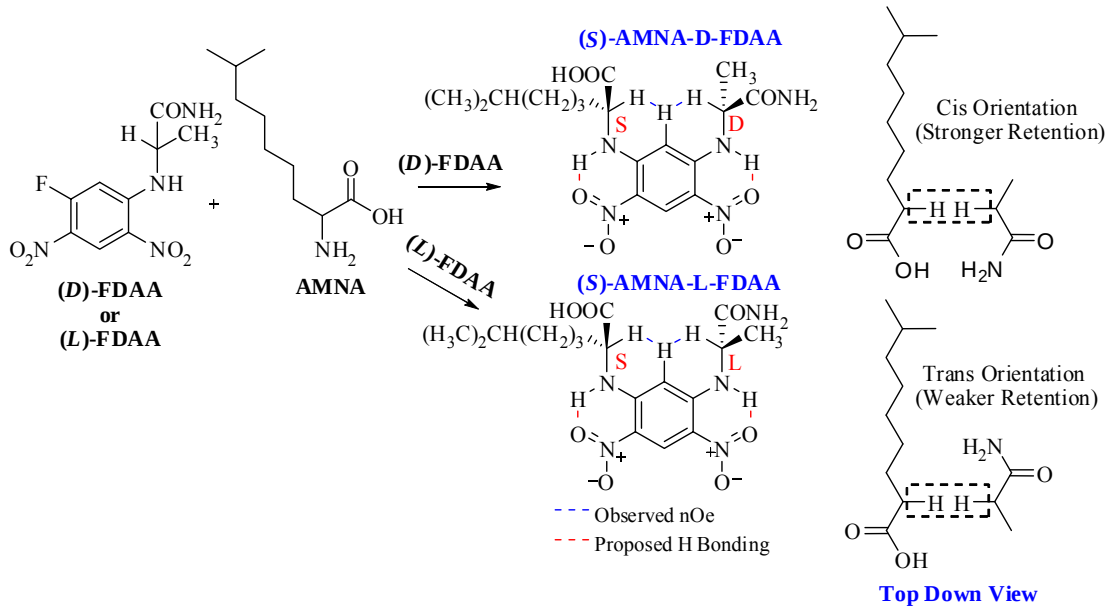

Figure II.6. Advanced Marfey Method for the Determination of the Absolute Configuration of the Reduced AMNA Residue in 30

Table II.4. Retention Times for the Amino Acids from 30 as their FDAA Derivatives

Residue	Mass FDAA Derivative	(t_R, min)	(t_R, min)
	ESI-LRMS $[M+H]^+$ *m/z*	L-FDAA	D-FDAA
[a](*R*)-αMeSer	372.3	28.7	23.8
[b]αMeSer	372.3	23.6	NA
[b,c]AMNA	440.2	59.3	63.8

[a]Standard of known configuration, [b]from acid hydrolysate of **30**, [c] from hydrogenate of **30**

II.4.2. Determination of the Absolute Configurations of the γOHPip Residues in 30 by Application of the Mosher NMR Method

Determination of the absolute stereochemistry of the γOHPip units was then attempted by derivatizing **30** with (*R*) and (*S*)-MTPACl and applying the modified Mosher method.[102] For a detailed explanation of the Mosher method and its use in the determination of the absolute configuration of secondary, alcohol bearing carbons, the reader is referred to section III.4. Subsequent interpretation of $\Delta\delta_{S-R}$ values for the tri-MTPA derivative yielded inconclusive results (data not shown) and no clear assignment of absolute configuration could be made by this method.[103]

II.4.3. X-ray Crystallographic Analyses and the Complete Relative Stereochemistry of Piperazimycin A (30)

X-ray crystallography is a technique in crystallography in which the pattern produced by the diffraction of X-rays through the closely spaced lattice of atoms in a crystal is recorded and then analyzed to reveal the nature of that lattice. X-ray diffraction is by far the most powerful technique for the structure determination of crystalline materials, from the smallest molecules that can be crystallized to the largest proteins.[104] In this method, X-rays of suitable wavelength are allowed to impinge on a single crystal, 0.1-1mm in length, of the material to be investigated.[105] The X-rays are scattered by the atoms (by the electrons rather than by the nuclei) and are re-radiated with the same frequency either interfering with each other constructively or

destructively (overlapping waves either add together to produce stronger peaks or subtract from each other to some degree). The interference of the scattered radiation is recorded as a diffraction pattern that can then be used for structure determination.[106] This technique is widely used in chemistry and biochemistry to determine the structures of an immense variety of molecules, including inorganic compounds, DNA, and proteins. Because a comprehensive examination of the theory and methods used in X-ray based structure determination is well beyond the scope of this discussion the interested reader is referred to the following specialized text for a thorough treatment of the subject.[107]

Because of the aforementioned difficulties in determining the absolute stereochemistry of the γOHPip and γClPip residues (see: sections II.4.1, II.4.2) of **30** by chemical methods, efforts were focused toward crystallization and a small crystal was ultimately obtained from methanol. The crystal structure of piperazimycin A (Figure II.7) confirmed the connectivity and relative stereochemistry assigned by NMR methods. However, due to the poor quality of the crystal, the absolute configuration, potentially determined by anomalous scattering from the chlorine atom, was not feasible. However, given that the absolute configuration of C-2 (*S*) and C-16 (*S*) had been determined by the Marfey method (Table II.4), the overall absolute configuration of **30** could be assigned as 2*S*, 6*S*, 8*S*, 11*R*, 13*S*, 16*S*, 26*R*, 28*R*.

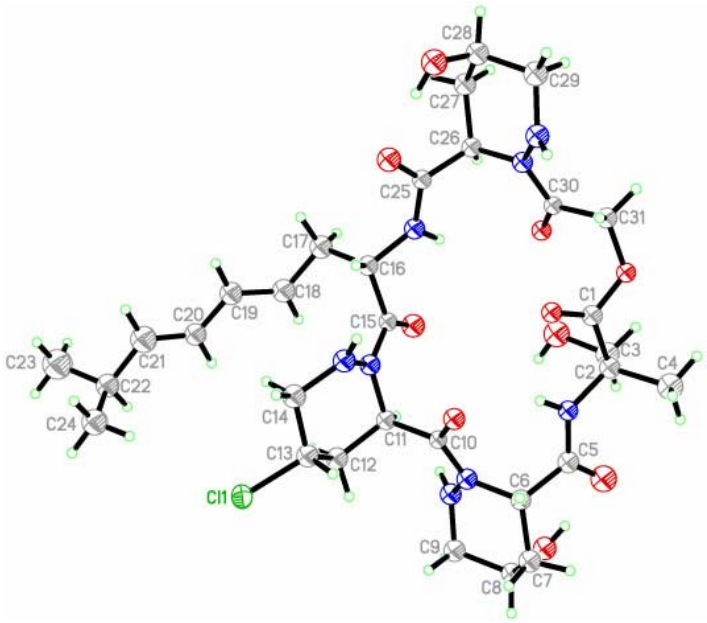

Figure II.7. Computer Generated Plot of the Final X-ray Structure of 30 Depicting Relative Stereochemistry Only

It should be noted that the γOHPip residue has been found in the chair conformation[108,109] with the alcohol in the axial position for each case where the stereochemistry has been reported.[97,108,109,110] Further, MTPA derivatives of axial alcohols have been shown to be susceptible to steric compression thus causing significant deviations from the assumed conformation.[111] Deviations caused by steric compression lead to irregular anisotropic shielding effects, which are reflected in $\Delta\delta_{S\text{-}R}$ values with little or no definitive pattern, exactly as we observed in this study. Therefore, it is concluded that the Mosher method would be ineffective in determining the absolute configuration of the γ-position in the γOHPip residue. It is also interesting to note that the absolute configurations of the γOHPip1 and the γOHPip2

residues of **30** were (*S*, *S*) and (*R*, *R*) respectively. While both the (*R*, *R*) and (*S*, *S*) γOHPip residues have been found independently in himastatin[93] and monamycin[112] respectively, to the best of our knowledge, this report represents the first time in which the (*R*, *R*) and (*S*, *S*) enantiomers have been found in the same molecule.

Assignment of the absolute configurations of **31** and **32** was approached by comparison of their respective CD spectra (Figure II.8) to that of **30**. The planar structures of **30** and **31**, which differ only in the presence of an alcohol at position C-8 in **23**, exhibited nearly identical CD behavior [Cotton effects: **30**: λ 235 (Δε –5.7), **31:** λ 240 (Δε –7.0)]. Piperazimycins A and C, **30** and **32**, which differ only in substitution at C-23, also exhibit very similar CD spectra [Cotton effects: **30**: λ 235 (Δε –5.7), **25:** λ 236 (Δε –4.5)]. Interpretation of the CD data suggests, but does not rigorously confirm that the configurations of all the identical centers in **30**-**32** are the same. The absolute configuration of the center at C-22 in **32** could not be suggested from these experiments.

II.5. Anticancer Drug Screening at the National Cancer Institute

Systematic drug screening began at the National Cancer Institute (NCI) in 1955 with the formation of the Cancer Chemotherapy National Service Center (NSC) screening program.[113] From the inception of the NSC program to the 1980s most of the screening was performed *in vivo* using a murine tumor cell line (P388) or leukemia

cell line (L1210).[114] These two hematologic tumor cell lines were chosen mainly due to the fact that they were inexpensive, stable, reproducible and easily handled. However, by using rapidly growing leukemia cells these *in vivo* experiments were biased toward compounds with activity against rapidly growing tumors. Therefore, the agents identified in these screens were relatively unsuccessful in treating human solid tumors and this limitation of the screening methodology translated to a relatively low success rate.

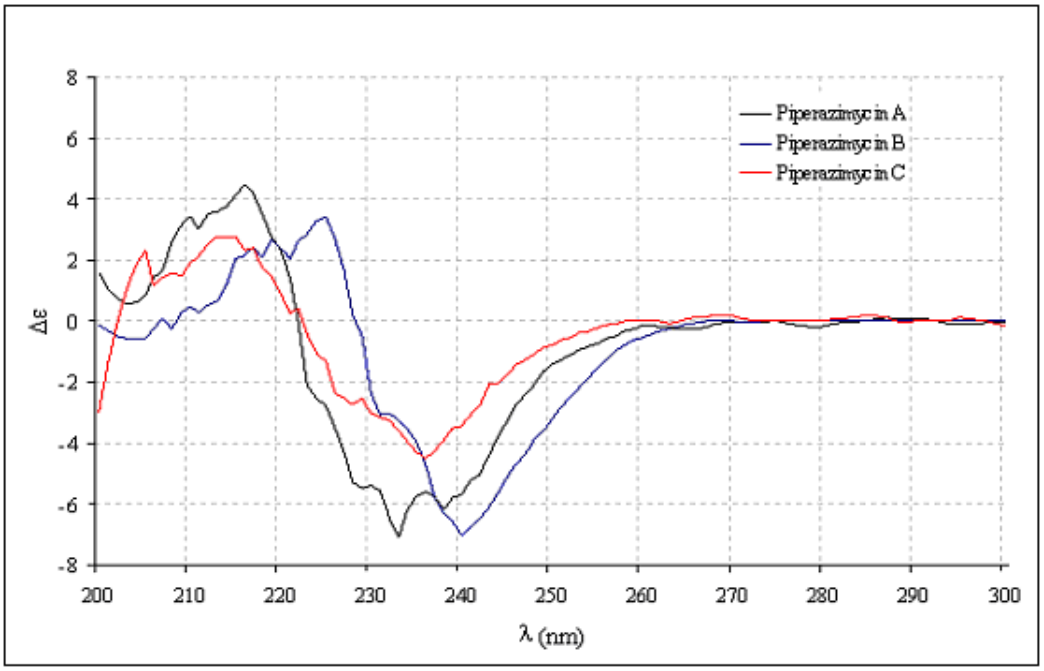

Figure II.8. CD Spectra for Piperazimycins A-C (30-32)

Because of these limitations, in 1989 the NCI changed to a rationally designed "disease-oriented" screening panel that incorporated 60 oncologically diverse cell lines derived from a variety of different human solid tumors.[115]

In addition, due to the fact that greater than 85% of the compounds submitted for screening to the NCI 60 cell-line panel are found to have no anticancer activity, the NCI adopted a three cell-line prescreen in 1999.[116] All compounds submitted to the NCI are now prescreened *in vitro* against a panel of three highly sensitive human tumor cell lines including breast (MCF-7), lung (NCI-H460) and glioma (SF-268) cells. Samples exhibiting anticancer activity in the 3 cell-line prescreen are then submitted to the NCI 60 cell-line panel which is composed of lines derived from nine different human histologic tumor types including brain, colon, leukemia, lung, melanoma, ovarian, renal, prostate and breast cancers. An automated sulforhodamine blue cytotoxicity assay is used to assess the relative potency of a compound against all 60 cell lines using five different drug concentrations incubated for a standard 48 hours.[116] Endpoint parameters calculated for each individual cell line include: GI_{50} (Growth Inhibition, 50%), which is defined as the drug concentration that inhibits tumor cell growth by 50%; TGI (Total Growth Inhibition) which is the lowest drug concentration that totally inhibits cell growth; and the LC_{50}, which is the lowest concentration that kills 50% of the cells.

The data points mentioned above are then analyzed by the COMPARE algorithm, which is a program that categorizes and compares different groups of agents based on their patterns of cytotoxic activity in the 60 cell-line panel (Figure II.13). This program can identify similar classes of anticancer molecules (e.g. microtubule agents) based solely on their cytotoxicity patterns.[117] This style of analysis enables NCI researchers to generate hypotheses about potential mechanisms of action of new

anticancer agents based on their similarity (or dissimilarity) to known anticancer drugs. Thus new agents with novel mechanisms of action may be identified by the screen if they exhibit a previously unseen pattern of antitumor activity.[116] In this manner the COMPARE program becomes a very valuable tool that converts the somewhat simple test of growth inhibition into an extremely valuable tool to study the pharmacology of a previously unknown agent.

Molecules that exhibit favorable profiles within the COMPARE program, biologically active molecules with extremely novel chemical structures or those that are extremely potent cytotoxins, are advanced to *in vivo* animal models following *in vitro* examination in the 60 cell-line panel. The initial animal studies are conducted using small hollow fibers (1mm diameter, 2cm long, MW exclusion of 500,000 Da) made of polyvinylidene fluoride that contain cells from twelve different human tumor cell lines including those from lung, breast, colon, melanoma, ovarian and central nervous system tumors.[118] Once formulated, the tumor cell containing hollow fibers are inserted underneath the skin and in the body cavity of a test mouse. Each mouse receives three intraperitoneal and three subcutaneous implants. The mice are then treated with experimental agents (via intraperitoneal injection) starting on day 3 or 4 of implantation and continuing daily for four days. The fibers are collected from the mice following the fourth treatment and subjected to the stable endpoint MTT assay that operates in a fashion very similar to the MTS assay described in section II.1. The percent net growth for each cell line in each treatment group is then assessed and compared to the percent net growth of control samples (implanted and receiving

treatment with drug diluent alone). A 50% or greater reduction in percent net growth of the treated samples compared to the control is considered a positive result. Test compounds that yield positive results or those that produce cell kill of any kind in the hollow fiber assay are then evaluated are considered for possible human xenograft testing.

Xenotransplantation is the transplantation of living cells, tissues or organs from one species to another with such cells, tissues or organs being termed xenografts. At the NCI, human tumor cell xenografts are implanted subcutaneously in mice and the drugs are administered intraperitoneally. A relative difference in the tumor weight ratio of treated to control animals of less than 0.5 is considered promising for further development.[116]

II.6. Anticancer Drug Development at the National Cancer Institute

For molecules exhibiting promising results in the early testing, two separate programs exist at the NCI to enable further development. The first is the Rapid Access to Intervention Development (RAID) program.[119] The RAID program is designed to assist academic investigators with the early steps required to initiate clinical trials allowing new agents to be developed under the umbrella of the NCI as an Investigational New Drug (IND) the license to which is held by the academic investigator or investigator's designee.[116] The RAID program thus enables "not-for-profit" scientists to have access to the extensive range of NCI resources for early

development but does not sponsor clinical trials. The second NCI sponsored drug development program is the Drug Development Group (DDG).[120] This program differs from the RAID program in that the NCI is the IND holder and the main sponsor of clinical development of the agent. The main goal of the DDG program is the full-scale clinical evaluation of a novel therapeutic agent.

II.7. Biological Activities of Piperazimycins A-C (30-32) and National Cancer Institute Screening of 30 in the 60 Cell Line Panel

Biological activities for the piperazimycins A-C (**30-32**) were initially evaluated *in vitro* against the human colon carcinoma cell line HCT-116. All compounds exhibited significant cytotoxicity with an average GI_{50} = 76 ng/mL for each. Piperazimycin A (**30**) also showed potent biological activity when evaluated against the oncologically diverse 60 cancer cell line panel at the National Cancer Institute, with mean values for all cell lines of GI_{50} = 100 nM (TGI = 300 nM, LC_{50} = 2 μM. Overall, piperazimycin A exhibited a nearly 3-fold more potent activity against solid tumors (average LC_{50} = 13.9 μM) than against the leukemia cell lines tested (average LC_{50} = 31.4 μM). Within the solid tumors, **30** was most active against the melanoma (average LC_{50} = 0.3 μM), CNS (average LC_{50} = 0.4 μM) and prostate cell lines (average LC_{50} = 0.6 μM) cancers. Piperazimycin A was also active against the colon cancer group (average LC_{50} = 1.2 μM), renal cancers (average LC_{50} = 9.5 μM), ovarian cancers (average

LC_{50} = 10.3 μM), non-small cell lung cancers (average LC_{50} = 12.9 μM) and breast cancers (average LC_{50} = 55.8 μM). Although some selectivity was observed, the general cytotoxicity noted in the 60 cell line panel indicates a general mode of cell toxicity. Unfortunately this result precluded application of the COMPARE analysis and does not support further development of these agents for the treatment of cancer. Additional studies ongoing at the National Cancer Institute will provide furher information to completely evaluate the drug-like potential of the piperazimycins.

It should also be noted that piperazimycin A (**30**) was a potent inhibitor of ornithine decarboxylase (ODC) activity exhibiting an IC_{50} = 0.28μg/mL. Although this activity could be attributed to broad spectrum cytotoxicity of **30** as the ODC assay is run in a whole cell format, another explanation is also plausible. If one envisions a reduction of the piperazic acid N-N bond via cellular processes, the resulting structure would be that of a cyclic depsipeptide containing three substituted ornithine residues. The structural similarities between these substituted ornithine residues and the known ODC inhibitor eflornithine (**10**) provide grounds for the possibility that **30** could also be a true ODC inhibitor. Additional studies ongoing with academic collaborators will provide further information to thoroughly evaluate the chemopreventative activity of the piperazimycins as well.

II.8. Conclusions and Direction for Future Study

The piperazimycins are composed of exclusively unusual amino acids including αMeSer, AMNA, AMDA and various γ-substituted piperazic acids including γ-OHPip and γ-ClPip. Examination of the literature reveals a number of studies in which bioactive piperazic acid containing cyclic peptides have been isolated. Examples include antitumor antibiotics,[121,122,123] tuberculostatics,[124] anti-inflammatory agents[125] and anti-HIV agents.[126,127] Originally identified by Hassall and coworkers in the monamycin series of antibiotics[112], molecules containing piperazic acids have since been isolated from the culture broth of numerous *Streptomyces* spp.[92,93,109,126-129] and also from strains of the genus *Actinomadura*.[123,130]

While synthetic routes to γ-substituted piperazic acids have been developed,[131] to the best of our knowledge the biosynthetic mechanisms by which piperazic acids are formed are poorly understood. Original work by Arroyo using [2-^{14}C]piperazic acid suggested that the piperazic acids, as well as γOHPIP and γClPip moieties, were incorporated into monamycin as intact residues.[132] Further studies by Arroyo indicated that ornithine was not a precursor to piperazic acids, as no labeled ornithine could be incorporated into the piperazic acid ring. Subsequent studies by Umezawa[133] showed that L-[1,2-$^{13}C_2$]glutamine was incorporated into the carbonyl group and α-carbon and DL-[5-^{13}C]glutamic acid was incorporated into δ-carbon of piperazic acid residues (Figure II.9). Additional work by Parry, defining the biosynthesis of the *Streptomyces*-derived natural product valanimycin, has suggested that N-N bond

formation occurs via the reaction of a hydroxylamine with an amine to yield a hydrazine.[134] Parry and Tao also suggested that the hydroxlamine is likely formed by a PIP specialized flavoprotein monooxygenase, as NADH and FAD are required for its formation.[135] It is possible that piperazic acids could be formed from glutamine following reduction of the δ-carbonyl and conversion of either the α or γ-amine to the hydroxylamine. A subsequent intramolecular cyclization would result in formation of the piperazic acid ring (Figure II.10). In the case of glutamic acid, the same scheme could be envisioned following conversion of glutamic acid to glutamine via a glutamine synthetase. Addition of hydroxyl or chloro groups to the γ-position of the piperazic acid ring, as is the case in **30**, could occur at any stage after reduction of the δ-carbonyl and elimination of water to form the enamine. Substitution at the now nucleophilic γ-position most likely occurs via oxygenase and halogenase enzymes.

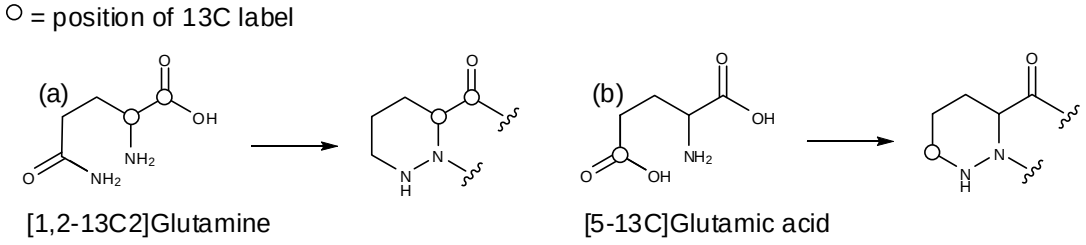

Figure II.9. Incorporation of Glutamine (a) and Glutamic acid (b) into Piperazic Acid Rings as Reported by Umezawa et al [133]

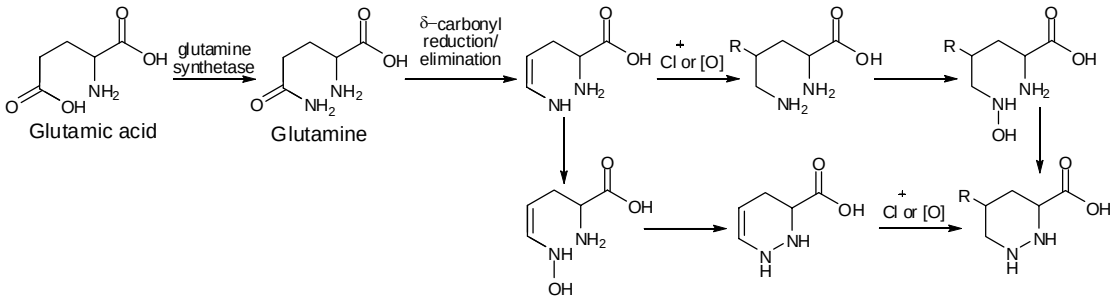

Figure II.10. Hypothetical Biosynthetic Pathways to γ-substituted Piperazic Acids

II.9. Acknowledgement

Chapter II, in full, was a reprint of material as it appears in The Journal of Organic Chemistry, 2007 *72*(2), 323-330, Miller, E.D.; Kauffman, C.A..; Jensen, P.R.; Fenical, W. The dissertation author was primary investigator and author of this paper.

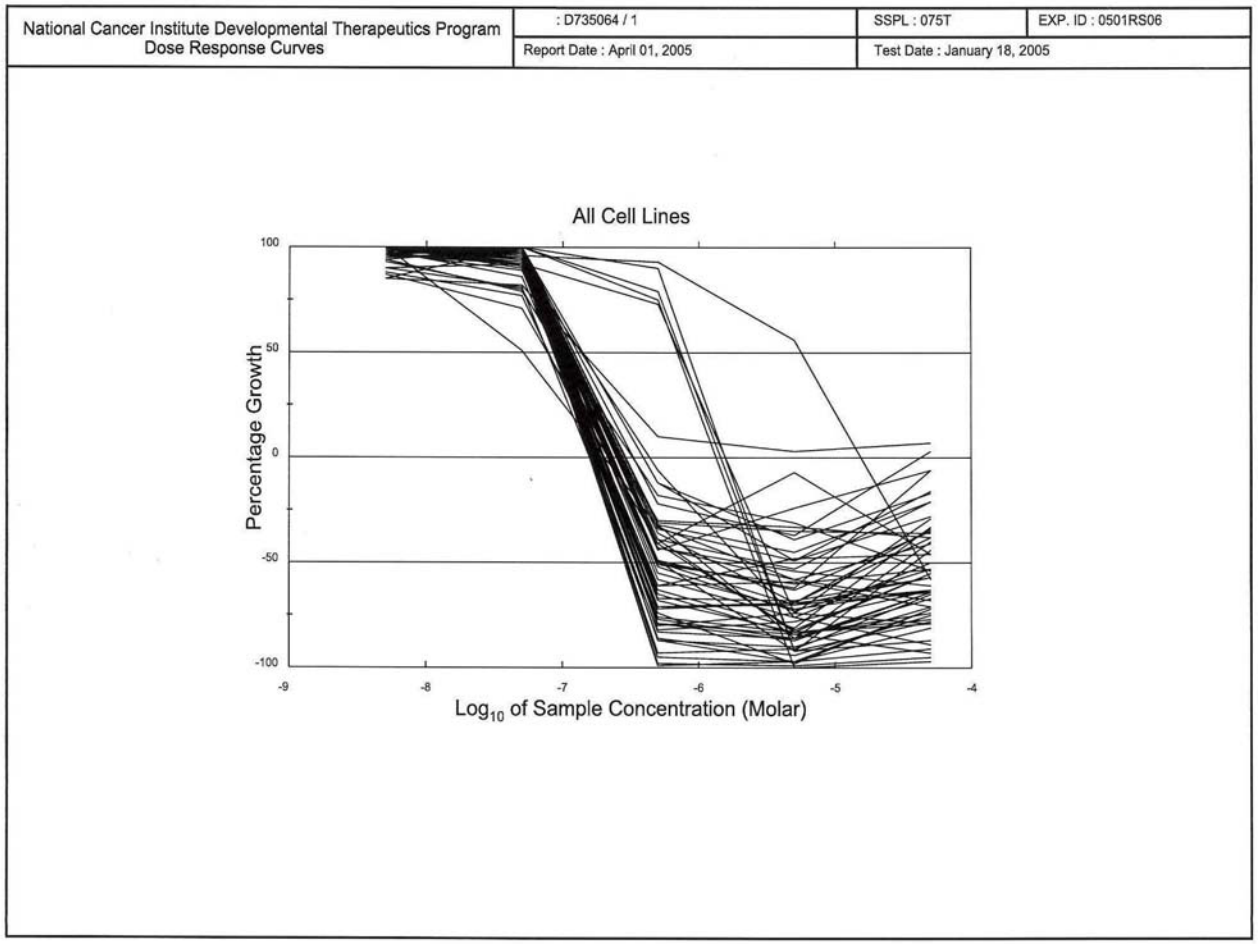

Figure II.11. Dose Response Curves For Piperazimycin A (30) All Cell Lines

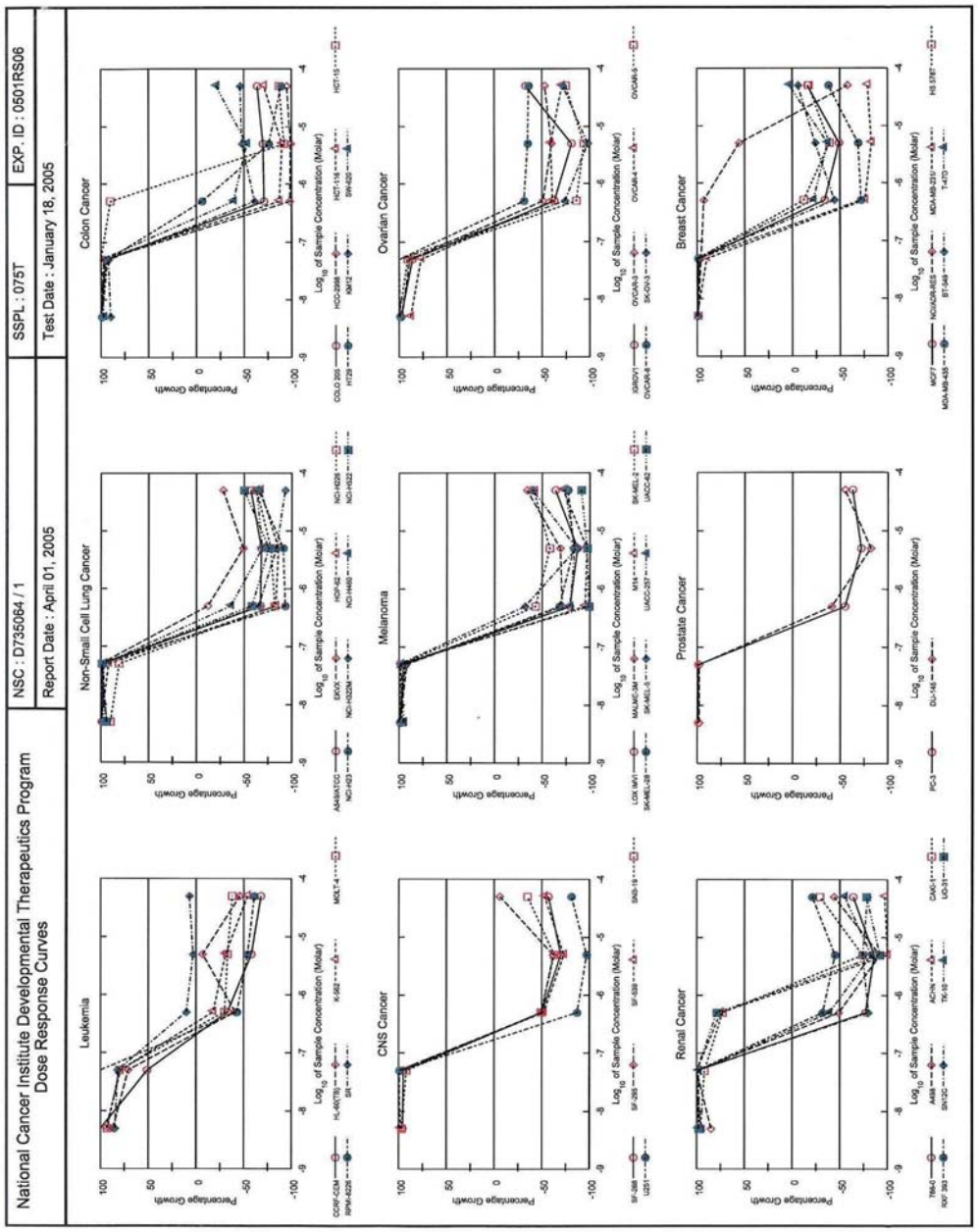

Figure II.12. Dose Response Curves for Piperazimycin A (30) by Cancer Type

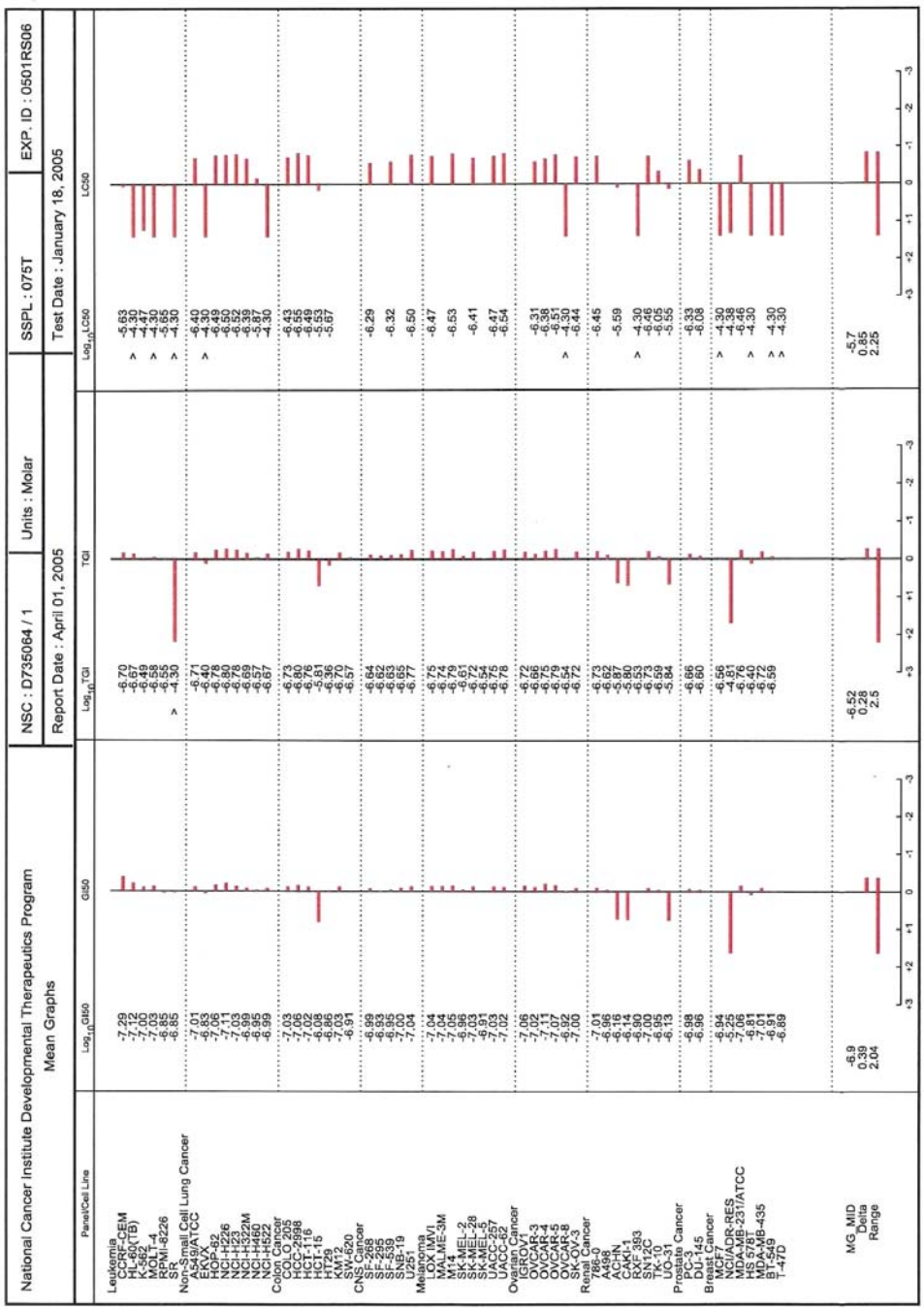

Figure II.13. Mean Graphs for Piperazimycin A (30)

References

(84) Satoh, T.; Isobe, H.; Ayukawa, K.; Sakai, H.; Nawata, H. *Life Sci*. **1996**, *59*, 1103-1108

(85) Shearman, M.S. *Neuropeptides* **1996**, *30*, 125-132

(86) Shearman, M.S.; Hawtin, S.R.; Tailor, V.J. *Neurochem*. **1995**, *65*, 218-227

(87) Marshall, N.J.; Goodwin, C.J.; Holt, S.J. *Growth Regul*. **1995**, *5*, 69-84

(88) Goodwin, C.J.; Holt, S.J.; Riley, P.A.; Downes, S.; Marshall, N.J. *Biochem*. *Biophys*. *Res*. *Commun*. **1996**, *226*, 935-941

(89) Liu, Y.; Schubert, D. *J*. *Neurochem*. **1997**, *69*, 2285-2293

(90) Prochaska, H.J.; Santamaria, A.B. *Anal*. *Biochem*. **1988**, *169*, 328-336

(91) Carpenter-Deyo, L.; Reed, D.J. *J*. *Pharmacol*. *Exp*. *Ther*. **1991**, *258*, 747-752

(92) Umezawa, K.; Ikeda, Y.; Uchihata, Y.; Naganawa, H.; Kondo, S. *J*. *Org*. *Chem*. **2000**, *65*, 459-463

(93) Leet, J.; Schroeder, D.; Golik, J.; Matson, J.; Doyle, T.; Lam, K.; Hill, S.; Lee, M.; Whitney, J.; Krishnan, B., *J. Antibiot*. **1996**, *49*, 299-311

(94) Marfey, P. *Carlsberg Res. Commun*. **1984**, *49*, 591-596

(95) Bhushan, R.; Brückner, H. *Amino Acids* **2004**, *27*, 231-247

(96) Huang, X.; Roemer, E.; Sattler, I.; Moellman, U.; Christner, A.; Grabley, S. *Angew. Chem. Int. Ed*. **2006**, *45*, 3067-3072

(97) Hassall, C.; Ogihara, Y.; Thomas, W. *J. Chem. Soc. C*. **1971**, 522-526

(98) Fujii, K.; Ikai, Y.; Mayumi, T.; Oka, H.; Suzuki, M.; Harada, K. *Anal. Chem.* **1997**, *69*, 3346-3352

(99) Harada, K.; Fuji, K.; Mayumi, T.; Hibino, Y.; Suzuki, M. *Tetrahedron Lett*. **1995**, *36*, 1515-1518

(100) Harada, K.; Fujii, K.; Hayashi, K.; Suzuki, M. *Tetrahedron Lett*. **1996**, *37*, 3001-3004

(101) Broberg, A.; Menkis, A.; Vasiliauskas, R. *J. Nat. Prod*. **2006**, *69*, 97-102

(102) Dale, J.; Dull, D.; Mosher, H. *J. Org. Chem*. **1969**, *34*, 2543-2549

(103) Seco, J.; Quiñoá, E.; Riguera, R. *Tetrahedron-Asymmetr*. **2000**, *11*, 2781-2791

(104) Glusker, J.P.; Trueblood, K.N. *Crystal Structure Analysis*. Oxford University Press, New York: **1985**

(105) Dunitz, J.D. *X-ray Analysis and the Structure of Organic Molecules*. Cornell Unversity Press, Ithaca, New York: **1979**

(106) Mills, H.H.; Speakman, J.C. *Prog. Stereochem*. **1969**, *4*, 273-281

(107) Ladd, M.C.F.; Palmer, R.A. *Structure Determination by X-ray Crystallography*. Plenum, New York: **1993**

(108) Hassall, C.; Thomas, A.; Moschidis, M. *J. Chem. Soc. Perk. T. 1*. **1977**, 2369-2376

(109) Umezawa, K.; Nalazawa, K.; Uemura, T.; Ikeda, Y.; Kondo, S.; Naganawa, H.; Kinoshita, N.; Hashizume, H.; Hamada, M.; Takeuchi, T.; Ohba, S. *Tetrahedron Lett*. **1998**, *39*, 1389-1392

(110) Umezawa, K.; Nakazawa, K.; Ikeda, Y.; Naganawa, H.; Kondo, S. *J. Org. Chem*. **1999**, *64*, 3034-3038

(111) Ohtani, I.; Kusumi, T.; Kashman, Y.; Kakisawa, H. *J. Org. Chem.* **1991**, *56*, 1296-1298

(112) Bevan, K.; Davies, J.; Hassall, C.; Morton, R.; Phillips, D. *J. Chem. Soc. C.* **1971**, 514-522

(113) Zubrod, C.G.; *JAMA* **1972**, *222*, 1161-1169

(114) Waud, W.R. *Murine L1210 and P388 Leukemia*. In: Teicher, B. (ed) *Anticancer Drug Development Guide*: *Pre-clinical Screening*, *Clinical Trials*, *and Approval*. Humana Press, Totowa, **1997**. 59-68

(115) Boyd, M.R. *The NCI In Vitro Anticancer Drug Discovery Screen*: *Concept, Implementation, and Operation*, *1985-1995*. In: Teicher, B. (ed) *Anticancer Drug Development Guide*: *Pre-clinical Screening*, *Clinical Trials*, *and Approval*. Humana Press, Totowa, **1997**. 59-68

(116) Takimoto, C.H. *Cancer Chemother. Pharmacol.* **2003**, *52 Suppl. 1*, S29-S33

(117) Rixe, O.; Ortuzar, W.; Alvarez, M.; Parker, R.; Reed, E.; Paull, K.; Fojo, T. *Biochem. Pharmacol.* **1996**, *52*, 1855-1874

(118) Hollingshead, M.G.; Alley, M.C.; Camalier, R.F.; Abbott, B.J.; Mayo, J.G.; Malspeis, L.; Grever, M.R. *Life Sciences* **1995**, *57*, 131-141

(119) http://dtp.nci.nih.gov/docs/raid/raid_pp.html

(120) http://dtp.nci.nih.gov/docs/ddg/ddg_descript.html

(121) Agatsuma, T.; Sakai, Y.; Mizukami, T.; Saitoh, Y. *J. Antibiot*. **1997**, *50*, 704-708

(122) Konishi, M.; Ohkuma, H.; Sakai, F.; Tsuno, T.; Koshiyama, H.; Naito, T.; Kawaguchi, H. *J. Am. Chem. Soc*. **1981**, *103*, 1241-1243

(123) Konishi, M.; Ohkuma, H.; Sakai, F.; Tsuno, T.; Koshiyama, H.; Naito, T.; Kawaguchi, H. *J. Antibiot*. **1981**, *34*, 148-159

(124) Morimoto, K.; Shimada, N.; Nakagawa, H.; Takita, T and Umezawa, H. *J. Antibiot*. **1982**, *35*, 378-380 and refs. cited therein.

(125) Hensens, O.; Borris, R.; Koupal, L.; Caldwell, C.; Currie, S.; Haidri, A.; Homnick, C.; Honeycutt, S.; Lindenmayer, S.; Schwartz, C.; Weissberger, B.; Woodruff, H.; Zink, D.; Zitano, L.; Fieldhouse, J.; Rollins, T.; Springer, M.; Springer, J. *J. Antibiot*. **1991**, *44*, 249-254

(126) Inouye, Y.; Take, Y.; Nakamura, S.; Nakashima, H.; Yamamoto, N.; Kawaguchi, H. *J. Antibiot*. **1987**, *50*, 100-104

(127) Lingham, R.; Hsu, A.; O' Brien, J.; Sigmund, J.; Sanchez, M.; Gagliardi, M.; Heimbuch, B.; Genilloud, I.; Diez, M.; Hirsch, C.; Zink, D.; Liesch, J.; Koch, G.; Gartner, S.; Garrity, G.; Tsuo, N.; Salituro, G. *J. Antibiot*. **1996**, *49*, 253-259

(128) Gräfe, U.; Schlegel, R.; Ritzau, M.; Ihn, W.: Dornberger, K.; Stengel, C.; Fleck, W.; Gutsche, W.; Härtl, A. *J. Antibiot*. **1995**, *48*, 119-125

(129) Maehr, H.; Liu, C.; Palleroni, N.; Smallheer, J.; Todaro, L.; Williams, T.; Blount, J. *J. Antibiot*. **1986**, *39*, 17-25

(130) Ogita, T.; Sato, A.; Enokita, R.; Suzuki, K.; Ishii, M.; Negishi, T.; Okazaki, T.; Tamaki, K.; Tanzawa, K. *J. Antibiot*. **1992**, *45*, 1723-1732

(131) Ushiyama, R.; Yonezawa, Y.; Shin, C. *Chem. Lett*. **2001**, 1172-1173

(132) Arroyo, V.; Hall, M.J.; Hassal, C.H.; Yamasaki, K. *J. Chem. Soc. Chem. Commun.* **1976**, 845-846

(133) Umezawa, K.; Ikeda, Y.; Kawase, O.; Naganawa, H.; Kondo, S. *J. Chem. Soc. Perk. T. 1*. **2001**, 1550-1553

(134) Parry, R.; Wenying, L. *J. Chem. Soc. Chem. Commun*. **1994**, 995-996

(135) Tao, T.; Alemany, L.B.; Parry, R.J. *Org. Lett*. **2003**, *5*, 1213-1215

III

Arenicolides A-C, 26-Membered Ring Macrolides from the Marine Actinomycete *Salinispora arenicola*

III.1. Introduction

Following the identification of the new marine actinomycete genus *Salinispora*[81] a vast amount of effort was invested into assessing the anticancer properties of the secondary metabolites produced by various members of that genus. The discovery of the nanomolar cytotoxin salinosporamide A (**26**) from *S. tropica*[82] and the early assessment that a high percentage of *Salinispora* isolates produced bioactive molecules,[82] provided good reason to thoroughly investigate the biomedical potential of secondary metabolites derived from members of the *Salinispora* genus. In order to accomplish this goal, an intensive fermentation and screening effort was initiated that utilized a HCT-116 colon adenocarcinoma whole cell assay (See: Chapter II for assay details) as the sole response variable. Even though multiple crude *Salinospora* fermentation extracts were potently cytotoxic (i.e. $IC_{50} \leq 76$ng/mL), more often than not, subsequent bioactivity guided isolation led to the identification of a small number of compounds, from classes that were already known. For instance, in the vast majority of cytotoxic fermentation extracts derived from *Salinospora arenicola*, HCT-116 whole cell bioassay guided fractionation led to the isolation of a member of the well known indole carbazole class of cytotoxins [e.g. staurosporine SV (**34**), (Figure III.1)]. The same occurrence was observed when screening *Salinispora arenicola* strains in a methicillin resistant *Staphylococcus aureus* (MRSA) antimicrobial assay wherein known molecules [e.g. rifamycin (**35**)] were often responsible for the observed bioactivity of the crude extract. .

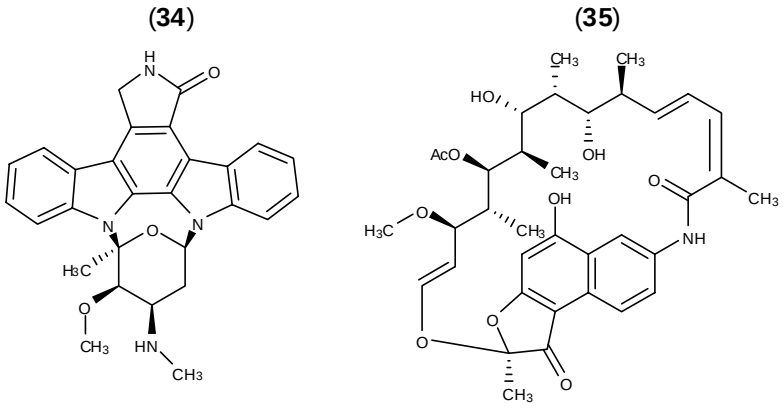

Figure III.1. Known Bioactive Compounds Produced by Members of the Genus *Salinispora*

Due to the fact that bioassay guided methodologies were leading to the isolation of a high proportion of known compounds, the discovery methodology was subsequently widened to a "target" based isolation strategy wherein we hoped to isolate new chemistry irregardless of activity. Not only would this approach ultimately provide insight into the biosynthetic potential of the *Salinispora*, once isolated, any new compounds (those with novel carbon skeletons) would be placed into a pure compound library that could be screened at a later date in various cancer relevant bioassays. A key component of this strategy was the incorporation of an analytical scale liquid chromatography system equipped with both a diode array detector and quadrupole mass detector (LCMS). Crude *Salinispora* fermentation extracts were injected into the system and the resulting chromatograms were carefully analyzed for the presence of new molecules. Examination of the UV profiles of peaks present in the chromatogram (Figure III.2, Figure III.3) and comparison of those profiles to the UV profiles of known compounds, allowed for new molecules produced by

Salinispora isolates to be identified. With the retention time, mass and UV profile of the "target" molecule known, production of that molecule could be optimized in subsequent fermentations and the isolation of that molecule could be guided by LCMS. This approach led to the isolation and identification of several new compounds from *Salinispora* including the cyclopenta[*a*]indenes cyanosporasides A (**36**) and B (**37**)[136] (Figure III.4) and the polyketide derived salinoketal (**38**)[137] (Figure III.4). Fermentation and investigation of an additional *S. arenicola* strain CNR005 led to the isolation and structure elucidation of three new oxygenated macrolides, arenicolides A - C (**39-41**) that comprise the subject matter for this chapter.

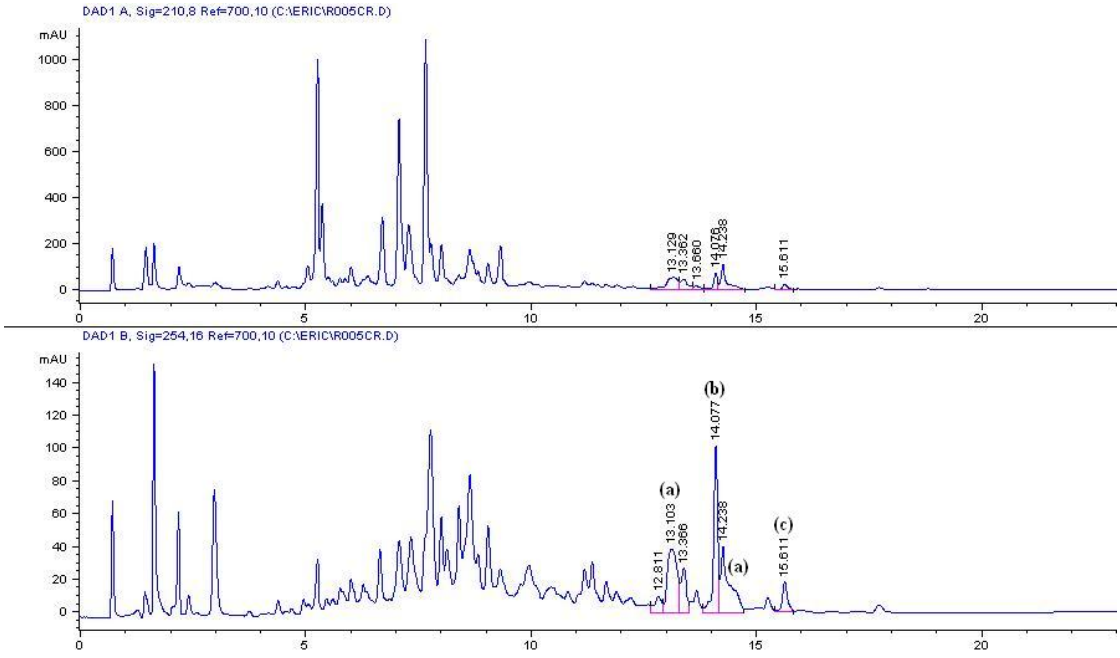

Figure III.2. LCMS Elution Profile of *Salinispora arenicola* Strain CNR005

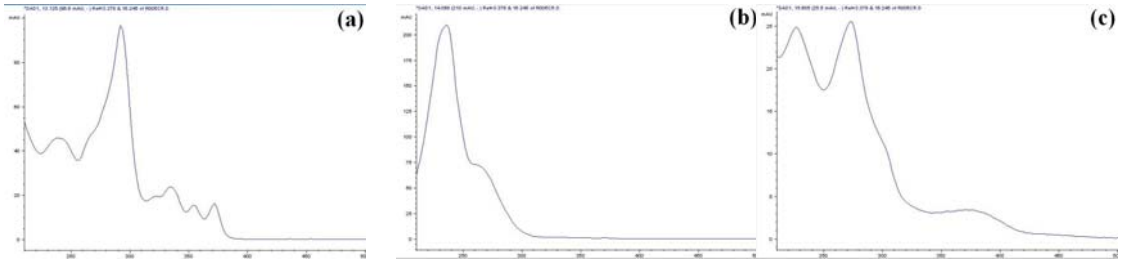

Figure III.3. Representative UV Profiles of Known Compound Staurosporine (a), New Compound Arenicolide A (b), and Known Compound Rifamycin (c)

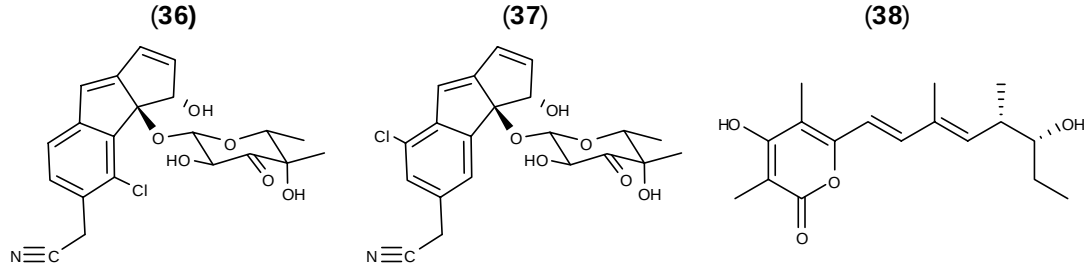

Figure III.4. New Compounds from *Salinispora* Identified by Target Based Approach

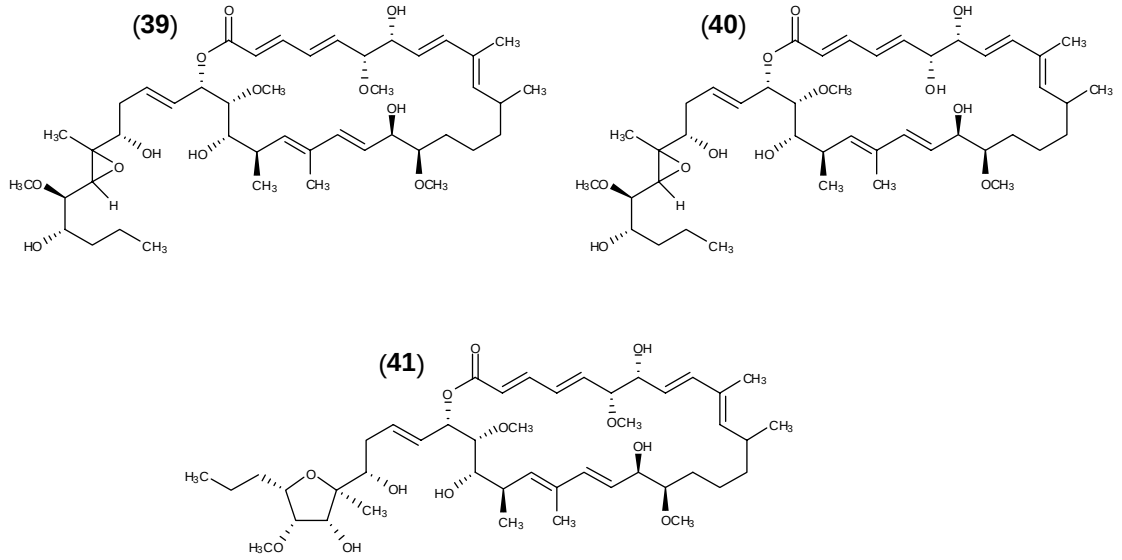

Figure III.5. Arenicolides A (39), B (40) and C (41)

III.2. Isolation and Planar Structure Elucidation of Arenicolides A-C (39-41)

Arenicolide A (**39**) was isolated by RP-HPLC from the 50% CH_3CN in water fraction obtained from a C_{18} flash column of the organic extract (0.37% of the crude extract; 0.55 mg/L). High-resolution mass spectral analysis of the optically active amorphous powder ($[\alpha]_D$ –72.4 *c* 0.26, MeOH) provided a pseudo-molecular ion peak at 827.4916 amu (0.5 mDa error) that, in conjunction with the ^{13}C NMR data, established the molecular formula of **39** as $C_{45}H_{72}O_{12}$. The IR spectrum of **39** contained bands consistent with alcohol and ester functional groups (3417 and 1738 cm^{-1} respectively), while the UV absorptions at 234 and 261 were suggestive of an extended system of conjugation. This supposition was supported by the 15-sp^2 carbon signals visible in the ^{13}C NMR spectrum. In total 45 carbon resonances were observed in the DEPT and ^{13}C NMR spectra, which were ascribed to 4 quaternary, 25 methine, 6 methylene, and 10 methyl carbons. Based on the carbon chemical shifts of these resonances, **39** was comprised of 1 ester and 7 double bonds that accounted for of the total 10 degrees of unsaturation implied by the molecular formula. This indicated arenicolide A contained 2 rings. The carbon NMR data also contained a multitude of oxymethine carbon resonances, which in conjunction with the aforementioned data demonstrated the likely polyketide origin of **39**.

Analysis of the 2D NMR data of arenicolide A (**39**) (Table III.1, III.2) established the six discrete spin systems shown in Figure III.6. From these data it became apparent that **39** contained a repeating structural motif of vicinal hydroxyl and methoxyl groups. The spectral overlap caused by this common subunit proved to be problematic in the structure elucidation of **39**. Nonetheless, the constitution of the

largest spin system (**A**) was defined starting from the ester carbonyl carbon C-1 that, based on HMBC correlations from H-2 [$\delta_{H\text{-}2}$ 5.96, $\delta_{C\text{-}2}$ 122.7] and H-3 [$\delta_{H\text{-}3}$ 7.23, $\delta_{C\text{-}3}$ 144.6], was in conjugation with a *trans* disubstituted olefin [$J_{2,3}$ = 14.9 Hz]. This chromophore was extended based on a COSY correlation from this latter proton signal H-3 to H-4, which belonged to another *trans* disubstituted olefin [$\delta_{H\text{-}4}$ 6.42, $\delta_{C\text{-}4}$ 132.6; $\delta_{H\text{-}5}$ 5.91, $\delta_{C\text{-}5}$ 140.7; $J_{4,5}$ = 15.4 Hz]. HMBC correlations from the δ-proton of this unsaturated system (H-5) to two oxymethine carbons [$\delta_{H\text{-}6}$ 3.57, $\delta_{C\text{-}6}$ 86.7; $\delta_{H\text{-}7}$ 3.96, $\delta_{C\text{-}7}$ 75.8] established the first spin system containing a vicinal hydroxyl methoxyl moiety. While partial structure **A** could not be extended beyond C-7 with any degree of confidence due to spectral overlap, HMBC NMR correlations at the other end of this unit to the ester carbonyl C-1 established H-25 [$\delta_{H\text{-}25}$ 5.40] as the acyloxy proton of this functional group. The two carbons adjacent to this methine could be identified by COSY correlations from this proton (H-25) to the oxygenated methine H-24 [$\delta_{H\text{-}24}$ 3.33] and to a second-order vinyl proton signal H-26 [$\delta_{H\text{-}26}$ 5.82]. Correlations observed in the COSY and HMBC spectra of **39** from the overlapping second order olefinic proton signals (H-26 and H-27) to methylene proton and methine carbon signals established the remaining carbon backbone of fragment **A**. Partial structure **B** was deduced as a β-substituted diene based on HMBC correlations from the methyl group H_3-41 to sp^2 carbon signals for C-19, C-20, and C-21 [$\delta_{C\text{-}19}$ 136.9; $\delta_{C\text{-}20}$ 133.8; $\delta_{C\text{-}21}$ 136.0]. A suite of COSY correlations starting from the proton signal of this latter carbon connected H-21 to the methine proton H-22 and to the methyl doublet H_3-42. Interestingly, NMR analysis indicated fragment **C** was identical to fragment **B**, but comprised of C-8 through C-12.

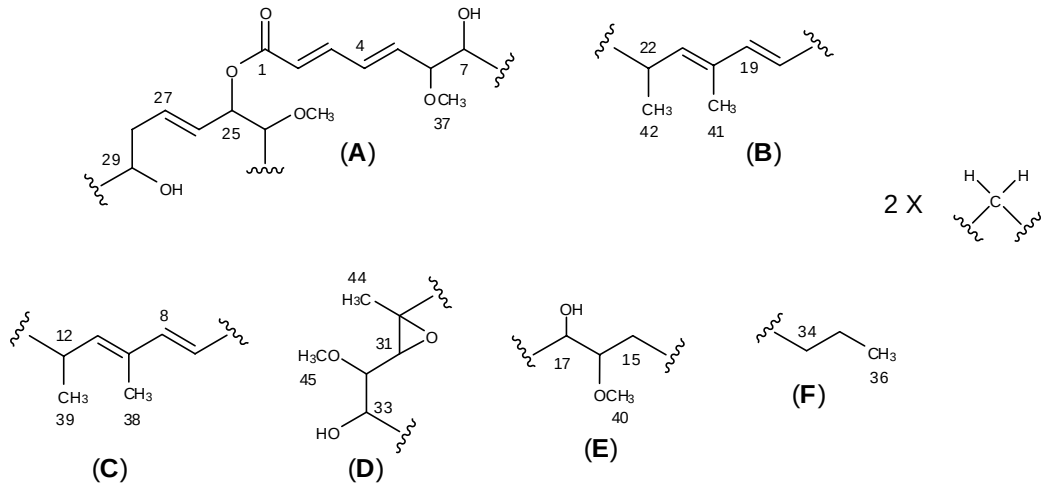

Figure III.6. Partial Structures Determined for 39 in Acetone-d_6

Table III.1. NMR Spectral Data for 39 Recorded in Acetone-d_6 (500 MHz) at 25°C

C/H #	δ_C, DEPT	δ_H mult (*J* in Hz)	COSY	HMBC
1	166.0, C			2, 3
2	122.7, CH	5.96, d (14.9)		4
3	144.6, CH	7.23, dd (14.9, 11.2)	2, 4	4, 5
4	132.6, CH	6.42, dd (15.4, 11.2)	3, 5	2, 6
5	140.7, CH	5.91, dd (15.4, 8.0)	6	3
6	86.7, CH	3.57, d (8.0)		4, 5, 8, 7, 37
7	75.8, CH	3.96, d (8.3)	8, 6	5
8	126.4, CH	5.35, dd (15.6, 8.3)	7	6, 7
9	139.3, CH	6.14, d (15.6)	8	7, 11, 38
10	132.3, C			8, 9, 38
11	140.6, CH	5.23, d (9.8)	12, 38	9, 38, 39
12	33.2, CH	2.49, m	13, 39	11, 13, 39
13	38.2, CH_2	1.24, m	12	39
14a	24.2, CH_2	1.39, m		12, 15, 16
14b		1.24, m		
15a	31.2, CH_2	1.43, m	16	
15b		1.29, m		
16	85.6, CH	3.02, dt (7.8, 4.9)	17	17, 18, 40
17	75.7, CH	3.96, m	18	
18	129.5, CH	5.60, dd (16.1, 8.3)	17	
19	136.9, CH	6.16, d (16.1)	18	21, 41
20	133.8, C			18, 19, 41
21	136.0, CH	5.27, d (10.3)	22, 41	19, 41, 42
22	38.0, CH	2.75, m	23, 42	22, 24, 42
23	76.5, CH	3.29, m	29-OH, 28	22, 24, 42
24	83.4, CH	3.33, m		45
25	78.5, CH	5.40, dd (6.3, 2.4)	24	24, 25
26	128.9, CH	5.82, m	25	24, 25, 28
27	132.0, CH	5.82, m		26, 28
28a	37.5, CH_2	2.30, ddd (16.1, 5.4,	27	27
28b		2.10, ddd (16.1, 9.3,	27	
29	76.7, CH	3.18, dd (9.3, 3.4)	29-OH, 28	31, 44, 28
30	62.1, C			31, 44
31	62.7, CH	2.85, d (8.3)	32	44, 32
32	83.9, CH	2.98, dd (8.3, 5.9)	33	33-OH, 31
33	72.0, CH	3.56, m	32, 34	32, 34
34a	36.1, CH_2	1.55, m	33, 35	32, 36, 35
34b		1.42, m	33, 35	
35a	19.5, CH_2	1.53, m	36	
35b		1.61, m	36	
36	14.4, CH_3	0.90, t (7.3)	35	
37	57.0, CH_3	3.29, s		6
38	12.9, CH_3	1.69, d (1.5)		
39	20.8, CH_3	0.94, d (6.8)	12	11
40	58.9, CH_3	3.36, s		16
41	13.0, CH_3	1.77, d (1.0)		
42	17.8, CH_3	1.02, d (6.3)		
43	60.5, CH_3	3.42, s		24
44	13.7, CH_3	1.29, s	22	
45	58.5, CH_3	3.41, s		32
29-OH		3.83, d (3.9)		

Table III.2. NMR Spectral Data for 39 Recorded in $CDCl_3$ (500 MHz) at 25°C

C/H #	δ_C, DEPT	δ_H mult (*J* in Hz)	COSY	HMBC
1	169.5, C			2, 3, 25
2	121.7, CH	5.89, d (16.0)	3	3, 4
3	144.2, CH	7.24, dd (16.0, 11.2)	2, 4	2, 4, 5
4	132.6, CH	6.25, dd (15.0, 11.2)	3, 5	2, 3, 6
5	139.2, CH	5.78, dd (15.0, 8.3)	4, 6	3
6	85.6, CH	3.49, dd (8.5, 8.3)	5, 7	4, 7, 8, 37
7	75.9, CH	3.98, bt (8.5)	6, 8	4, 6, 9
8	123.0, CH	5.28, dd (15.6, 8.3)	7, 9	6, 7, 9
9	140.6, CH	6.10, d (15.6)	8, 11	6, 7, 8, 38
10	130.4, C			7, 8, 9, 38
11	141.4, CH	5.24, d (10.8)	9, 12, 38	9, 38, 39
12	32.8 CH	2.44, m	11, 13, 39	11, 39
13	37.5, CH_2	1.28, m	12, 14ab	11, 12, 39
14a	31.3, CH_2	1.52, m	13, 14b, 15ab	16
14b		1.50, m	13, 14a, 15ab	16
15a	23.9, CH_2	1.48, m	14ab	17
15b		1.26, m	14ab	
16	84.6, CH	3.09, m	14ab, 15b, 17	17, 18, 40
17	76.0, CH	3.94, dd (8.8, 6.3)	16, 18	19
18	127.0, CH	5.52, dd (15.6, 8.8)	17, 19	17
19	138.2, CH	6.19, d (15.6)	18	17, 41
20	133.4, C			18, 19, 22, 41, 42
21	135.3, CH	5.15, bd (10.0)	22, 41	18, 19, 22, 23, 42
22	37.9, CH	2.65, tp (10.0, 6.5)	21, 23, 42	21, 23, 24, 42
23	75.7, CH	3.17, bd (10.0)	22, 24	21, 22, 24
24	81.4, CH	3.36, bd (2.2)	23, 25	43
25	78.9, CH	5.33, dt (5.9, 2.2)	24, 26	23, 24, 26, 27
26	131.8, CH	5.80, m	25	25, 28, 29
27	128.8, CH	5.80, m	25, 26, 28ab	24, 25, 28
28a	36.3, CH_2	2.39, m	27, 28b, 29	25, 26, 27
28b		2.13, m	27, 28a, 29	
29	74.1, CH	3.39, dd (11.0, 2.5)	28ab	28, 44
30	60.7, C			29, 32, 33, 44
31	60.9, CH	3.04, s	32	29, 32, 33, 44
32	82.5, CH	3.07, d (3.9)	31, 33	45
33	71.4, CH	3.68, dt (8.3, 3.9)	32, 34	34, 35
34	34.5, CH_2	1.46, m	33, 35ab	35, 36
35a	19.0, CH_2	1.58, m	34, 35b, 36	
35b		1.38, m	34, 35a, 36	36
36	14.0, CH_3	0.94, t (7.0)	35ab	
37	56.8, CH_3	3.33, s		6
38	12.5, CH_3	1.68, s	11	9, 11
39	19.9, CH_3	0.95, d (7.0)	12	11, 12
40	58.9, CH_3	3.47, s		
41	12.7, CH_3	1.76, s	21	19, 21
42	17.4, CH_3	1.02, d (6.5)	22	21, 22, 23
43	60.8, CH_3	3.52, s		24
44	14.1, CH_3	1.34, s		
45	58.4, CH_3	3.51, s		

Table III.3. NMR Spectral Data for 40 Recorded in $CDCl_3$ (500 MHz) at 25°C

C/H #	δ_C, DEPT	δ_H mult (*J* in Hz)	COSY	HMBC
1	166.0, CH			2, 3
2	121.6, CH	5.85, d (15.1)	3	
3	144.3, CH	7.21, dd (15.1, 11.2)	2, 4	
4	130.6, CH	6.30, dd (15.1, 11.2)	3, 5	
5	140.4, CH	5.93, dd (15.1, 7.6)	4, 6	3
6	75.7, CH	4.04, t (7.6)	5, 7	3
7	77.4, CH	3.912, dd (8.8, 7.6)		9
8	123.5, CH	5.30, dd (15.1, 8.8)		9
9	140.7, CH	6.12, d (15.1)		
10	130.5, C			9, 10-Me
11	141.8, CH	5.26, dd (9.1)		9, 10-Me
12	32.9, CH	2.45, m		
13	37.5, CH_2	1.29, m		
14a	24.0, CH_2	1.42, m		
14b		1.27, m		
15	31.2, CH_2	1.50, m		
16	84.6, CH	3.14, m		18, 17, 16-OMe
17	75.7, CH	3.92, t (9.3)	18	18, 19
18	127.1, CH	5.53, dd (15.6, 9.3)	17, 19	
19	138.0, CH	6.17, d (15.6)	18	20-Me, 21
20	133.4, C			19, 20-Me, 22
21	135.2, CH	5.14, d (10.3)	20-Me, 22	19, 20-Me, 22-Me, 22
22	37.7, CH	2.65, m	21 ,23	22-Me
23	75.6, CH	3.16, m	22	21, 22-Me, 22
24	81.3, CH	3.37, m		22, 26, 24-OMe
25	78.6, CH	5.29, m		26
26	128.8, CH	5.80, m		24
27	131.8, CH	5.80, m		29
28a	36.3, CH_2	2.39, m	27	26, 27
28b		2.13, m	27	
29	74.2, CH	3.38, m	28	30-Me, 31
30	61.0, C			30-Me, 29
31	61.0, CH	3.03, m		30-Me, 29
32	82.5, CH	3.07, m		
33	71.4, CH	3.05, m		35_d
34	38.7, CH_2	1.69, m		
35a	19.0, CH_2	1.58, m		
35b		1.37, m		
36	14.0, CH_3	0.94, t (7.0)		
37	12.5, CH_3	1.69, s		9, 21
38	20.2, CH_3	0.95, (6.8)		11
39	58.9, C	3.47, s		16
40	12.7, CH_3	1.76, s		19
41	17.4, CH_3	1.02, d (6.5)		21
42	60.8, CH_3	3.49, s		24
43	14.1, CH_3	1.33,		
44	58.3, CH_3	3.49, s		

Table III.4. NMR Spectral Data for 41Recorded in Acetone-d_6 (500 MHz) at 25°C

C/H #	δ_C , DEPT	δ_H mult (*J* in Hz)	COSY	HMBC	ROESY
1	165.9, C			2, 3	
2	122.4, CH	5.96, d (15.6)	3	4	4
3	144.4, CH	7.24, dd (15.6, 11.1)	2, 4	5	5
4	132.4, CH	6.43, dd (15.6, 11.1)	3, 5	2, 6	2
5	140.5, CH	5.93, dd (15.6, 7.3)	6		3
6	86.6, CH	3.58, m	7	37, 7	
7	76.2, CH	3.98, m	6, 9	6, 9	
8	126.2, CH	5.37, dd (15.6, 8.8)	9		38
9	139.1, CH	6.14, d (15.6)	8	7, 11, 38	11
10	132.2, C			8, 9, 38	
11	140.4, CH	5.24, m	12, 13	38, 39	
12	33.1, CH	2.50, m	13, 39	39	38
13a	38.1, CH_2	1.52, m	11	39	
13b		1.25, m	11, 14		
14a	24.3, CH_2	1.42, m		12	
14b		1.30, m	13		
15	31.1, CH_2	1.43, m	16	14	
16	85.6, CH	3.04, m	15, 17	17, 40	
17	75.6, CH	3.98, m	18	19	
18	129.2, CH	5.62, dd (15.6, 8.1)	19	17	41
19	136.7, CH	6.17, d (15.6)	18	21, 41	20
20	133.9, C			18, 41	21
21	135.9, CH	5.30, d (10.3)	22	19, 41, 42	
22	38.1, CH	2.76, m	21, 23, 42	42	41
23	76.5, CH	3.31, m	22	24, 42	42
24	83.4, CH	3.35, m	25	43	
25	78.4, CH	5.41, dd (6.4, 2.5)	24, 26	24	
26	128.4, CH	5.77, m	25	25, 28	
27	133.1, CH	5.80, m	28, 29	29	
28a	35.4, CH	2.39, m	29	26	
28b		2.06, m			
29	75.4, CH	3.54, m	28	44	
30	85.3, C			33, 44	
31	79.6, CH	4.26, d (5.9)	32	44	29
32	92.4, CH	3.45, m	33	31, 33, 45	31, 33
33	79.4, CH	3.62, m	32, 34		44
34	38.1, CH_2	1.53, m	33, 35	36	
35	19.7, CH_2	1.42, m	36	36	
		1.31, m	34, 36		
36	14.4, CH_3	0.90, t (7.3)	35		
37	57.0, CH_3	3.31, s		6	
38	12.9, CH_3	1.70, d (1.4)		9, 11	
39	20.8, CH_3	0.95, d (6.9)	12	11	
40	58.9, CH_3	3.38, s			
41	12.9, CH_3	1.78, d (1.1)		19	
42	17.8, CH_3	1.03, d (6.8)	22		
43	60.6, CH_3	3.44, s		24	
44	17.6, CH_3	1.07, s			34
45	58.0, CH_3	3.42, s			

Table III.5. NMR Spectral Data for 41 Recorded in $CDCl_3$ (500MHz) at 25°C

C/H #	δ_C, DEPT	δ_H mult (*J* in Hz)	COSY	HMBC
1	166.0, C			2, 3, 25
2	121.7, CH	5.86, d (15.3)	3	3
3	144.2, CH	7.24, dd (15.3, 11.2)	2, 4	5
4	132.4, CH	6.23, dd (15.1, 11.2)	3, 5	2, 6
5	139.1, CH	5.76, dd (15.1, 8.9)	4, 6	2
6	85.6, CH	3.46, t (8.9)	5	4, 7, 37
7	76.0, CH	3.95, t (8.9)	6, 8	9
8	123.0, CH	5.24, dd (15.6, 8.8)	7, 9	7
9	140.6, CH	6.08, d (15.6)	8	7, 38
10	130.4, C			8, 38
11	141.4, CH	5.21, d (9.8)	12	9, 38, 39
12	32.8, CH	2.39, m	11, 13, 39	39
13	37.5, CH_2	1.54, m	12	39
14a	24.0, CH_2	1.48, m		12
14b		1.23, m		
15	31.4, CH_2	1.46, m	14, 16	
16	84.6, CH	3.07, m	15, 17	17, 18, 40
17	76.0, CH	3.91, dd (8.8, 6.5)	16, 18	19
18	127.1, CH	5.50, dd (15.6, 8.8)	17, 19	17,
19	138.2, CH	6.17, d (15.6)	18	17, 21
20	133.4, C			18, 41
21	135.1, CH	5.14, d (10.3)	22	19, 42
22	38.0, CH	2.60, ddd (10.3, 9.5, 6.5)	21, 23, 42	24, 42
23	75.6, CH	3.14, d (9.5)	22	22
24	81.2, CH	3.36, d (2.2)	25	43
25	79.1, CH	5.28, dd (8.8, 1.8)	24, 26	23, 24,
26	127.9, CH	5.74, m	25	24, 25, 28
27	133.6, CH	5.79, m	28	25, 28, 29
28a	34.7, CH_2	2.44, m	27, 29	26, 27
28b		2.00, m		
29	76.1, CH	3.51, m	28	31
30	82.8, C			28
31	81.5, CH	4.20, d (6.3)	32	45
32	89.5, CH	3.50, m	31, 33	31, 33, 45
33	78.9, CH	3.66, ddd (12.2, 7.3, 4.6)	32	31
34	37.4, CH_2	1.24, m	35	32, 36
35a	19.0, CH_2	1.43, m	34, 36	36
35b		1.34, m		
36	14.1, CH_3	0.90, t (7.4)	35	
37	56.8, CH_3	3.31, s		6
38	12.5, CH_3	1.65, s		9, 11
39	19.9, CH_3	0.93, d (6.5)	12	11
40	59.0, CH_3	3.45, s		
41	12.7, CH_3	1.74, s		19, 21
42	17.4, CH_3	1.01, d (6.5)	22	
43	61.0, CH_3	3.53, s		24
44	16.9, CH_3	1.07, s		31
45	58.2, CH_3	3.48, s		

Table III.6. ^{1}H and ^{13}C NMR Data for 39-41 Recorded in $CDCl_3$ (500 MHz) at 25°C

	1		**2**		**3**	
C/H #	δ, DEPT	δ_H mult (*J* in Hz)	δ_C, DEPT	δ_H mult (*J* in Hz)	δ_C, DEPT	δ_H mult (*J* in Hz)
1	169.5, C		166.0, C		166.0, C	
2	121.7, CH	5.89, d (16.0)	121.6, CH	5.85, d (15.1)	121.7, CH	5.86, d (15.3)
3	144.2, CH	7.24, dd (16.0, 11.2)	144.3, CH	7.21, dd (15.1, 11.2)	144.2, CH	7.24, dd (15.3, 11.2)
4	132.6, CH	6.25, dd (15.0, 11.2)	130.6, CH	6.30, dd (15.1, 11.2)	132.4, CH	6.23, dd (15.1, 11.2)
5	139.2, CH	5.78, dd (15.0, 8.3)	140.4, CH	5.93, dd (15.1, 7.6)	139.1, CH	5.76, dd (15.1, 8.9)
6	85.6, CH	3.49, dd (8.5, 8.3)	75.7, CH	4.04, t (7.6)	85.6, CH	3.46, t (8.9)
7	75.9, CH	3.98, bt (8.5)	77.4, CH	3.91, dd (8.8, 7.6)	76.0, CH	3.95, t (8.9)
8	123.0, CH	5.28, dd (15.6, 8.3)	123.5, CH	5.30, dd (15.1, 8.8)	123.0, CH	5.24, dd (15.6, 8.8)
9	140.6, CH	6.10, d (15.6)	140.7, CH	6.12, d (15.1)	140.6, CH	6.08, d (15.6)
10	130.4, C		130.5, C		130.4, C	
11	141.4, CH	5.24, d (10.8)	141.8, CH	5.26, dd (9.1)	141.4, CH	5.21, d (9.8)
12	32.8, CH	2.44, m	32.9, CH	2.45, m	32.8, CH	2.39, m
13	37.5, CH_2	1.28, m	37.5, CH_2	1.29, m	37.5, CH_2	1.54, m
14a	31.3, CH_2	1.52, m	24.0, CH_2	1.42, m	24.0, CH_2	1.48, m
14b		1.50, m		1.27, m		1.23, m
15a	23.9, CH_2	1.48, m	31.2, CH_2	1.50, m	31.4, CH_2	1.46, m
15b		1.26, m				
16	84.6, CH	3.09, m	84.6, CH	3.14, m	84.6, CH	3.07, m
17	76.0, CH	3.94, dd (8.8, 6.3)	75.7, CH	3.92, t (9.3)	76.0, CH	3.91, dd (8.8, 6.5)
18	127.0, CH	5.52, dd (15.6, 8.8)	127.1, CH	5.53, dd (15.6, 9.3)	127.1, CH	5.50, dd (15.6, 8.8)
19	138.2, CH	6.19, d (15.6)	138.0, CH	6.17, d (15.6)	138.2, CH	6.17, d (15.6)
20	133.4, C		133.4, C		133.4, C	
21	135.3, CH	5.15, bd (10.0)	135.2, CH	5.14, d (10.3)	135.1, CH	5.14, d (10.3)
22	37.9 CH	2.65, tp (10.0, 6.5)	37.7, CH	2.65, m	38.0, CH	2.60, ddp (10.3, 9.5, 6.5)
23	75.7, CH	3.17, bd (10.0)	75.6, CH	3.16, m	75.6, CH	3.14, d (9.5)
24	81.4, CH	3.36, bd (2.2)	81.3, CH	3.37, m	81.2, CH	3.36, d (2.2)
25	78.9, CH	5.33, dt (5.9, 2.2)	78.6, CH	5.29, m	79.1, CH	5.28, dd (8.8, 1.8)
26	131.8, CH	5.80, m	128.8, CH	5.80, m	127.9, CH	5.74, m
27	128.8, CH	5.80, m	131.8, CH	5.80, m	133.6, CH	5.79, m
28a	36.3, CH_2	2.39, m	36.3, CH_2	2.39, m	34.7, CH_2	2.44, m
28b		2.13, m		2.13, m		2.00, m
29	74.1, CH	3.39, dd (11.0, 2.5)	74.2, CH	3.38, m	76.1, CH	3.51, m
30	60.7, C		61.0, C		82.8, C	
31	60.9, CH	3.04, s	61.0, CH	3.03, m	81.5, CH	4.20, d (6.3)
32	82.5, CH	3.07, d (3.9)	82.5, CH	3.07, m	89.5, CH	3.50, m
33	71.4, CH	3.68, dt (8.3, 3.9)	71.4, CH	3.05, m	78.9, CH	3.66, ddd (12.2, 7.3, 4.6)
34	34.5, CH_2	1.46, m	38.7, CH_2	1.69, m	37.4, CH_2	1.24, m
35a	19.0, CH_2	1.58, m	19.0, CH_2	1.58, m	19.0, CH_2	1.43, m
35b		1.38, m		1.37, m		1.34, m
36	14.0, CH_3	0.94, t (7.0)	14.0, CH_3	0.94, t (7.0)	14.1, CH_3	0.90, t (7.4)
37	56.8, CH_3	3.33, s			56.8, CH_3	3.31, s
38	12.5, CH_3	1.68, s	12.5, CH_3	1.69, s	12.5, CH_3	1.65, s
39	19.9, CH_3	0.95, d (7.0)	20.2, CH_3	0.95, (6.8)	19.9, CH_3	0.93, d (6.5)
40	58.9, CH_3	3.47, s	58.9, C	3.47, s	59.0, CH_3	3.45, s
41	12.7, CH_3	1.76, s	12.7, CH_3	1.76, s	12.7, CH_3	1.74, s
42	17.4, CH_3	1.02, d (6.5)	17.4, CH_3	1.02, d (6.5)	17.4, CH_3	1.01, d (6.5)
43	60.8, CH_3	3.52, s	60.8, CH_3	3.49, s	61.0, CH_3	3.53, s
44	14.1, CH_3	1.34, s	14.1, CH_3	1.33, s	16.9, CH_3	1.07, s
45	58.4, CH_3	3.51, s	58.3, CH_3	3.49, s	58.2, CH_3	3.48, s

Substructures **D** and **E** both contained this repeating vicinal hydroxy methoxy motif [δ_{C-32} 83.9/δ_{C-33} 72.0 and δ_{C-16} 85.6/δ_{C-17} 75.7 respectively] based on analysis of the gDQF-COSY and gHMBC data. One of these two carbon fragments, substructure **D**, could be expanded through analysis of the HMBC correlations to these two carbons from a methine doublet [δ_{H-31} 2.85], which allowed this unit to be connected to one end of a trisubstituted epoxide. Evidence supporting the existence of this three-member ring was the distinctive carbon chemical shifts of C-30 and C-31 [δ_{C-30} 62.1; δ_{C-31} 62.7]. The final spin-system, substructure **F,** was assigned as an *n*-propyl chain based on the NMR data recorded in acetone-d_6. This was established from HMBC correlations from the methyl triplet (δ_{H-36} 0.90, $J_{36,35}$ = 7.3 Hz) to two methylene carbons C-35 and C-34 [δ_{C-35} 19.5; δ_{C-34} 36.1]. An inventory of the atoms remaining revealed 2 methylene carbons [δ_{C-13} 38.2; δ_{C-14} 24.2] and one oxygenated methine [δ_{C-23} 76.5] that still needed to be connected to these partial structures.

Unfortunately, due to overlap of several of the key residues in the proton and carbon NMR spectra, e.g., C-7 and C-17 [δ_{H-7} 3.96, δ_{C-7} 75.8; δ_{H-17} 3.96, δ_{C-17} 75.7], these partial structures could not be assembled with a high degree of confidence. In the end it became necessary to acquire the NMR spectra of **39** in a different solvent ($CDCl_3$, Table III.2) in which key proton signals were sufficient dispersed. It should be noted that it would not have been possible to confidently assign the structure of **39** solely based on the data recorded in $CDCl_3$ due to spectral overlap. In this solvent, it was now possible to link C-7 of unit **A** to C-8 of unit **C** based on a COSY correlation from H-8 to H-7 and a HMBC correlation from H-9 to C-7. With the position of this center clearly established, C-17 of fragment **E** could be joined to C-18 of fragment **B**

due to similar COSY and HMBC cross peaks as previously mentioned. Likewise, the conclusive placement of C-7/C-8 suggested fragment **F**, the propyl chain, was connected to C-33 of unit **D** based on an HMBC correlation from H-33 [$\delta_{H\text{-}33}$ 3.68] to C-34 and C-35. The other end of substructure **D** was attached to unit **A** on the basis of HMBC correlations from H-29 [$\delta_{H\text{-}29}$ 3.39] to C-30 [$\delta_{C\text{-}30}$ 60.7], C-31 [$\delta_{C\text{-}31}$ 60.9] and C-44 [$\delta_{C\text{-}44}$ 14.1]. Finally, the one remaining oxymethine carbon [$\delta_{H\text{-}23}$ 3.17, $\delta_{C\text{-}23}$ 75.7] that could not be connected to any of the fragments based on the NMR data recorded in acetone was used to join fragment **A** to **B** on the basis of a network of COSY correlations, spanning H-24 to H-22, observed in $CDCl_3$.

What remained were methylene carbons that, on the basis of the structural fragments proposed so far, appeared to connect fragment **E** to **C** to form a 26-membered macrocyclic ring. The NMR evidence for the placement of these two carbons within the macrocycle was, however, equivocal and there was some uncertainty about the assignment of H_2-34 and H_2-35 to the side chain. This left the possibility that **39** contained either a 26- or 27-membered macrocycle. To unambiguously resolve this issue would require degradation of **39** in a manner that would discriminate between the two ring sizes. Therefore, a small sample of **39** was degraded by ozonolysis with a reductive workup and the resulting complex mixture analyzed by LC-MS and ^{1}H NMR spectrometry. While **39** was completely consumed, this experiment yielded no clear evidence of fragments consistent with any of the proposed ring structures. A search of the literature for alternative strategies revealed an elegant report using olefin cross-metathesis to degrade a simple polyacetylenic oxylipid.[138] Arenicolide A (**39**)

represented a much more daunting problem as cross metathesis with this complex polyene could potentially yield a myriad of reaction products.

III.2.1. Olefin Cross-Metathesis of 39

A cross-metathesis reaction can be considered as a bimolecular process formally involving the exchange of a bond (or bonds) between similar interacting chemical species such that the bonding affiliations in the products are identical (or closely similar) to those in the reactants.[139] Olefin cross metathesis refers to the set of reactions in which an olefin is cleaved and subsequently reassembled and if the substitution pattern was different on each side of the olefin, the reassembly will yield two new olefins (Figure III.7).

The commonly accepted mechanism for the olefin metathesis reaction involves a [2+2] cycloaddition reaction between a transition metal alkylidene complex and the olefin to form an intermediate metallacyclobutane. The metallacycle then breaks up in a fashion opposite to that in which it was formed to yield a new alkylidene and a new olefin (Figure III.7).[140]

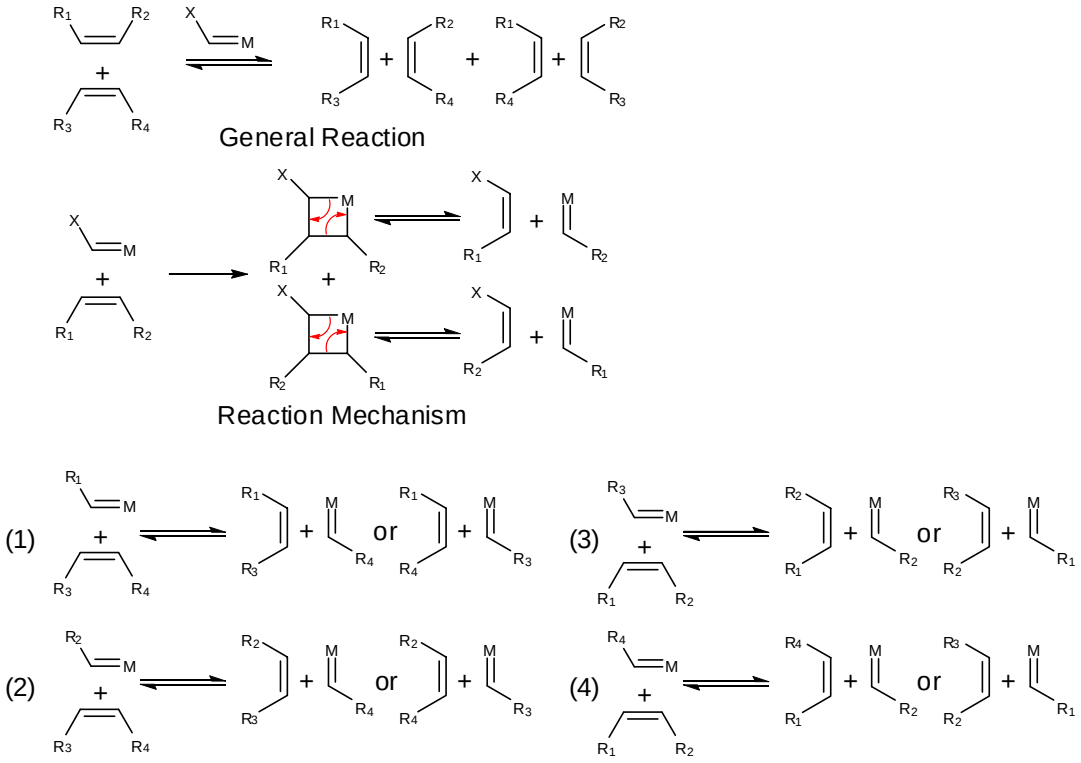

Figure III.7. General Schematic of Olefin Cross Metathesis Reaction

Given the electrophilic nature of the metathesis initiators and their sensitivity to steric bulk, the predominant metathesis product should result from cleavage of the isolated Δ_{26} olefin as compared to the lower energy dienes. Arenicolide A (**39**) was stirred with the commercially available second-generation Grubb's catalyst in DCM under 5 atmospheres of ethylene (Figure III.8). Despite the slow rate of cross metathesis, analysis of the reaction mixture by LC-MS indicated the presence of a small amount of the 27-carbon backbone macrocycle (**42**, C-1 through C-27). The corresponding macrocycle was identified by its molecular weight and the distinctive chromophore associated with the arenicolides (Figure III.9-III.11). Concurrent to

these degradation experiments, the structure of arenicolide C (**41**) was established and unlike **39**, the carbon backbone of **41** was unambiguously assigned by interpretation of NMR spectroscopic data. On the basis of the information gained from the structure of **41**, arenicolide A was identified as a 26-membered macrolide and therefore no further characterization of the metathesis reaction products was undertaken.

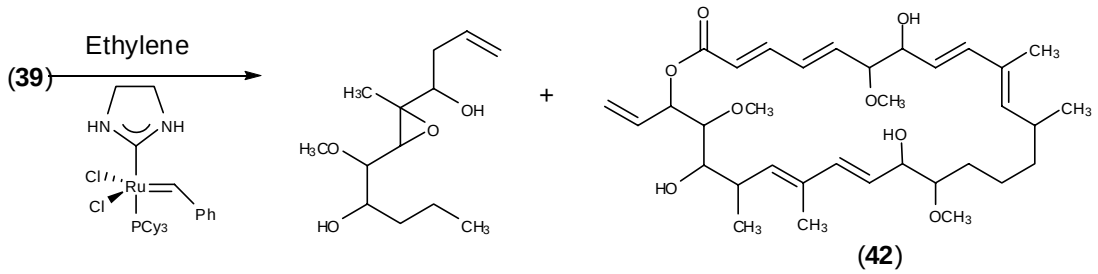

Figure III.8. Olefin Cross Metathesis Reaction of 39

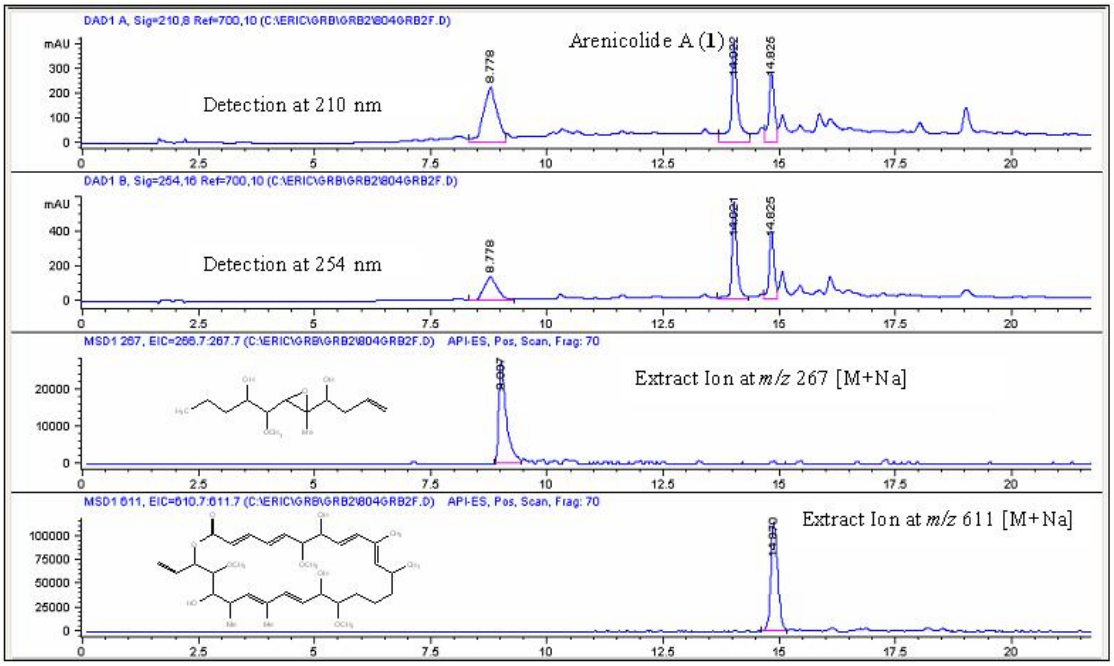

Figure III.9. LCMS Analysis of Metathesis Reaction Mixture

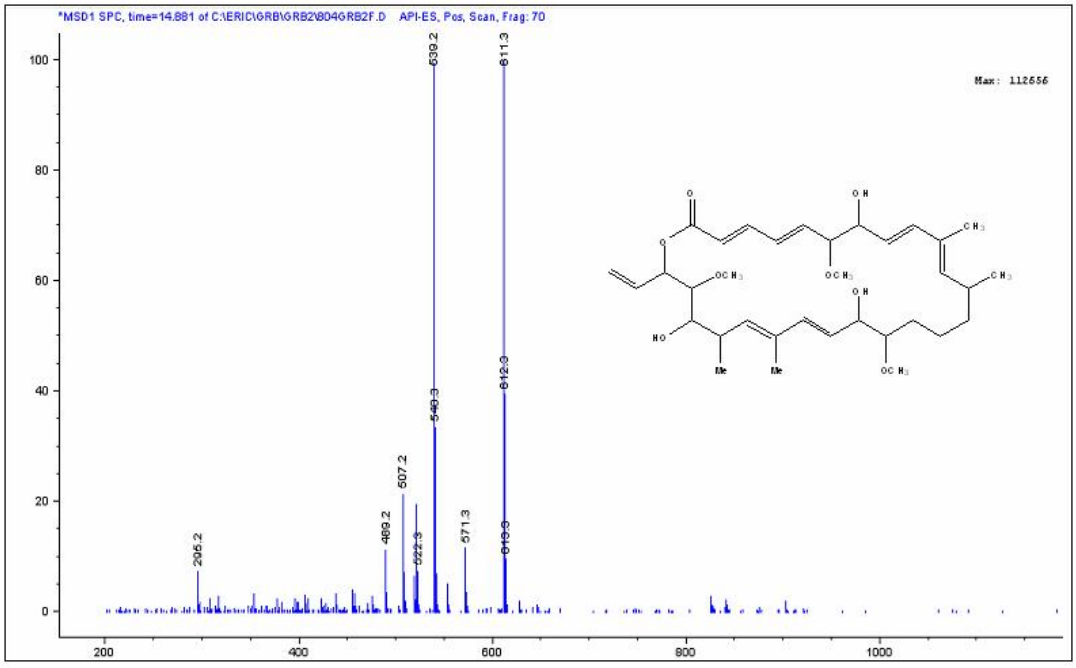

Figure III.10. ESI Mass Spectrum of 42 from Metathesis Reaction Mixture

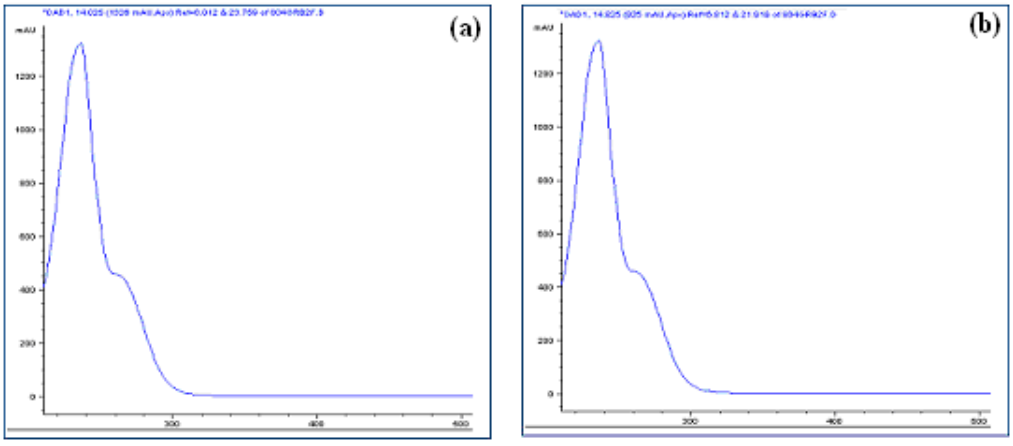

Figure III.11. UV Spectrum of 39 (a) and 42 (b) from Metathesis Reaction Mixture

Arenicolide B (**40**) eluted from the C_{18} HPLC column prior to **39** (**39** t_R = 69 min; **40** t_R = 55 min) and was assigned the molecular formula $C_{44}H_{70}O_{12}$ (HRESI-TOFMS $[M+Na]^+$ ion at *m/z* 813.4751), indicating **40** was 14 amu smaller than **39**. Comparison of the proton and carbon NMR spectra of **39** and **40** (Table III.3, Table III.6) established that **40** was 37-desmethoxyarenicolide A, as indicated by loss of the corresponding methoxy singlet and the upfield shift of C-6 [$\delta_{C\text{-}6}$ 75.7]. Analysis of the 2D NMR data conclusively established the gross structure as depicted for **40**.

Arenicolide C (**41**), isolated from the same fraction that contained **39** and **40**, was identified as a congener of **39** given the similarity of its spectral data. The high-resolution mass spectrum of **39** suggested a molecular formula of $C_{45}H_{72}O_{12}$, which confirmed that **39** and **41** were isomeric. Several differences in the resonances for the side chain (H-29 – H-35) were visible in the ^1H and ^{13}C NMR spectra (Table III.4, Table III.5, Table III.6). In particular, the large downfield shifts of C-30 and C-31 ($\delta_{C\text{-}30}$ 82.8, $\delta_{C\text{-}31}$ 81.5) indicated that the oxirane ring was not a structural feature of **41**. Analysis of the 2D NMR data provided evidence for a substituted tetrahydrofuran ring formed from C-30 through C-33. Specifically, a clear HMBC correlation was observed between H-33 and C-30, as well as a NOE correlation between H-34 and H-45, indicative of the proposed ring structure assigned for **41**. For a comparison of the ^1H and ^{13}C NMR chemical shifts for **39**-**41** see Table III.6.

III.3. Relative Stereochemical Determination of Arenicolide A (39)

Over the past 20 years many important bioactive molecules containing acyclic or macrocyclic motifs have been isolated from microorganisms. The planar structures of these molecules have been successfully solved by modern NMR methods however the stereochemical determination has proven to be a significant challenge. In many cases the stereochemistry has been solved via X-ray crystallography or extremely labor intensive syntheses. Examples where complete stereochemical description has been achieved include palytoxin,[141,142] amphotericin B,[143,144] calyculin,[145] fumonisins,[146] the swinholides[147] and aflastatin.[148] However, because these types of molecules are both difficult to crystallize and often possess multiple chiral centers making syntheses challenging, a large portion of these molecules have remained stereochemically unassigned. Examples of this include the amphidinols,[149,150] the prymensins[151] and the zooxanthellatoxins.[152]

In the case of **39**, examination of the planar structure revealed seven olefins the stereochemistries of which were determined via examination of $^{3}J_{HH}$ coupling constants and ROESY NMR correlations that will be covered in section III.3.1. Additional examination of the planar structure revealed that **39** consisted of a 26-carbon backbone macrocyclic system attached to an 11-carbon backbone acyclic system that together contained a total of 14 chiral centers arranged into six discrete stereochemical units (Figure III.12). Because five of the six units contained a secondary, alcohol bearing carbon, a methodology was devised to determine the stereochemistry of all of the chiral centers in a given unit relative to the alcohol

bearing carbon of that unit. The absolute configuration of the alcohol bearing carbon could then be determined by the Mosher NMR method (See: Section III.4) and with the configurations of the remaining centers in that unit relative to the alcohol bearing carbon known, the absolute configurations of all centers could then be determined. With this in mind, assignment of the relative stereochemistry of five of the six stereochemical units in **39** was approached by a combination of spectral, chemical and biosynthetic arguments and is covered in sections III.3.2, III.3.3 and III.3.4. The sixth unit consisted of an isolated secondary, methyl bearing carbon, the stereochemistry of which was not deduced herein.

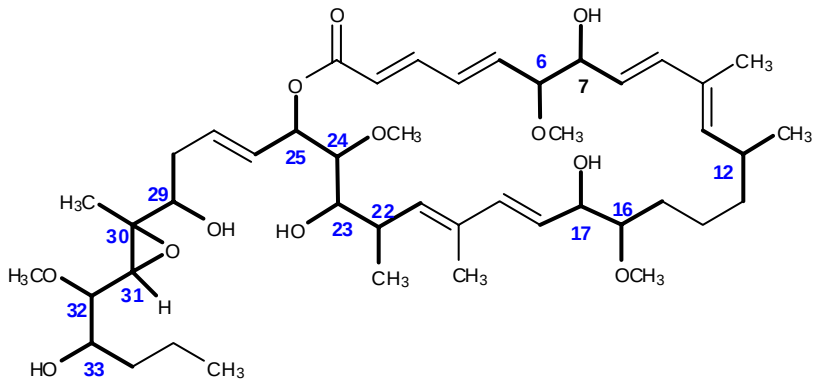

Figure III.12. Arenicolide A Planar Structure with Isolated Stereochemical Units Shown in Bold

III.3.1. Configurations of the Olefins

The relative stereochemistry of each of the seven olefins in **39** was assigned as follows. The configurations of the two-trisubstituted olefins (Δ_{10}, Δ_{20}) were deduced as *E* from analysis of the ROESY spectral data recorded in acetone-d_6. In both cases,

ROE correlations were observed from the methyl proton signals to the neighboring sp^3 methine proton signals; i.e., for the Δ_{10} and Δ_{20} double bonds, cross-peaks were observed from H_3-38 to H-12 and from H_3-41 to H-22, respectively. The *E* configurations of four of the five disubstituted double bonds were assigned based on their characteristic $^3J_{H,H}$ values observed in acetone-d_6 ($J_{\Delta 2}$ = 14.9 Hz, $J_{\Delta 4}$ = 15.4 Hz, $J_{\Delta 8}$ = 15.6 Hz and $J_{\Delta 18}$ = 16.1 Hz). The configuration of the remaining disubstituted double bond (Δ_{26}) could not be established at this time from the NMR data of **39-41**, recorded in a variety of solvents, due to apparent second-order coupling between H-26 and H-27. This configuration was determined by analyzing the corresponding $^3J_{H,H}$ values in the derivative **43** (See: section III.3.3).

III.3.2. Relative Configuration of C-6/C-7, C-22/C-23 and C-16/C-17: Spectral Methods

Prior to beginning this section, it is appropriate to define some of the key terms used to describe the stereochemical configurations determined herein. To begin, the terms *threo* and *erythro* stem from the four carbon sugars threose and erythrose (Figure III.13) and provide an "at a glance" description of the relative configuration of two adjacent chiral centers without individually specifying the configuration of either one. Specifically, isomers with two identical (or similar) ligands attached to the same side of the carbon chain are termed *erythro* as in erythrose and those isomers wherein the respective ligands are on opposite sides are termed *threo* akin to the four carbon sugar threose. Applying these designations to a newman projection (a projection

formula representing the spatial arrangement of bonds on two adjacent atoms in a molecule viewed along the bond joining the two atoms) provides a convenient way to visualize these configurations (Figure III.13.) and is used predominantly in the following sections to represent the deduced stereochemistry. Further stereochemical designations used herein include the term *gauche* which is used to describe relative configurations of A and D in a molecule A-C_1-C_2-D where A and D are the functionalities and the torsion angle AC_1C_2D about the bond C_1-C_2 is near +60° or -60° (Figure III.13). In addition, the term *anti*, derived from antiperiplanar, is used to describe the relative configuration of X and Y in the moecule X-C_1-C_2-Y if the torsion angle XC_1C_2Y about the bond C_1-C_2 is between +150° and -150°. Finally, the term *syn* derived from synperiplanar (sometimes referred to as eclipsed) is used to describe the relative configurations of X and Y in the molecule X-C_1-C_2-Y if the torsion angle XC_1C_2Y about the bond C_1-C_2 is between +30° and -30° (Figure III.13)

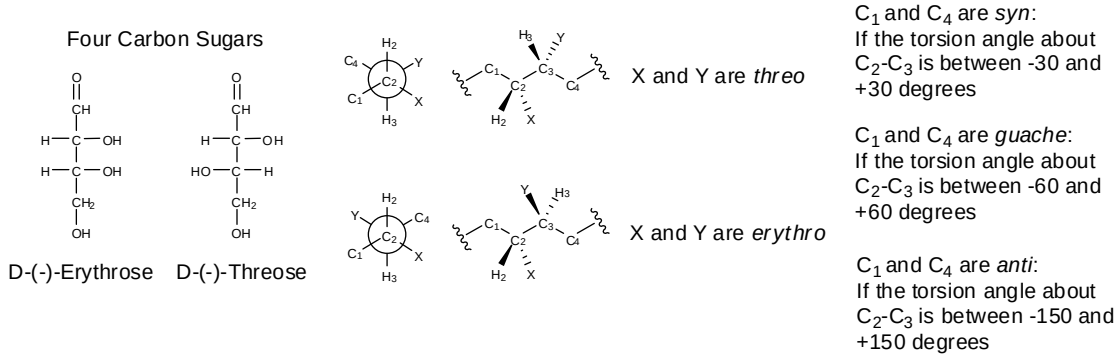

Figure III.13. Diagrammatic Representations of the Stereochemical Terms Used to Describe the Relative Configurations of the Respective Centers in 39-41

To continue with the relative stereochemical determination of arenicolide A, for three of the five stereogenic units, (C-6/C-7, C-16/C-17 and C-22/C-23) a publication by Murata *et al.*[153] was consulted as a key reference. By assuming that the conformation of adjacent asymmetric centers in acyclic systems is represented by low energy staggered rotamers, Murata argued that the relative stereochemistry of those systems can be determined using a combination of carbon-proton spin-coupling constants [($^{2,3}J_{CH}$), measured herein by G-BIRD$_R$-HSQMBC NMR experiments)],[154,155] proton-proton spin-coupling ($^3J_{HH}$) constants and nOe correlations. This methodology, termed *J*-based configurational analysis, enables the identification of the predominant staggered rotamer(s) out of the six possible derived from the *threo* and *erythro* configurations, by solely non-destructive NMR methods.

In arenicolide A (**39**), initial investigations indicated that two sets of the vicinal stereogenic centers (C-6/C-7 and C-22/C-23) had proton-proton coupling constants whose magnitude was defined as "large" according to Murata *et al.,*[149,153] thus allowing the configuration of these centers to be determined by ROESY or NOESY correlations. A *threo* configuration could be assigned between the vicinal stereocenters C-6 and C-7 based on the magnitude of the $^3J_{H\text{-}6,\ H\text{-}7}$ constant (8.5 Hz; $CDCl_3$) and the NOE observed between H-5 and H-8 (Figure III.14). Likewise, a *threo* configuration was assigned between stereocenters C-22 and C-23 based on a proton-proton coupling constant of 10.0 Hz between their respective protons, and an observed NOE between H-21 and H-24 that established a *gauche* orientation for these two substituents (Figure III.14). The stereochemical relationship between H-22/H-23 could not be extended to the adjacent stereocenters (C-24 & C-25) using a *J*-based

configuration analysis approach due to an insufficient signal-noise ratio for these resonances in a G-BIRD$_R$-HSQMBC experiment.[150] A *J*-based configuration analysis approach was also used to establish the *threo* configuration between the vicinal centers C-16 and C-17. The intermediate magnitude of the homonuclear coupling constant ($^3J_{H\text{-}16/H\text{-}17}$ = 6.3 Hz) for this dioxygenated unit suggested a mixture of rotamers at these two vicinal stereocenters. Three-bond proton-carbon coupling constants measured between H-16/C-18 and H-17/C-15 were also of an intermediate magnitude. Taken together these data are most consistent with an interconverting mixture of the *anti* (-)- and (+)-*gauche* rotamers as shown in Figure III.15.

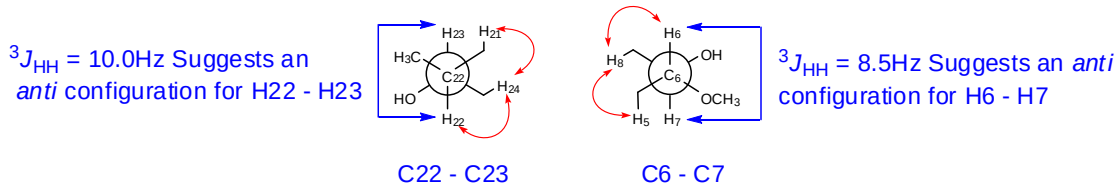

Figure III.14. NOE Correlations (Red) and $^3J_{CH}$ Values Used to Assign the Relative Configurations of C-6/C-7 and C-22/C-23 in 32

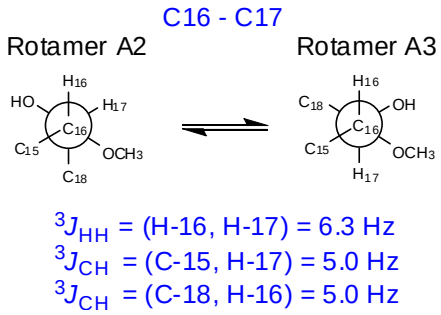

Figure III.15. $^3J_{HH}$ and $^3J_{CH}$ Values Used to Assign the Relative Configurations of the Interconverting Rotamers Present in C-16/C-17 in 39

III.3.3. Relative Configuration of C-24/C-25 and Relation to C-22/C-23: Chemical and Spectral Methods

To relate the centers at C-24 and C-25 to C-22 and C-23 required methanolysis of **39** and conversion of the resulting diol to the acetonide derivative (**43**) by reaction with PPTS (pyridinium toluenesulfonate) and dimethoxypropane. Once converted to the acteonide, the stereochemistry of the *syn*-or *anti*-1,3-diol can be assigned from the ^{13}C chemical shifts of the acetal methyl groups.[156] In general, the *syn*-1,3-diol acetonides have acetal methyl shifts at 19 and 30 ppm and acetal carbon shifts at 98.5 ppm, while the *anti*-acetonides have methyl shifts at 25 ppm and acetal carbon shifts at 100.5 ppm. The chemical shift differences are attributed to the fact that the *syn*-acetonide exists in a well defined chair conformation with the C(4) and C(6) alkyl substituents in equatorial positions (Figure III.16). An *anti*-acetonide exists in a twist-boat conformation in order to avoid the 1,3-diaxial interactions that would be present in either chair conformation so long as the groups involved in the 1,3-diaxial interaction possess sufficient steric bulk as to make the interaction unfavorable (as is the case in **43**).

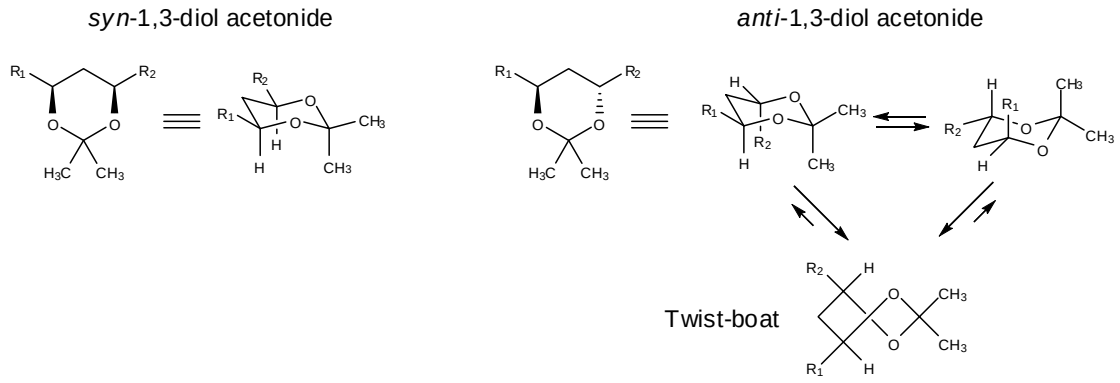

Figure III.16. Conformations of Acetonides Formed from *syn* and *anti*-1,3 diols

Analysis of the NMR spectroscopic data for **43,** recorded in MeOH-d_4, established the 1,3-dioxane ring existed in a twist-boat conformation as defined by the carbon chemical shifts of the ketal carbon ($\delta_{C\text{-}49}$ 102.9) and the nearly identical chemical shifts of the *gem*-dimethyl carbons ($\delta_{C\text{-}47}$ 25.2 and $\delta_{C\text{-}48}$ 24.8).[156] Taken together these data established the *anti* configuration of H-23 and H-25 in compound **43**. The configuration of these centers relative to H-24 was deduced by analysis of the proton-proton coupling constants ($J_{23,24}$ = 2.4 Hz; $J_{24,25}$ = 5.8 Hz) in the 1,3-dioxane ring and comparison with a model compound (**44**), present in the literature (Figure III.17).[157] These data established the *anti* and *syn* stereochemical relationships in **39** between H-24/H-25 and H-23/H-24, respectively.

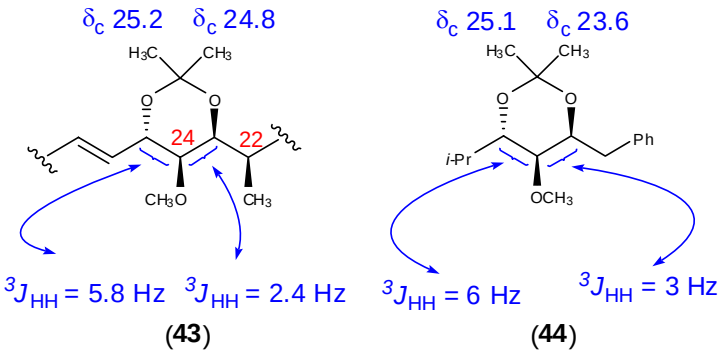

Figure III.17. Comparison of NMR Spectroscopic Data for the Acetonide Derivative of the Methanolysis Product of 32 (43) and a Model Compound (44)

III.3.4. Relative Configuration of the Side Chain C-26 to C-36: Biosynthetic Arguments

In the side chain (C-26 to C-36), the configuration of the epoxide was assigned based upon a ROESY correlation observed in acetone-d_6 due to a large amount of signal overlap for H-31 and H-32 in $CDCl_3$. A cross peak between H_3-44 and H-32 established their likely *cis* relationship thus implying the *trans* configuration of the epoxide (C-30/C-31). Unfortunately, relating the configuration of the epoxide to the adjacent centers (C-29 or C-32) was not possible by *J*-based configuration analysis due to a combination of poor signal-to-noise in the G-BIRD$_R$-HSQMBC spectrum and the lack of appropriate comparison data from models systems. It is also important to note that recent work has shown that the J_{CH} values at centers directly adjacent to epoxides varies significantly from those in acyclic systems. [158]

Based on the structural similarity, **39** is likely either a biosynthetic precursor to **41** or they share a late stage biosynthetic intermediate. Therefore, the relative and absolute configurations deduced for the stereocenters in **39** are likely the same in **41** and vice versa. The near superimposable negative cotton effect observed in the CD spectra of **39-41** (Figure III.18) is evidence to support the hypothesis that the absolute stereochemistry of **39-41** is the same within the macrocycle and likely also within the side chain. Given the strong structural similarity between **39** and **41**, the stereochemical relationship between C-32 and C-33 in **39** could be inferred from the corresponding centers in arenicolide C (**41**), as shown in Figure III.19. Specifically, NOE correlations observed in DPFGSE-1D NOE experiments on **41**, in $CDCl_3$ and acetone-d_6, between H-33, H-32 and H-31 in the side chain established the relative configuration of these centers in **41**. Extrapolating this to the linear compounds **39** and **40**, by opening up the THF ring, suggests the stereochemistry depicted in Figure III.19 for C-32 and C-33 in **39**.

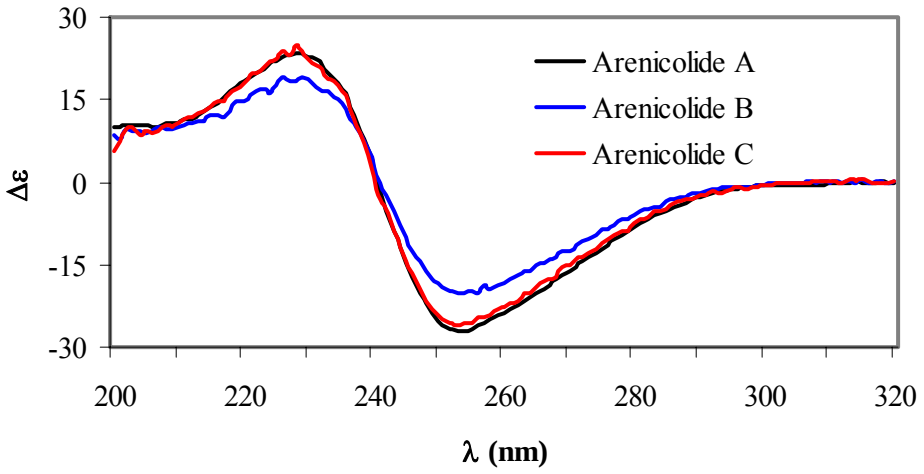

Figure III.18. CD Spectra of 39-41 in MeOH

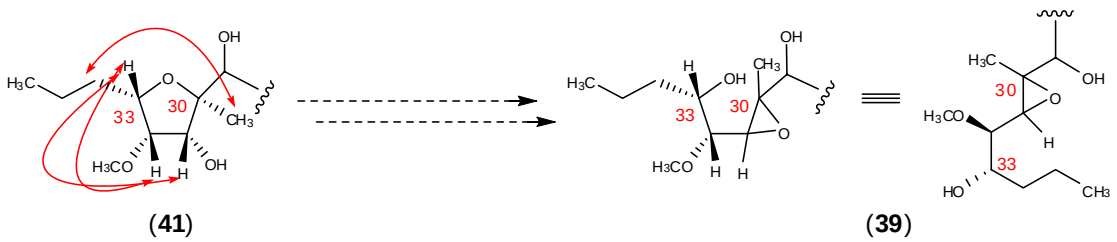

Figure III.19. Relative Configuration of the THF Ring of 41 and Extrapolation to the Epoxides in 39and 40

Two stereocenters in the side chain of **39**, at C-30 and C-31, cannot be assigned based on this analysis because multiple mechanisms exist for the conversion of **39** to **41** involving either inversion or retention of configuration at those centers. For example, analogous to the Cane-Celmer-Westley model[159,160] for the biosynthesis of monensin, substitution of 33-OH at C-30 by an S_N2 mechanism inverts the stereochemistry at this latter center if **39** is directly converted to **41** (Figure III.20).

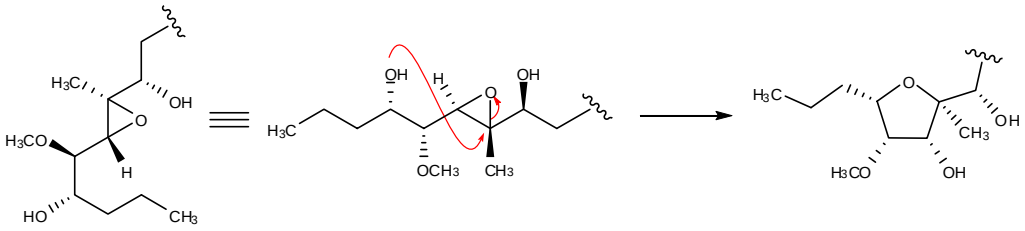

Figure III.20. Application of Cane-Celmer-Westley Model to the Formation of the THF Ring of 41 from the Epoxide of 39

This corresponds to a 5-endo-tet cyclization, which is disfavored according to Baldwin's rules,[161] but not without precedent as electron donating groups can stabilize a "disfavored" transition state[162] and lewis acids can induce disfavored cyclizations.[163] The same disfavored cyclization can be accomplished with a catalytic antibody, which

demonstrates the biosynthetic feasibility of the proposal.[164] Disfavored cyclizations are also postulated in the biosynthesis of marine polyether brevetoxin, which is believed to involve a series of nine disfavored endo-tet cyclizations.[165,166] This all serves to reinforce the likelihood of a S_N2 conversion of **39** to **41** involving an inversion of stereochemistry at C-30,[167] but while cyclizations of epoxides clearly have the most biosynthetic precedent, other mechanisms exist, since despite always being present in the crude extract, **41** may still be an artifact of a non-enzymatic transformation. In this case, a mechanism involving an initial epoxide migration through a Payne rearrangement[168] and subsequent formation of the tetrahydrofuran ring by a favored 5-exo-tet S_N2 cyclization would result in retention of configuration at C-30 due to double inversion at this center. The aforementioned mechanism is unlikely in the context of this report as NOESY correlations suggest that C-30/C-31 of the epoxide in **39** exists in a *trans* configuration. Therefore, double inversion of C-30, as would be the case with the Payne rearrangement followed by a favored 5-*exo*-tet S_N2 cyclization, would lead to retention of the C-30/C-31 *trans* configuration that is not observed in the all *cis* THF ring of **41**.

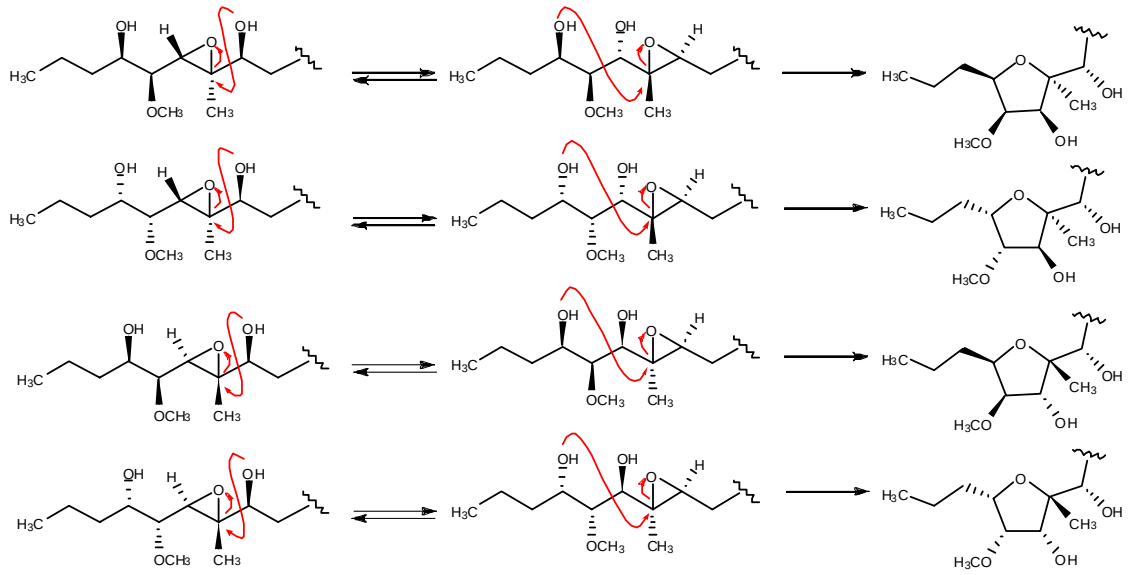

Figure III.21. Mechanism for Conversion of the Epoxide Containing Side Chain of 39 to the THF ring in 41 by Payne Rearrangement and Subsequent 5-*exo*-tet S_N2 Cyclization (Note: Not All Side Chain Diastereomers are Shown)

However, a mechanism involving a S_N2 nucleophilic opening of the epoxide at C-31 by water, subsequent loss of the resulting tertiary alcohol at C-30 to give a carbocation that is quenched intramolecularly by the C-33 hydroxyl group has the potential to invert both stereocenters. It is this latter possible mechanism that prevents relating the stereochemistry of C-30/C-31 between **39** and **41** due to the fact that both the side chain shown in figure III.20 and in figure III.22 could generate the observed THF ring configuration shown in figure III.19. Thus, the relative configuration of the epoxide in **39** with respect to the adjacent centers (C-29 & C-32) remains unassigned.

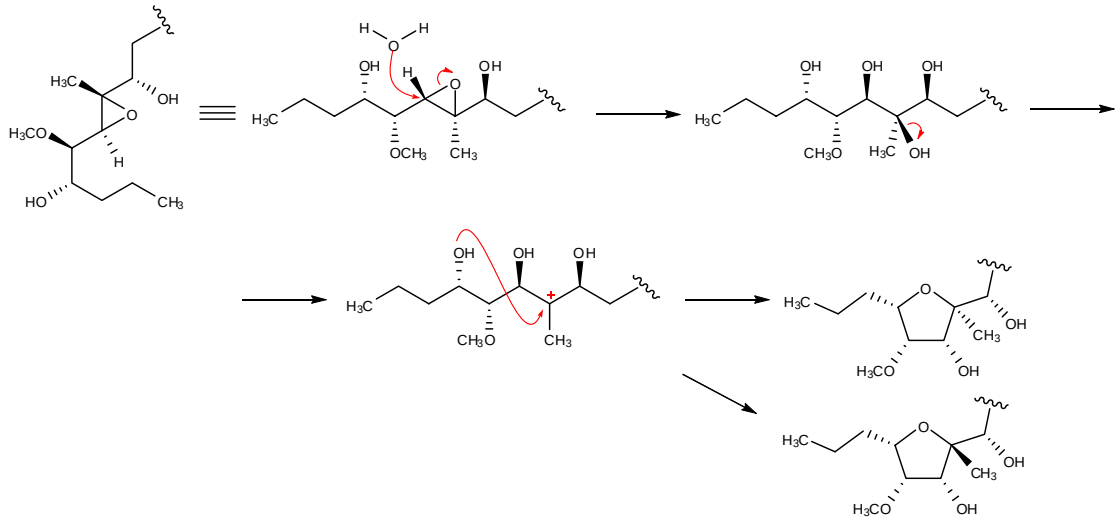

Figure III.22. Nucleophilic Opening of the Epoxide in 39 at C-31 by Water Followed by Loss of the Resulting Tertiary Alcohol at C-30 to Give a Carbocation that is Quenched Intramolecularly by the C-40 Hydroxyl Group

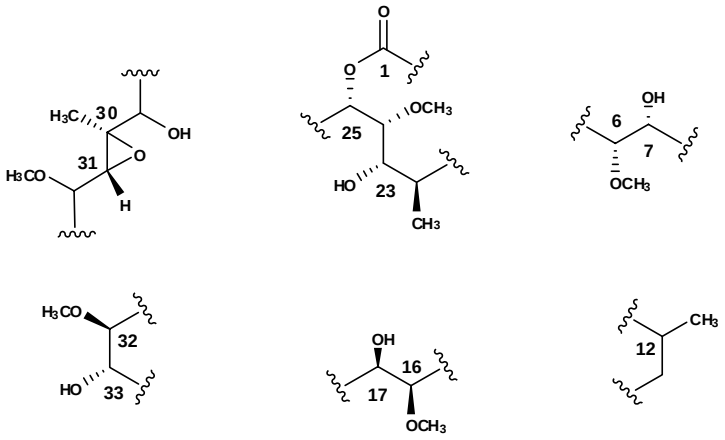

Figure III.23. Relative Stereochemistry of the Isolated Units Deduced

The evidence presented thus far established the relative configuration of five of the six isolated stereochemical units, which could not be directly related to each other

through any obvious means (Figure III.23). This necessitated determining the absolute stereochemistry of each of these isolated units.[169] Several strategies were considered involving complete degradation of **39** via either ozonolysis or cross-metathesis. In general, these approaches eventually required either NMR analysis of the degradation products using chiral auxiliaries or necessitated the synthesis of a significant portion of **32** in order to generate standards for comparative purposes by GC- or LCMS or circular dichroism.[170,171,172] In the end, our inability to conclusively identify fragments from the small scale ozonolysis of **39** (*vide supra*) weighed heavily on the decision to explore approaches that did not involve substantial degradation of **39**. It should be noted that both substantial degradation with the Grubb's reagent and attempts at crystallization were both unsuccessful. Given that five of these stereochemical units contained a secondary alcohol, a strategy for determining the absolute stereochemistry of intact arenicolide A (**39**) using the Mosher NMR spectroscopic method was devised.

III.4. Mosher NMR Method for Determining the Absolute Configuration of Secondary Alcohols and Application to Arenicolide A (39)

The Mosher method, developed by Mosher and Trost in the 1970s, is a NMR based method for the determination of the absolute configurations of unknown chiral substrates.[102] The ranges of substrates whose configuration can be assigned by these methods include primary, secondary and tertiary alcohols, diols, carboxyclic acids, primary and secondary amines and sulfoxides. In the case of secondary alcohols, α-

methoxy-α-(trifluoromethyl)phenylacetyl chloride (MTPACl) has been the most commonly used chiral derivatizing agent (CDA) and is also the reagent used in this study (Figure III.24).

The process of determining the absolute configuration of the alcohol bearing carbon begins with the esterification of the alcohol with the two enantiomers of MTPA-Cl. After the two diastereomeric esters have been prepared, their respective NMR spectra are recorded and compared. Most commonly, ^{1}H and ^{13}C NMR are used to ascertain the chemial shifts of the protons and carbon atoms of the derivatized, chiral, alcohol bearing carbon and the carbons and protons that are α and β to it. This method is based on the anisotropic shielding effect that the phenyl group of the chiral auxillary MTPA exerts on the substituents L_1/L_2 attached the alcohol bearing carbon. Specifically, the anisotropic shielding effect of the MTPA phenyl group allows the position of L_1 and L_2 to be determined with respect to that phenyl group on the basis of the signs of $\Delta\delta_{S-R}$ values (see below). For this argument Mosher assumed that the most representative MTPA conformer is that in which the proton of the derivatized methine, the carbonyl group, and the CF_3 group are situated in the same plane (Figure III.25). Taking this assumption into consideration, the protons of the substituent L_2 are shielded by the phenyl ring in the (*R*)-MTPA ester, whereas those of L_1 remain unaltered. In opposition, when the same alcohol is derivatized with the (*S*)-MTPA derivative, L_1 and its attached protons are shielded while L_2 is unaffected (Figure III.25). Therefore, the substituent L_1 will be more shielded in the (*S*)-MTPA ester than in the (*R*)-MTPA ester and L_2 will be more shielded in the (*R*)-MTPA ester than in the

(*S*)-MTPA ester derivative. These selective shielding effects are expressed using the parameter $\Delta\delta_{S-R}$ which is defined as the difference between the chemical shift of a particular proton in the (*S*)-MTPA ester and the chemical shift of the same proton in the (*R*)-MTPA derivative. All of the protons shielded in the (*R*)-MTPA will exhibit a positive $\Delta\delta_{S-R}$ value, whereas those shielded in the (*S*)-MTPA derivative will exhibit a negative $\Delta\delta_{S-R}$ value (Figure III.25).

In order for confident assignments to be made, the NMR data used for assignments should conform to the following regulations: (1) The $\Delta\delta_{S-R}$ must be sufficiently large and be above the level of experimental error, (2) All of the protons on the same side of the plane of the MTPA ester should have the same sign and (3) If the sign of $\Delta\delta_{S-R}$ is negative for one substituent (e.g. L_1), then the sign of $\Delta\delta_{S-R}$ for the other substituent (e.g. L_2) must be positive.

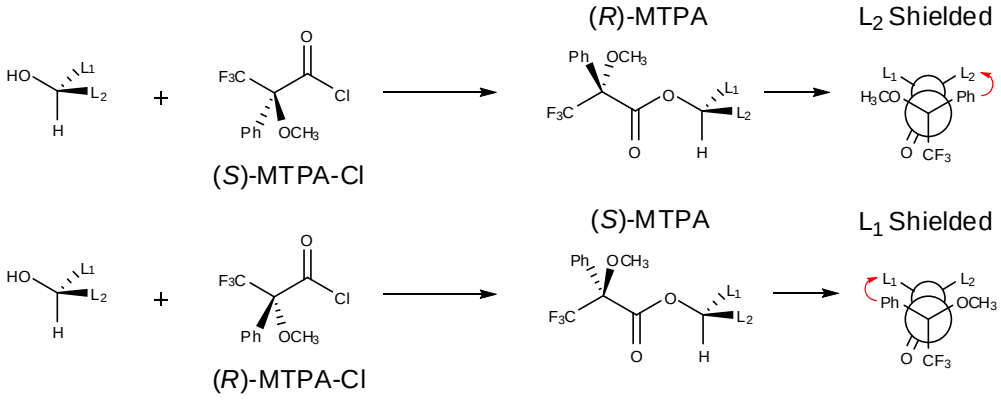

Figure III.24. Shielding Effect of MTPA Derivatives and Application to Determination of the Absolute Configuration of Secondary Alcohols

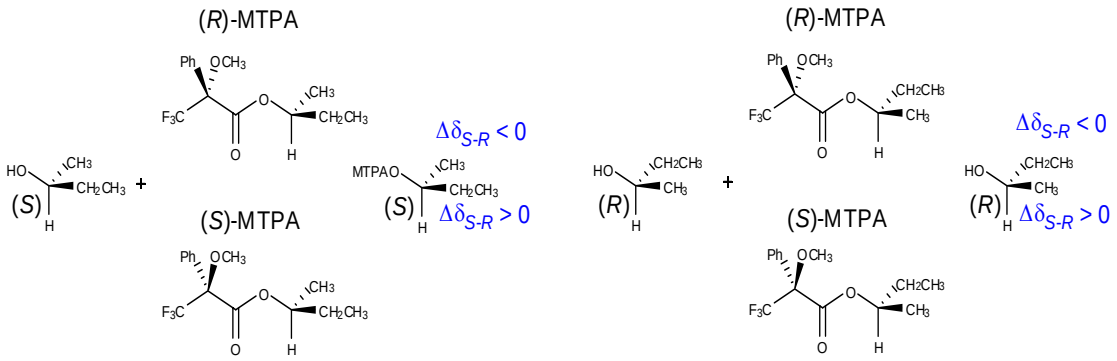

Figure III.25. Determination of the Absolute Configuration of a Secondary Alcohol Using MTPA-Cl and the Mosher NMR Method.

When applied to polyols in which multiple chiral centers are derivatized, $\Delta\delta_{S-R}$ values can become complicated due to undesired shielding from distal CDAs upon the center of interest. To overcome this dilemma, approaches have been devised where specific centers are protected allowing for each alcohol in a polyol to be derivatized singularly and the configuration of each center determined one at a time. In the case of **39**, formation of partial per-MTPA derivatives involving protection of the individual alcohols and subsequent derivatization with MTPA were precluded by sample size and the inherent reactivity of **39**. In a separate set of experiments, we attempted to prepare the tetra-MTPA derivatives of the acetonide protected methanolysis product of **39**. Unfortunately, were we not able to prepare an adequate amount of the *R*-MTPA derivative of this compound for NMR analysis. Therefore, efforts were focused on formation of the penta-MTPA derivative. Recent studies have established that MTPA is inferior to α-methoxyphenylacetic or 9-anthrylmethoxyacetic acid because of the smaller differences between the ^{1}H NMR chemical shifts in the MTPA derivatives. These smaller differences have been

proposed to arise from the comparatively more complex conformational ratios inherent to MTPA.[173] In the case of **39**, this attribute was deemed desirable, as it should minimize the undesired cumulative shielding effects due to distal chiral auxiliaries. Therefore, treatment of **39** in separate experiments, with (*R*)- and (*S*)-α-methoxy-α-(trifluoromethyl)phenylacetyl chloride (*R*- and *S*-MTPA-Cl) initially yielded a complex mixture of Mosher derivatives which eventually coalesced into the penta-(*S*)- and penta-(*R*)-MTPA derivatives of **39**.[174] It should be noted that the rate of formation of *R*-**39** was significantly slower than the corresponding *S*-derivative with the former requiring twice as long to obtain an adequate amount of material for NMR analysis. Despite the prolonged reaction time we observed no appreciable amount of elimination at the allylic alcohols C-7 and C-17. Assuming the conformation of the acetylated derivative at these centers is analogous to **39**, elimination at these centers would require a sterically unfavorable *syn*- rather than the favored *anti*-periplanar elimination owing to a *gauche* orientation between the acyloxy bond and the adjacent methine proton.

Analysis of ^{1}H NMR chemical shift differences ($\Delta\delta_{S-R}$) yielded the values shown in Figure III.26. As expected, the $\Delta\delta_{S-R}$ values on each side of the respective derivatized chiral centers were complicated presumably due to shielding effects arising from MTPA units not directly bound to the carbon of interest. Nonetheless, consistent $\Delta\delta_{S-R}$ values for the protons α and β to the derivatized centers suggest the absolute configuration for **39** depicted in Figure III.26. It should be noted however that the absolute stereochemistry of C-12, C-30 and C-31 in **39** could not be determined via

the experiments described. Based on biosynthetic considerations, and the similarity of the CD spectra, the same absolute configuration is suggested for **40** and **41**.

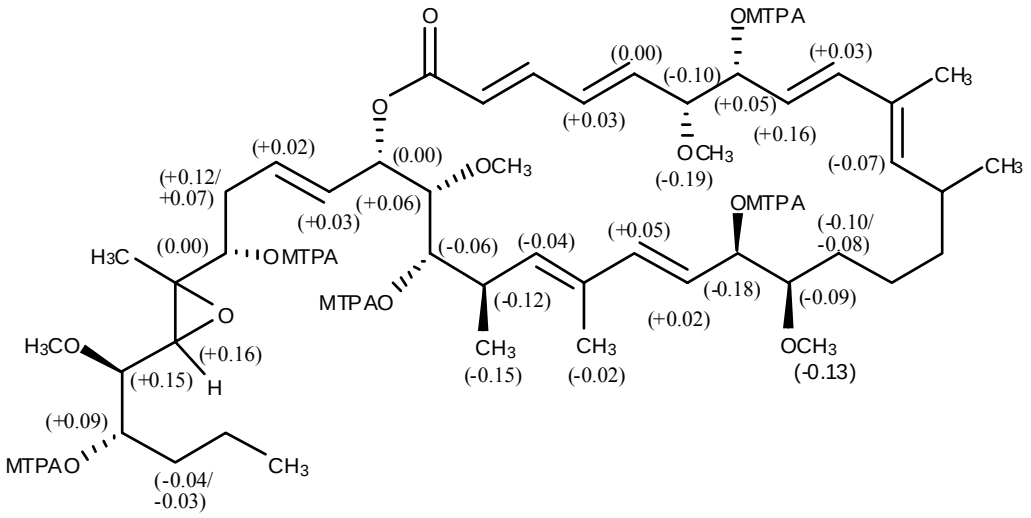

Figure III.26. $\Delta\delta_{S\text{-}R}$ Values for the Penta-MTPA Derivatives of Arenicolide A (39)

As stated earlier, although the Mosher method was originally developed to determine the absolute configuration of monoalcohols, it has been widely applied to polyols.[175-180] Recently, Riguera *et al.* have sought to rigorously validate this approach for the configurational assignment of acyclic 1,2-, 1,3-, 1,4-, and 1,5-diols by examining the combined anisotropy effects of two phenylacetic acid derivatives.[181] In general, it appears that the combined chemical shift differences of the acyloxy protons are indicative of the relative and absolute stereochemistry. The configurations proposed from the Mosher analysis of C-29 and C-33 in the side chain are consistent with the trends noted by Riguera for acyclic systems (Figure III.26). Specifically, the positive $\Delta\delta_{S\text{-}R}$ values for C-29 through C-33 are distinctive of the absolute stereochemistry depicted. While this work begins to address the potential problems

raised by Mosher analysis of a complex polyol, a number of crucial factors, including the different conformational preference of the macrocycle as compared to the acyclic diols and exactly how to parse **39** into diol units, complicate the application of Riguera's predictive models for C-7, C-17, and C-23.

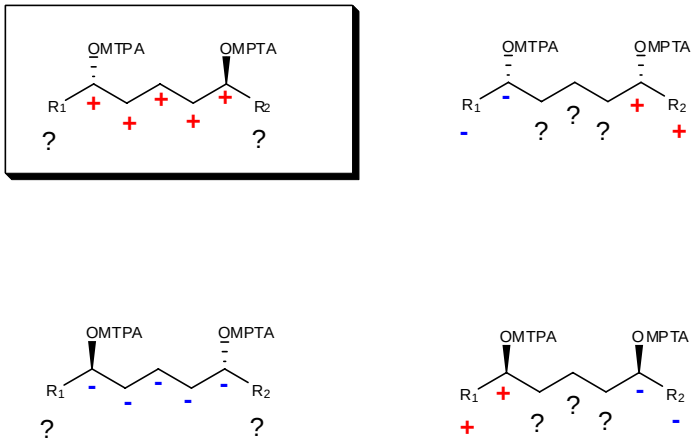

Figure III.27. Predictive $\Delta\delta_{S\text{-}R}$ (+ or -) Patterns for bis-MTPA Derivatives Atoms Labeled "?" Are Not Used for that Configurational Assignment

III.5. Evaluation of the Biological Activity of Arenicolides A-C (39-41)

Given the impressive bioactivity that is often associated with macrolides, Arenicolide A was evaluated in all of the biological assays available to us. Arenicolide A exhibited moderate cytotoxicity toward the human adenocarcinoma cell line HCT-116 (IC_{50} = 30 µg/mL) and all cell lines in the National Cancer Institute's 3-cell line screen. Further testing in the NCI 60-cell line screen was originally deemed unwarranted by the NCI but is currently under reinvestigation. Further, through academic and industrial collaboration, the enzyme target based activity of Arenicolide A is currently being examined in a variety of cancer chemoprevention assays (See:

Chapter I.3) and against also the specific enzymes NF-κB and HDAC (See: Chapter I.3).

III.6. Conclusions and Direction for Future Study

After a thorough search of the literature it became apparent that in the last 10 years, there are no clear examples where the analysis of a poly-MTPA derivative was later conclusively proven wrong by synthesis because of a failure of the Mosher method to account for the combined anisotropy. Far more common are errors relating the stereochemistry of that secondary alcohol to the other stereogenic centers in the molecule, which are responsible for the needed structure revision.[182,183] The problem arises because although examples of molecules whose stereochemistry was determined by multiple Mosher's analysis are common, cases in which those molecules were then synthesized and the stereochemistry corroborated or corrected are quite rare. More data is clearly needed in this area to truly understand the limitation of the technique. Therefore, the absolute configuration of the secondary alcohols derivatized with the Mosher chiral auxiliary in this study are suggested based on the historically more precedented analysis of the $\Delta\delta_{S\text{-}R}$ values directly adjacent to that chiral center.

Finally, while the role of ring-closing metathesis (RCM) and ring-opening metathesis polymerization (ROMP) has been cemented in organic synthesis, the area of olefin cross-metathesis has been slower to develop.[184,185,186] The slow development of the cross metathesis is due in part to the statistical yields of products observed with simple olefins which limits the synthetic utility of the reaction since the yield of any

one product is low.[186] Recently developed guidelines now allow the outcome of cross metathesis reactions to be predicted based on the relative rates of homodimerization of the alkenes using the commercially available ruthenium- and molybdenum-based initiators.[187] For natural product chemists, olefin cross metathesis becomes an attractive alternative to ozonolysis and periodate oxidation of alkenes due to its wide functional group tolerance and comparatively mild reaction conditions. As importantly, we demonstrate here the utility of olefin cross metathesis for the degradation of a single alkene within a polyunsaturated macrolide for the purpose of gross structure determination.[188,189] Thus, using the predictive guidelines for cross metathesis it is now possible to fine tune the regioselectivity to utilize fully this powerful transformation in degradation studies of complex natural products.

III.7. Acknowledgement

Chapter III, in full, was a reprint of material as it appears in The Journal of Organic Chemistry, 2007 *ASAP*, Miller, E.D.; Williams, P.G.; Asolkar, R.N.; Jensen, P.R.; Fenical, W. The dissertation author was primary investigator and author of this paper.

References

(136) Oh, D.C.; Williams, P.; Kauffman, C.; Jensen, P.; Fenical, W. *Org*. *Lett*. **2006**, *8*, 1021-1024

(137) Williams, P.; Asolkar, R.; Kondratyuk, T.; Pezzuto, J.; Jensen, P.; Fenical,.*J*. *Nat*. *Prod*. **2007**, *70*, 83-88

(138) Ratnayake, A. S; Hemscheidt, T. *Org. Lett.* **2002**, *4*, 4667-4669

(139) Calderon, N.; Ofstead, E.; Ward, J.; Judy, W.; Scott, K. *J*. *Am*. *Chem*. *Soc*. **1968**, *90*, 4133

(140) Hérisson, J-L.; Chauvin, Y. *Makromol*. *Chem*.**1971**, *141*, 161

(141) Uemura, D.; Ueda, K.; Hirata, Y.; Katayama, C.; Tanaka, J. *Tetrahedron Lett*. **1980**, *21*, 4861-4864

(142) Cha, J.K.; Christ, W.J.; Fiana, J.M.; Fujioka, H.; Kishi, Y.; Klein, L.L.; Ko, S.S.; Leder, J.; McWhorter, W.W.; Pfaff, K.P.; Yonaga, M.; Uemurar, D.; Hirata, Y. *J*. *Am*. *Chem*. *Soc*. **1982**, *104*, 7369-7371

(143) Mechlinski, W.; Schnaffer, C.P.; Ganis, P.; Avitabile, G. *Tetrahedron Lett*. **1970**, 3873-3876

(144) Ganis, P.; Avitabile, G.; Mechilinski, W.; Schnaffer, C.P. *J*. *Am*. *Chem*. *Soc*. **1971**, *93*, 4560-4564

(145) Kato, Y.; Fusetani, N.; Matsunaga, S.; Hashimoto, K.; Fujita, S.; Furuya, T. *J*. *Am*. *Chem*. *Soc*. **1986**, *108*, 2780-2781

(146) Harmange, J.C.; Boyle, C.D.; Kishi, Y. *Tetrahedron Lett*. **1994**, *35*, 6819-6822

(147) Kitagawa, I.; Kobayashi, M.; Katori, T.; Yamashita, M.; Tanaka, J.; Doi, M.; Ishida, T. *J. Am. Chem. Soc.* **1990**, *112*, 3710-3712

(148) Sakuda, S.; Ono, M.; Furihata, K.; Nakayama, J.; Suzuki, A.; Isogai, A. *J. Am. Chem. Soc.* **1996**, *118*, 7855-7856

(149) Satake, M.; Murata, M.; Yasumoto, T.; Fujita, T.; Naoki, H. *J. Am. Chem. Soc.* **1991**, *113*, 9859-9861

(150) Paul, G.K.; Matsumori, N.; Murata, M.; Tachibana, K. *Tetrahedron Lett.* **1995**, *36*, 6279-6282

(151) Igarashi, T.; Satake, M.; Yasumoto, T. *J. Am. Chem. Soc.* **1996**, *1183*, 479-480

(152) Nakamura, H.; Asari, T.; Murai, A.; Kan, Y.; Kondo, T.; Yoshida, K.; Ohizumi, Y. *J. Am. Chem. Soc.* **1995**, *117*, 550-551

(153) Matsumori, N.; Kaneno, D.; Murata, M.; Nakamura, H.; Tachibana, K. *J. Org. Chem.* **1999**, *64*, 866-876

(154) Marquez, B.L.; Gerwick, W.H.; Williamson, R.T. *Magn. Reson. Chem.* **2001**, *39*, 499-530

(155) Williamson, R.T.; Marquez, B.L.; Gerwick, W.H.; Kover, K.E. *Magn. Reson. Chem.* **2000**, *38*, 265-273

(156) Rychnovsky, S.D.; Rogers, B.; Yang, G. *J. Org. Chem.* **1993**, *58*, 3511-3515

(157) See compound **33** in Tsuboi, K.; Ichikawa, Y.; Naganawa, A.; Isobe, M.; Ubukata, M.; Isono, K. *Tetrahedron* **1997**, *53*, 5083-5102

(158) Chevallier, C.; Bugni, T.S.; Feng, X.; Harper, M.K.; Orendt, A.M.; Ireland, C. M. *J. Org. Chem.* **2006**, *71*, 2510-2513

(159) Westley, J.W.; Evans, R.H.; Harvey, G.; Pitcher, R.G.; Pruess, D.L. Stempel, A.; Berger, J. *J. Antibiot.* **1974**, *27*, 288-297

(160) Cane, D.E.; Celmer, W.B.; Westley, J.W. *J. Am. Chem. Soc.* **1983***, 105*, 3594-3600

(161) Baldwin, J. E. *J. C. S. Chem. Comm.* **1976**, *18*, 734-736

(162) Nicalaou, K.C.; Prasad, C.V.C.; Somer, P.K.; Hwang, C.K. *J. Am. Chem. Soc.* **1989**, *111*, 5335-5340

(163) Valentine, J.C.; McDonald, F.E.; Neiwert, W.A.; Hardcastle, K.I. *J. Am. Chem. Soc.* **2005**, *127,* 4586-4587

(164) Janda, KD.; Shevlin, C.G.; Lerner, R.A. *Science* **1993**, *259*, 490-493

(165) Shimizu, Y. *Natural Toxins* In.: *Animals, Plant and Microbial* J. B. Harris (ed), Clarendon, Oxford, **1986,** p. 123

(166) Nakanishi, K. *Toxicon*. **1985***, **23***, 473-479

(167) Spencer, J.B.; Gallimore, A.R. *Angew. Chem. Int. Ed.* **2006**, *45*, 4406-4413

(168) Payne, G. B. *J. Org. Chem.* **1962**, *27*, 3819-3822

(169) Constantine, K.L.; Mueller, L.; Huang, S.; Abid, S.; Lam, K.S.; Li, W.; Leet, J.E. *J. Am. Chem. Soc.* **2002**, *124*, 7284-7285

(170) Zhao, N.; Zhou, P.; Berova, N.; Nakanishi, K. *Chirality* **1995**, 7, 636-651

(171) MacMillan, J.B.; Molinski, T.F. *J. Am. Chem. Soc*. **2004**, *126*, 9944-9945

(172) MacMillan, J.B.; Linington, R.G.; Andersen, R.J.; Molinski, T. F. *Angew. Chem., Int. Ed*. **2004**, *43*, 5946-5951

(173) Latypov, S.K.; Seco, J.M.; Quiñoá, E.; Riguera, R. *J. Org. Chem.* **1996**, *61*, 8569-8577

(174) Kwon, H.C.; Kauffman, C.A.; Jensen, P.R.; Fenical, W. *J. Am. Chem. Soc.* **2006**, *128*, 1622-1632

(175) Kobayashi, J.; Shimbo, K.; Sato, M.; Shiro, M.; Tsuda, M. *Org. Lett.* **2000**, *2*, 2805-2807

(176) Jansen, R.; Kunze, B.; Reichenbach, H.; Höfle, G. *Eur. J. Org. Chem.* **2000**, *6*, 913-919

(177) Tsuda, M.; Endo, T.; Kobayashi, J. *Tetrahedron* **1999**, *55*, 14565-14570

(178) Yamada, K.; Ueda, K.; Uemura, D. *Tetrahedron Lett.* **1999**, *40,* 6309-6312

(179) Tanahashi, T.; Takenaka, Y.; Nagakura, N.; Nishi, T. *J. Nat. Prod.* **1999**, *62*, 1311-1315

(180) Harrigan, G.G.; Luesch, H.; Yoshida, W.Y.; Moore, R.E.; Nagle, D.G.; Biggs, J.; Park, P.U.; Paul, V. *J. Nat. Prod.* **1999**, *62*, 464-467

(181) Freire, F.; Manuel, J.; Quiñoá,, E.; Riguera, R. *J. Org. Chem.* **2005**, *70*, 3778-3790

(182) Chávez, D.; Acevedo, L.A.; Mata, R. *J. Nat. Prod.* **1998**, *61*, 419-412

(183) Takahashi, S.; Maeda, K.; Hirota, S.; Nakata, T. *Org, Lett.* **1999**, *1,* 2025-2028

(184) Grubbs, R. H. *Tetrahedron* **2004**, *60*, 7117-7140

(185) Connon, S.J.; Blechert, S. *Angew Chem., Int. Ed.* **2003**, *42*, 1900-1923

(186) Astruc, D. *New. J. Chem.* **2005**, *29*, 42–56

(187) Chatterjee, A.K.; Choi, T.L.; Sanders, D.P.; Grubbs, R.H. *J. Am. Chem. Soc.* **2003**, *125*, 11360-11370

(188) Tanaka, K.; Nakanishi, K.; Berova, N. *J. Am. Chem. Soc.* **2003**, *125*, 10802-10803

(189) Tanaka, K.; Itagaki, Y.; Satake, M.; Naoki, H.; Yasumoto, T.; Nakanishi, K.; Berova, N. *J. Am. Chem. Soc.* **2005**, *127*, 9561-9570

IV

Pyridinopyrones: Aromatase Inhibitors from a Marine-Derived Bacterium of the Genus *Streptomyces*

IV.1. Introduction

As mentioned in chapter I.3 inhibition or inactivation of the enzyme aromatase is one of the most successful contemporary achievements in cancer therapy.[53,190,191] Aromatase is the key enzyme involved in the production of estradiol, the most potent estrogen that has long been implicated as a central player in the initiation and promotion of breast cancer. Estradiol is biosynthesized from androgens by the cytochrome P450 enzyme complex aromatase[190] with the highest levels of aromatase being found in the ovaries of premenopausal women, in the placenta of pregnant women and in the peripheral adipose tissues of postmenopausal women and of men.[190] Active aromatase has been identified in breast tissue *in vitro*[192-194] and has also been shown to be most active in or near breast tumor sites.[192, 195] The enzyme complex is bound in the endoplasmic reticulum of the cell and is comprised of two major proteins.[196,197] One protein is cytochrome $P450_{arom}$, a hemoprotein that converts C19 steroids (androgens) into C18 steroids (estrogens) containing a phenolic A ring (Figure IV.1).[196,198] The second protein is NADPH-cytochrome P450 reductase, which transfers reducing equivalents to cytotchrome $P450_{arom}$. Three moles of NADPH and three moles of oxygen are used in the conversion of one mole of substrate into one mole of estrogen product. Aromatization of androstenedione proceeds in three successive oxidation steps, with the first being two hydroxylations of the C-19 methyl group. The final oxidation step proceeds with the aromatization of the A ring of the steroid, and loss of the C-19 carbon atom as formic acid. This third and final step in the aromatase reaction cleaves the C10-C19 bond although the mechanism of this reaction has yet to be elucidated (Figure IV.1).[190]

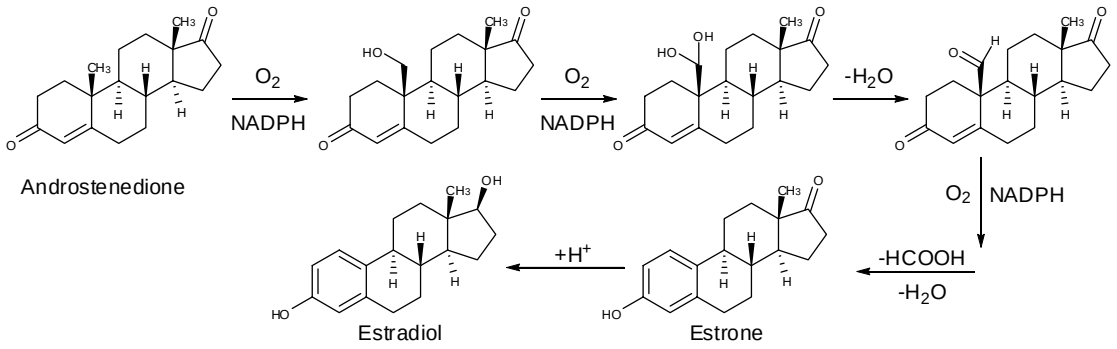

Figure IV.1. Aromatase Mediated Conversion of Androstenedione to Estrone

Two approaches have been developed to control the cancer promoting effects of estrogens on breast cancer cells including: (1) interfering with estrogen binding to its receptor [e.g. tamoxifen (**11**), (See: Chapter I.3)] and (2) decreasing the levels of endogenous estrogen in circulation by inhibition of the enzyme aromatase. Currently the aromatase enzyme is widely accepted as a valid anticancer target and many aromatase inhibitors have been developed that are effective therapeutic agents for controlling breast cancer. The reader is thus referred to several excellent reviews that have been written on the subject.[199-205] Aromatase inhibitors have also been shown to be superior to the estrogen receptor blockers such as tamoxifen in that they lack the significant toxicities associated with that class of molecules. According to their structure, aromatase inhibitors are classified as steroidal and nonsteroidal.[206] The first class, the steroidal inhibitors, are those that compete with the substrate androstenedione for binding to aromatase and are built on the androstenedione pharmacophore. These steroidal inhibitors have a high affinity for the aromatase binding pocket and reversibly inhibit the binding of androstenedione to the aromatase

cytochrome P450 enzyme complex thereby blocking the conversion of androstenediol to estradiol. Several structure activity relationship studies have been conducted on the stereoidal class of aromatase inhibitors in order to enhance the binding affinity to the aromatase enzyme.[207-220] Examples of steroidal aromatase inhibitors include formestane (**45**), 1-methyl ADD (**46**), 7α-APTA (**47**) and 7α-arylaliphaticandrostene (**48**) (Figure IV.2).

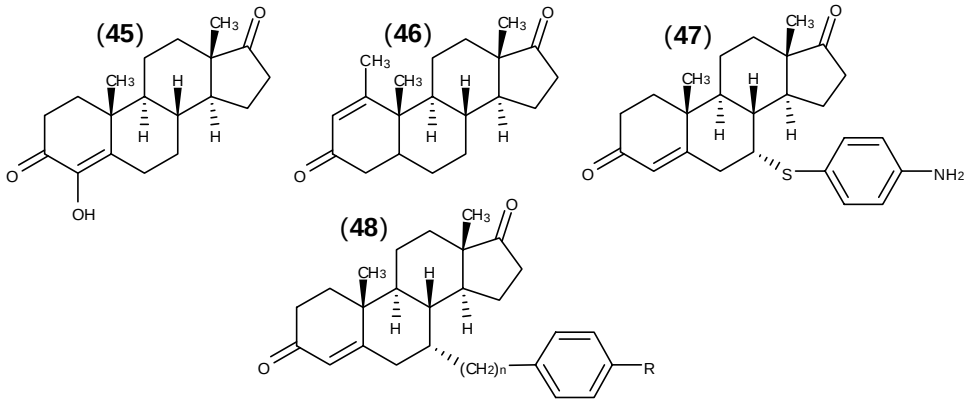

Figure IV.2. Steroidal Inhibitors of the Enzyme Aromatase

The second class of steroidal inhibitors also mimic the substrate androstenedione but upon binding to the aromatase enzyme, are subsequently converted to a reactive intermediate that causes irreversible inhibition of the enzyme.[190] Members of this class of inhibitors share in common a chemical functionality that is acted upon by the enzyme during the normal catalytic process. These mechanism based aromatase enzyme inhibitors produce time-dependent inactivation of the enzyme and require cofactors (e.g. NADPH) in order to deactivate it. Several of these types of inhibitors have also been developed that are all structurally related to androstenedione.

Examples include MDL 18,962 (**49**), exemestane (**50**), 7α-APTADD (**51**) and 7α-PEADD (**52**) (Figure IV.3).[190]

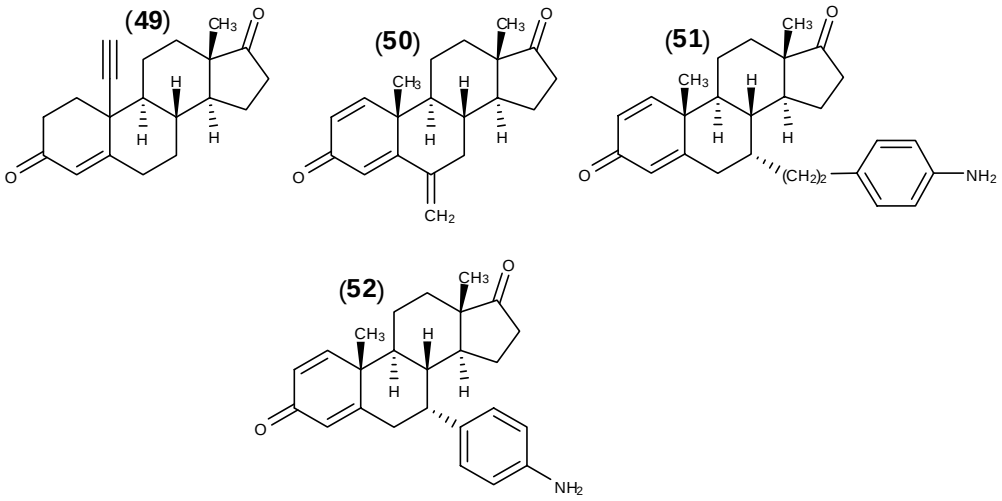

Figure IV.3. Mechanism Based Inhibitors of the Enzyme Aromatase

A third class of aromatase inhibitors, are nonsteroidal in structure and all possess a heteroatom as a common chemical feature. These molecules interfere with steroid hydroxylations via the binding of this heteroatom to the heme iron of the cytochrome P450s.[190] First- and second-generation nonsteroidal inhibitors were nonspecific P450 inhibitors and many side effects were associated with them. Examples of these early generation nonsteroidal aromatase inhibitors include aminoglutethimide (**53**) and fadrazole (**54**) (Figure IV.4). In subsequent years, third-generation nonsteroidal inhibitors containing a triazole ring have been successfully developed and used in the clinic. Examples of clinically accepted, third-generation aromatase inhibitors that contain a triazole ring include anastrozole (**12**) and letrozole (**55**).

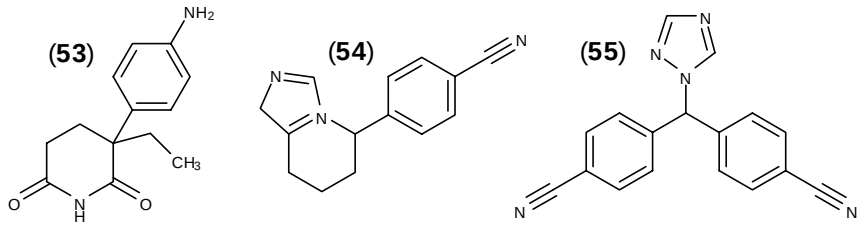

Figure IV.4. Nonsteroidal Inhibitors of the Enzyme Aromatase

Natural products representing several different biosynthetic classes and exhibiting potent aromatase inhibitory activity have also been identified. The majority of these molecules are plant-derived flavanoids that contain a characteristic benzopyranone ring system and include molecules such as chrysin (**56**), apigenin (**57**), biochanin A (**58**), flavone (**59**), flavanone (**60**), quercetin (**61**) and 7,8-benzoflavone (**62**). Many plant-derived fatty acids have also been identified as "interference" compounds exhibiting potent activity in noncellular aromatase assays although their clinical relevance is in question as none have displayed any activity in whole cell based assay systems.[221] Aromatase inhibitors have also been isolated from microbial sources including FR-901537 (**63**) from an unidentified *bacillus* strain[222, 223] and TAN-1085 (**64**) from an unidentified strain belonging to the genus *streptomyces*.[224-226]

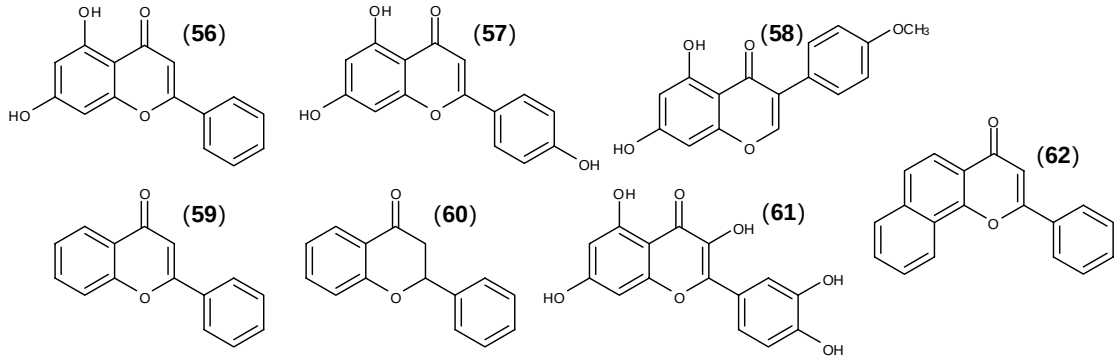

Figure IV.5. Flavanoid-Derived Inhibitors of the Enzyme Aromatase

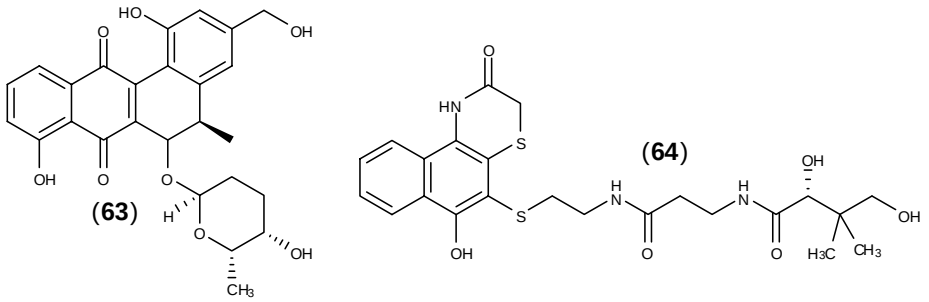

Figure IV.6. Microbially Derived Inhibitors of the Enzyme Aromatase

A significant portion of this thesis research was focused toward the identification of small molecule aromatase inhibitors using marine sediment-derived bacteria as a source for the chemical entities. The beginning of this chapter (section IV.2) is focused on the isolation and structure elucidation of two new molecules, pyridinopyrones A and B [Figure IV.7, (**65**) and (**66**)], that were isolated from the fermentation broth of a marine sediment-derived bacterium of the genus *streptomyces*. Section IV.3 contains the results of a thorough literature search that was initiated to identify known aromatase inhibitors that possessed the same functionalities as the pyridinopyrones (i.e. pyridine ring, conjugated tetraene and γ-pyrone). By focusing on structure activity relationship (SAR) studies that had been done on those molecules we hoped to ascertain the importance of those functionalities to the overall aromatase inhibitory activity of the pyridinopyrones. The ultimate goal of this endeavor was to provide a logical starting point to improve upon the inherent activity of the pyridinopyrones through chemical manipulation. Finally, in section IV.4 a

hypothetical biosynthetic pathway to the pyridinopyrones is formulated based off of what is known of the biosynthesis of compounds of similar structure.

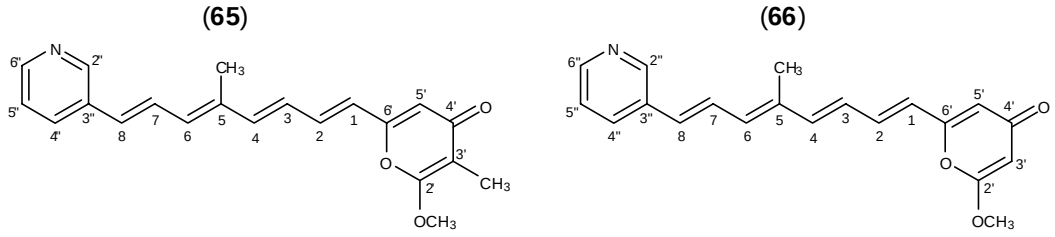

Figure IV.7. Pyridinopyrones A (65) and B (66)

IV.2. Isolation and Planar Structure Elucidation of Pyridinopyrones A (65) and B (66)

Actinomycete strain CNQ301 was isolated from marine sediments at a depth of 40m near San Diego, California. Fermentation in seawater based media followed by organic extraction (acetone/ HP-20 resin) of the resulting culture broth yielded a crude extract that was identified as possessing aromatase inhibitory activity in a whole cell assay.[227] Examination of the crude extract by LCMS revealed several peaks with interesting UV profiles (See: Figure IV.8) that did not match any of the known compounds in the UV profile database. Subsequent target based purification (See Chapter III) led to the isolation of a new class of highly conjugated molecules, the pyridinopyrones, that were later found to be responsible for the overall aromatase inhibitory activity of the extract.

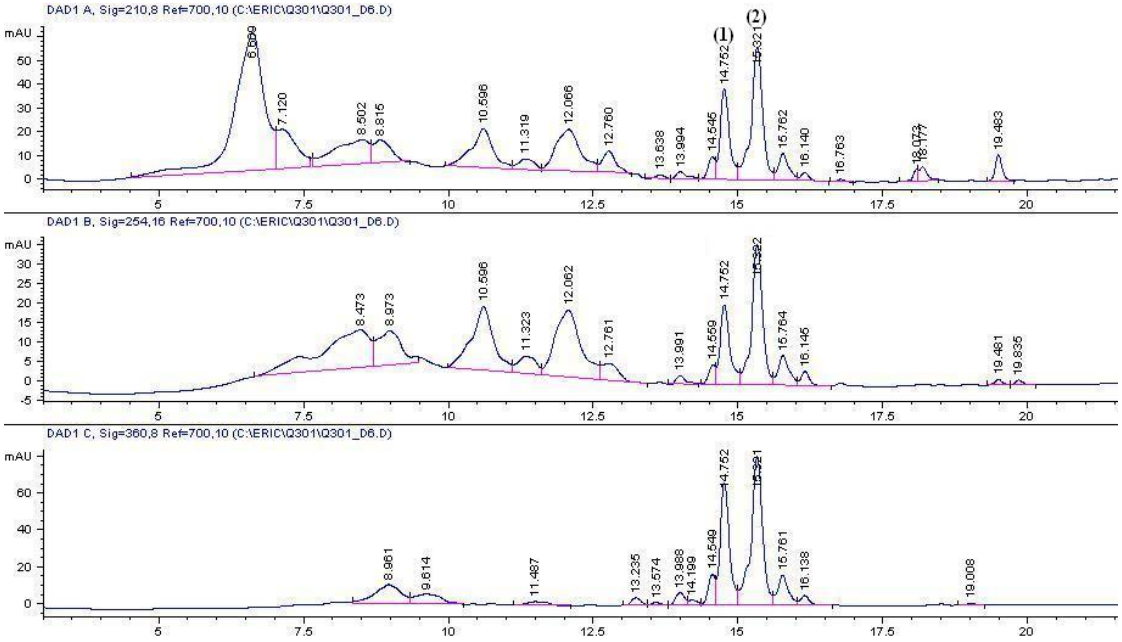

Figure IV.8. LCMS Elution Profile of the Crude Culture Extract Derived from Fermentation of Strain CNQ301 Showing the Presence of Pyridinopyrone B (1) and A (2)

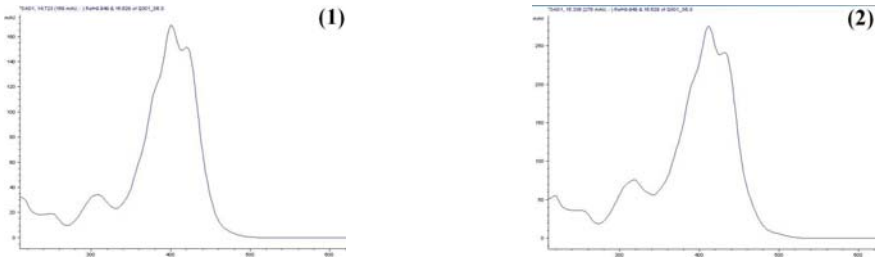

Figure IV.9. Characteristic UV Profiles of Pyridinopyrone B (1) and Pyridinopyrone A (2) Used for Dereplication and Peak Identification During Target Based Isolation

The first molecule to be isolated, pyridinopyrone A (**65**) was purified from the crude culture extract by normal phase (Si) column chromatography followed by reversed phase (C_{18}) HPLC [(52% CH_3CN:H_2O), **65** t_R = 41 min]. In the purified form, **65** was obtained as a yellow powder that analyzed for the molecular formula $C_{21}H_{21}NO_3$ by HRESIMS [$(M+H)^+$ m/z = 336.1589] and careful analysis of the ^1H and ^{13}C NMR spectral data. The UV spectrum displayed an absorbtion band at 394 nm that was suggestive of a highly conjugated polyene. Interpretation of ^1H, ^{13}C and gHSQC spectral data allowed all protons to be assigned to their respective carbons indicating that all of the heteroatoms designated by the molecular formula were un-protonated.

The presence of a substituted γ-pyrone in **65** was proposed following the observation of correlations within the respective gHMBC spectrum extending from a methine proton singlet [$\delta_{H\text{-}5'}$ 6.66 (1H, s), $\delta_{C\text{-}5'}$ 96.6] to a quaternary carbon C-3' ($\delta_{C\text{-}3'}$ 100.6), a carbonyl carbon C-4' ($\delta_{C\text{-}4'}$ 165.9), and an additional quaternary carbon C-6' ($\delta_{C\text{-}6'}$ 156.9). A characteristic signal in the IR spectrum of **65** at 1650 cm^{-1} was also supportive of a γ-pyrone moiety.[226, 228] Additional structural insight was gained from the observation of correlations within the gHMBC NMR spectrum originating from a methyl group, C-3'Me [$\delta_{H\text{-}C3'Me}$ 1.81 (3H, s), $\delta_{C\text{-}C3'Me}$ 8.8] to carbons C-2' ($\delta_{C\text{-}2'}$ 163.4), C-3' and C-4' and from the protons of a methoxyl group, [$\delta_{H\text{-}C2'OMe}$ 3.90 (3H, s), $\delta_{C\text{-}C2'OMe}$ 56.7], to C-4'. Further gHMBC correlations were observed from the protons of a *trans* olefin [$\delta_{H\text{-}1}$ 6.41 (1H, dd, J = 15.5 Hz), $\delta_{C\text{-}1}$ 122.6] and [$\delta_{H\text{-}2}$ 7.11 (1H, dd, J = 15.5, 11.0 Hz), $\delta_{C\text{-}2}$ 134.8] to C-6' ($\delta_{C\text{-}6'}$ 156.9). Taken together, the spectral data

indicated that the γ-pyrone in **65** was methoxylated at C-2', methylated at C-3' and bound to a *trans* olefin at C-6' (Figure IV.7).

The *trans* olefin bound to C-6' of the γ-pyrone was extended to a conjugated *trans* diene [$\delta_{H\text{-}1}$ 6.41 (1H, dd, J = 15.5 Hz), $\delta_{C\text{-}1}$ 122.6], [$\delta_{H\text{-}2}$ 7.11 (1H, dd, J = 15.5, 11.0 Hz), $\delta_{C\text{-}2}$ 134.8], [$\delta_{H\text{-}3}$ 6.59 (1H, dd, J = 15.5, 11.0 Hz), $\delta_{C\text{-}3}$ 127.8], [$\delta_{H\text{-}4}$ 6.79 (1H, dd, J = 15.5, 2.0 Hz), $\delta_{C\text{-}4}$ 142.2] by interpretation of signals present in the ^{1}H, ^{13}C, *J*-resolved, COSY and gHMBC NMR spectral data of **65**. Additional correlations within the gHMBC spectrum of **65** extending from the protons of a methyl group [($\delta_{H\text{-}C5Me}$ 2.05 (3H, d, J = 2.0 Hz), $\delta_{C\text{-}C5Me}$ 12.6] to C-4 and a quaternary carbon, C-5 ($\delta_{C\text{-}5}$ 137.0) and the observation that the methyl group was allylically coupled to H-4 (J = 2.0 Hz) indicated that a methylated, quaternary carbon (C-5), was present in the conjugated chain. Interpretation of additional correlations within the ^{1}H, *J*-resolved, COSY and gHMBC NMR spectra of **65** [($\delta_{H\text{-}6}$ 6.49 (1H, d, J = 11.5 Hz), $\delta_{C\text{-}6}$ 134.3], [$\delta_{H\text{-}7}$ 7.46 (1H, dd, J = 15.5, 11.5 Hz), $\delta_{C\text{-}7}$ 127.4], [$\delta_{H\text{-}8}$ 6.76 (1H, d, J = 15.5 Hz), $\delta_{C\text{-}8}$ 130.5] indicated that **65** contained an all *trans*, conjugated tetraene with methylation at C-5 as shown in figure IV.7.

The presence of 3-substituted pyridine ring was proposed following the observation of characteristic signals within the ^{1}H, *J*-resolved, and ^{13}C NMR spectra of **65** [$\delta_{H\text{-}2''}$ 8.67 (1H, d, J = 3.5 Hz), $\delta_{C\text{-}2''}$ 148.1], ($\delta_{C\text{-}3''}$ 130.6), [$\delta_{H\text{-}4''}$ 8.04 (1H, dt, J = 8.0, 2.0 Hz), $\delta_{C\text{-}4''}$ 132.8], [$\delta_{H\text{-}5''}$ 7.37 (1H, dd, J = 8.0, 5.0 Hz), $\delta_{C\text{-}5''}$ 123.6], [$\delta_{H\text{-}6''}$ 8.42 (1H, dd, J = 5.0, 2.0), $\delta_{C\text{-}6''}$ 148.4], interpretation of correlations within the gHMBC and COSY

spectral data (Table IV.1) and the fact that a nitrogen atom had yet to be assigned from the molecular formula. Correlations within the gHMBC spectrum of **65** from H-4" and H-2" to C-3" and from H-8 to C-2", C-3", C-4" and C-5" indicated that the conjugated tetraene in **65** was bound to the pyridino moiety at the 3-position thereby completing the structure as shown in figure IV.7.

Pyridinopyrone B (**66**) eluted from the C_{18} reversed phase HPLC column prior to **65** [(52% CH_3CN:H_2O), **66** t_R = 33 min] and was assigned the molecular formula $C_{20}H_{19}NO_3$ by HRESIMS [$(M+H)^+$ m/z = 322.1439] and careful analysis of the ^1H and ^{13}C NMR spectral data which together indicated that **66** was 14 amu smaller than **65**. Comparison of the ^1H and ^{13}C NMR spectra of **65** and **66** (See Table IV.3) established that pyridinopyrone B (**66**) was the C-3' desmethyl isomer of pyridinopyrone A (**65**). Specifically, the ^1H and ^{13}C NMR spectra of **66** did not contain the characteristic signals corresponding to the C-3' methyl substituent (C-3'Me) that were present in the ^1H and ^{13}C NMR spectra of **65**. In addition, the ^1H and ^{13}C NMR spectra of **66** contained a new methine signal, C-3' [$\delta_{H\text{-}3'}$ 5.61 (1H, d, J = 2.0 Hz), $\delta_{C\text{-}3'}$ 88.5] not present in the spectra of **65**. Further, the corresponding proton of this new methine, H-3' exhibited gHMBC correlations to C-2', C-4' and C-5' (Table IV.2) thus confirming the structure of **66** as shown in figure IV.7.

Table IV.1. NMR Spectral Data for Pyridinopyrone A (65) in DMSO-d_6 (500MHz) 25°C

Carbon #	δ_H mult ($^3J_{HCCH}$, Hz)	δ_C, DEPT	gHMBC	gCOSY
2'	NA	163.4, C	NA	NA
3'	NA	100.6, C	NA	NA
4'	NA	165.9, C	NA	NA
5'	6.66, s	96.6, CH	C3', C4', C6', C1	NA
6'	NA	156.9, C	NA	NA
1	6.41, d (15.5)	122.6, CH	C5', C6', C2, C3	H2
2	7.11, dd (15.5, 11.0)	134.8, CH	C6', C4	H1, H3
3	6.59, dd (15.5, 11.0)	127.8, CH	C1, C2, C4, C5	H2, H4
4	6.79, d (15.5)	142.2, CH	C6, C7	H3
5	NA	137.0, C	NA	NA
6	6.49, d (11.5, 2.0)	134.3, CH	C4, C7, C8	H7, H5Me
7	7.46, dd (15.5, 11.5)	127.4, CH	C5, C6	H6, H8
8	6.76, d (15.5)	130.5, CH	C2",C4", C5"	H7, H5", H5Me
2"	8.67, dd(2.0, 2.0)	148.1, CH		H4"
3"	NA	130.6	NA	NA
4"	8.04, ddd (8.0, 2.0, 2.0)	132.8, CH	C8, C6"	H2", H5", H6"
5"	7.37, dd (8.0, 5.0)	123.6, CH	C4", C6"	H4", H6"
6"	8.42, dd (5.0, 2.0)	148.4, CH		H4", H5"
5Me	2.05, d (2.0)	12.6, CH_3	C4, C5	NA
2'OMe	3.90, s	56.7, CH_3	C4'	NA
3'Me	1.81, s	8.8, CH_3	C2', C3', C6'	NA

* All multiplicity reported as obtained by interpretation of *J*-resolved NMR

Table IV.2. NMR Spectral Data for Pyridinopyrone A (66) in DMSO-d_6 (500MHz) 25°C

Carbon	δ_H mult (*J* in Hz)	δ_C, DEPT	gHMBC	gCOSY
2'	NA	162.6, C	NA	NA
3'	5.61, d (2.0)	88.5, CH	C2', C4', C5'	H5'
4'	NA	170.8, C	NA	NA
5'	6.26, d (2.0)	100.9, CH	C3', C4', C6', C1	H3'
6'	NA	158.3, C	NA	NA
1	6.39, d (15.5)	122.3, CH	C5', C6', C2	H2
2	7.10, dd (15.5, 11.0)	135.4, CH	C6', C5, C5Me	H1, H3
3	6.57, dd (15.5, 11.0)	128.2, CH		H2, H4
4	6.80, d (15.5)	142.5, CH	C2, C3	H2, H3
5	NA	130.6, C	NA	NA
6	6.49, dd (11.5, 2.0)	134.4, CH	C4, C5, C5Me	H7
7	7.46, dd (15.5, 11.0)	123.7, CH		H6, H8
8	6.76, d (15.5)	130.1, CH	C4", C2"	H7
2"	8.72, dd (2.0, 2.0)	148.4, CH	C3", C4", C6"	NA
3"	NA	130.6, C	NA	NA
4"	8.05, ddd (8.0, 2.0, 2.0)	132.9, CH	C3", C6", C2"	H5"
5"	7.37, dd (8.0, 5.0)	123.5, CH	C4", C6"	H4", H6"
6"	8.42, d (5.0)	148.3, CH	C4", C2"	H5"
5Me	2.04, d (2.0)	12.6, CH3	C2, C5	NA
2'OMe	3.82, s	56.4, CH3	C3', C4'	NA

* All multiplicity obtained by interpretation of *J*-resolved NMR spectral data

Table IV.3. ^{1}H and ^{13}C NMR Spectral Data for 65 and 66 in DMSO-d_6 (500MHZ) 25°C

Carbon #	Pyridinopyrone A δ_C, DEPT	Pyridinopyrone B δ_C, DEPT	Pyridinopyrone A δ_H mult ($^3J_{HCCH}$, Hz)	PyridinopyroneB δ_H mult ($^3J_{HCCH}$, Hz)
2'	163.4, C	162.6, C	NA	NA
3'	100.6, C	88.5, CH	NA	5.61, d (2.0)
4'	165.9, C	170.8, C	NA	NA
5'	96.6, CH	100.9, CH	6.66, s	6.26, d (2.0)
6'	156.9, C	158.3, C	NA	NA
1	122.6, CH	122.3, CH	6.41, d (15.5)	6.39, d (15.5)
2	134.8, CH	135.4, CH	7.11, dd (15.5, 11.0)	7.10, dd (15.5, 11.0)
3	127.8, CH	128.2, CH	6.59, dd (15.5, 11.0)	6.57, dd (15.5, 11.0)
4	142.2, CH	142.5, CH	6.79, d (15.5)	6.80, d (15.5)
5	137.0, C	130.6, C	NA	NA
6	134.3, CH	134.4, CH	6.49, d (11.5, 2.0)	6.49, dd (11.5, 2.0)
7	127.4, CH	123.7, CH	7.46, dd (15.5, 11.5)	7.46, dd (15.5, 11.0)
8	130.5, CH	130.1, CH	6.76, d (15.5)	6.76, d (15.5)
2"	148.1, CH	148.4, CH	8.67, dd(2.0, 2.0)	8.72, dd (2.0, 2.0)
3"	130.6	130.6, C	NA	NA
4"	132.8, CH	132.9, CH	8.04, ddd (8.0, 2.0,	8.05, ddd (8.0, 2.0, 2.0)
5"	123.6, CH	123.5, CH	7.37, dd (8.0, 5.0)	7.37, dd (8.0, 5.0)
6"	148.4, CH	148.3, CH	8.42, dd (5.0, 2.0)	8.42, d (5.0)
5Me	12.6, CH_3	12.6, CH3	2.05, d (2.0)	2.04, d (2.0)
2'OMe	56.7, CH_3	56.4, CH3	3.90, s	3.82, s
3'Me	8.8, CH_3	NA	1.81, s	NA

IV.3. Known Aromatase Inhibitors: Structure Activity Relationships and the Potential for Improving the Activity of the Pyridinopyrones

When tested in its purified form, pyridinopyrone A exhibited aromatase enzyme inhibitory activity with an IC_{50} = 20μg/mL. In contrast, the clinically accepted aromatase inhibitor anastrozole (**12**) exhibits an order of magnitude greater potency (IC_{50} = 15nM) in an *in vitro* aromatase inhibition assays.[229] Although this comparison may be somewhat misleading due to the fact that the assays are being run under different conditions in different laboratories, the order of magnitude difference serves to show the need to improve upon the efficacy of the pyridinopyrones if they are to become clinically relevant molecules. This desire to improve activity combined with the relatively simple chemical scaffold of the pyridinopyrones provides ample reason

to pursue chemical transformation and structure activity experiments (SAR). An exhaustive examination of the literature was therefore conducted in an effort to ascertain what role the respective functionalities (e.g. pyridine, conjugated tetraene, γ-pyrone) contained within the pyridinopyrones were playing in the overall aromatase inhibitory activity of other molecules containing those functionalities. The ultimate goal of this endeavor was to use this information to formulate logical starting points for chemical manipulation of the pyridinopyrone scaffold in order to improve the inherent activity of the natural product.

Upon initial examination of the literature it becomes apparent that the majority of competitive, non-steroidal aromatase inhibitors (e.g. Figure IV.4), possess a heteroatom that is reported to interfere with hydroxylation of androstenedione by coordinating with the heme iron of aromatase.[190] Although several heteroatoms such as sulfur, oxygen and nitrogen are known to show abilities to bind to heme iron, the majority of compounds in this class possess a nitrogen-containing heterocyclic moiety such as imidazole, triazole, pyrimidine or pyridine.[230] To continue, the structures of these third-generation aromatase inhibitors [e.g. anastrozole (**12**) and letrozole (**55**)] can be regarded as consisting of two parts, one being the azole part with the nitrogen atom which binds to the heme iron atom of cytochrome P450 on aromatase and the other, the bulky aryl part which mimics the steroid ring of the natural substrate androstenedione.[231] The common structural moieties of the third-generation inhibitors include (1) the presence of a free amine in the triazole ring system, which coordinates

the heme iron and (2) a flat aromatic ring that can fill the same volume as the A ring of androstenedione.[232]

Additional research using isoflavones as a substrate for chemical modification suggest that the substitution at the 2-position of the isoflavone scaffold with a (pyridylmethyl)thio functionality plays a key role in inhibiting the aromatase enzyme as molecules that do not contain this functionality are completely inactive.[233] The authors go on to assert that the position of the nitrogen atom in the pyridyl moiety is important for inhibitory activity with the 4'-pyridyl analog being more potent than the 3'-pyridyl analog that in turn is more potent that the 2'-pyridyl analog. Further, the effect that the position of the pyridyl nitrogen atom had on aromatase inhibitory activity when bound via a thio linkage to the 2-position of the tested isoflavones was evident regardless of substitution at other positions on the isoflavone core.

A literature search with the goal of understanding the aromatase inhibitory role of the tetraene yielded no results in terms of SAR studies. However, some information was gained from a report in which several fatty acids of varying chain lengths and degrees of unsaturation were analyzed for their aromatase inhibitory activities.[221] The authors concluded that in an *in vitro* aromatase inhibition assay, the saturated fatty acids showed no significant inhibitory activity while the majority of the unsaturated fatty acids did display some degree of activity. However, in fatty acids of identical chain length (e.g. 18, 20 or 22 carbons) there was no significant difference observed between molecules with differing degrees of unsaturation. These results indicated that within the fatty acid class of natural products, although unsaturation is important, the

degree of unsaturation has no significant effect on aromatase inhibitory activity. An additional report that tested the aromatase inhibitory activity of a series of synthetic, acylated nornicotines and anabasines, showed an interesting correlation of activity with length of the acyl carbon chain with maximum activity being associated with chain lengths of 11 carbons.[234]

In addition to the previously discussed molecules, the activity of another tetraene, fenretinide [*N*-(4-hydroxyphenyl) retinamide], [Figure IV.10 (**67**)] was examined due to the fact that its structure is very similar to that of the pyridinopyrones. The molecule fenretinide is a synthetic version of retinoic acid [Figure IV.10 (**68**)] and exhibits potent acitivity against estradiol receptor positive (ER+) MCF-7 breast cancer cells.[235] In addition **67** has been shown to be more effective in reducing the reoccurrence of breast cancer in post-menopausal women as compared to pre-menopausal women.[236] In later studies, fenretinide was found to have a multifactorial inhibitory effect on the aromatase enzyme.[237] Specifically, fenretinide was found to increase the K_m of the substrate androstenedione indicating that fenretinide was a competitive inhibitor of the endogenous substrate. However, these studies also concluded that V_{max} of the binding reaction was decreased in the presence of fenretinide suggesting that non-competitive inhibition was also a factor. Additional studies indicated that fenretinide also interfered with transcription of the aromatase enzyme itself. Although these studies provide insight into a possible mode of action for the pyridinopyrones, an assessment of the structure activity relationships of

fenretinide with respect to its aromatase inhibitory activity, to the best of our knowledge, does not exist.

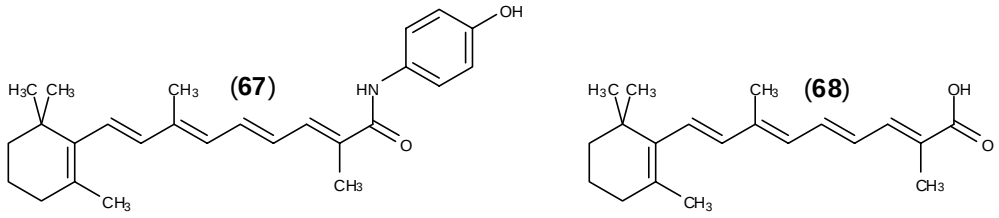

Figure IV.10. Chemical Structures of Fenretinide (67) and Retinoic Acid (68)

Finally, a search of the literature with the goal of understanding the aromatase inhibitory role of the γ-pyrone moiety yielded no results in terms of SAR studies save those reported within the context of the flavonoids.[190,230,233] Because the γ-pyrone functionality in the flavanoids is always found in the form of a benzopyranone, extensive analysis of the SAR studies conducted in the cited references is deemed unwarranted in the context of this section.

In conclusion, the aforementioned literature survey of similar molecules revealed several interesting aspects of the chemical structure of the pyridinopyrones with regard to their aromatase inhibitory activity. Deconstructing the pyridinopyrones into two units,[232] the first being the heme deactivating pyridine and the second being the possibly androstenedione-like tetraene/γ-pyrone functionality allows for logical starting points for SAR to be formulated. First and possibly most important is the presence of the pyridine ring that due to its incorporation of a tertiary nitrogen atom may be responsible for complexing of the aromatse heme iron and therefore essential to activity. Potency of the pyridinopyrones may be improved by altering the position

of alkyl substitution from the 3' to the 4' position[233] or by substituting the pyridine ring with another nitrogen containing substituent such as a triazole.[200]

Further, chain length may also increase activity as was found to be the case in the acylated nornicotine and anabasine derivatives.[234] Assuming that the γ-pyrone functions as some sort of androstenedione A-ring mimic (see below), the tetraene functionality may serve as a molecular tether connecting the A ring mimic to the heme deactivating pyridine moiety. Therefore alterations in chain length, degree of unsaturation and configuration of the olefins may have drastic effects on the orientation of the pyridine ring and thus its ability to deactivate the heme iron. The degree and type of olefin substitution may also have an effect on the aromatase inhibitory activity of the pyridinopyrones

As mentioned in the previous paragraph, it is possible that the γ-pyrone moiety may be acting as a mimic of the androstenedione A ring thus allowing for binding to the aromatase enzyme prior to heme inhibition.[232] Modification of the γ-pyrone substitution pattern or replacement of the γ-pyrone with a benzopyranone as is the case with the flavanoids may also improve activity. [190,230,233]

Finally, all of the above arguments were formulated based on the premise that the pyridinepyrones are acting as post-transcriptional inhibitors of the enzyme aromatase. Based on what is known about the aromatase inhibitory activity of fenretinide (**67**) as mentioned in the previous paragraph, and its structural similarity to the pyridinopyrones, it is also with the realm of reason to postulate that the

pyridinopyrones may be acting as inhibitors of aromatase transcription. Therefore, it is suggested that future analyses of molecules synthesized for SAR studies be tested in assays that are relevant to transcriptional inhibitors to ensure that this possibility is accounted for.

Photoinduced rearrangement is another possible method for generating new molecules based on the pyridinopyrone scaffold for testing in the aromatase system. It is well known that polyketide-derived polyene systems, in particular those equipped with strong chromophores, easily undergo light-induced photoisomerization which can lead to rearrangement cascades that often result in the formation of multiple new carbon skeletons.[238-240] In the case of neoaureothin (**69**),[238] Müller et al. were able to show that upon exposure to daylight, neoaureothin undergoes rearrangement to an *E*,*Z*,*Z*,*Z*-tetraene intermediate that forms a rare bicyclo[4.2.0]octadiene through an 8π-6π electrocyclization cascade the products of which undergo a subsequent retro-[2+2] cycloadditon to form the novel compound orinocin (**70**), (Figure IV.11).

Given the structural similarity of neoaureothin (**69**) and the pyridinopyrones (**65-66**) it is reasonable to assume that photoinduced rearrangement of the **65** and **66**, if present, would follow the same mechanism as that of **69** and a hypothetical mechanism for the photoinduced rearrangement of **66** from extrapolation of the mechanism proposed for **69** is presented in figure IV.12. This realization of the potential for photoinduced rearrangement coupled with the early observation that the pyridinopyrones undergo some form of chemical transformation in ambient sunlight, led us to investigate the photoreactivity of pyridinopyrone B (**66**)

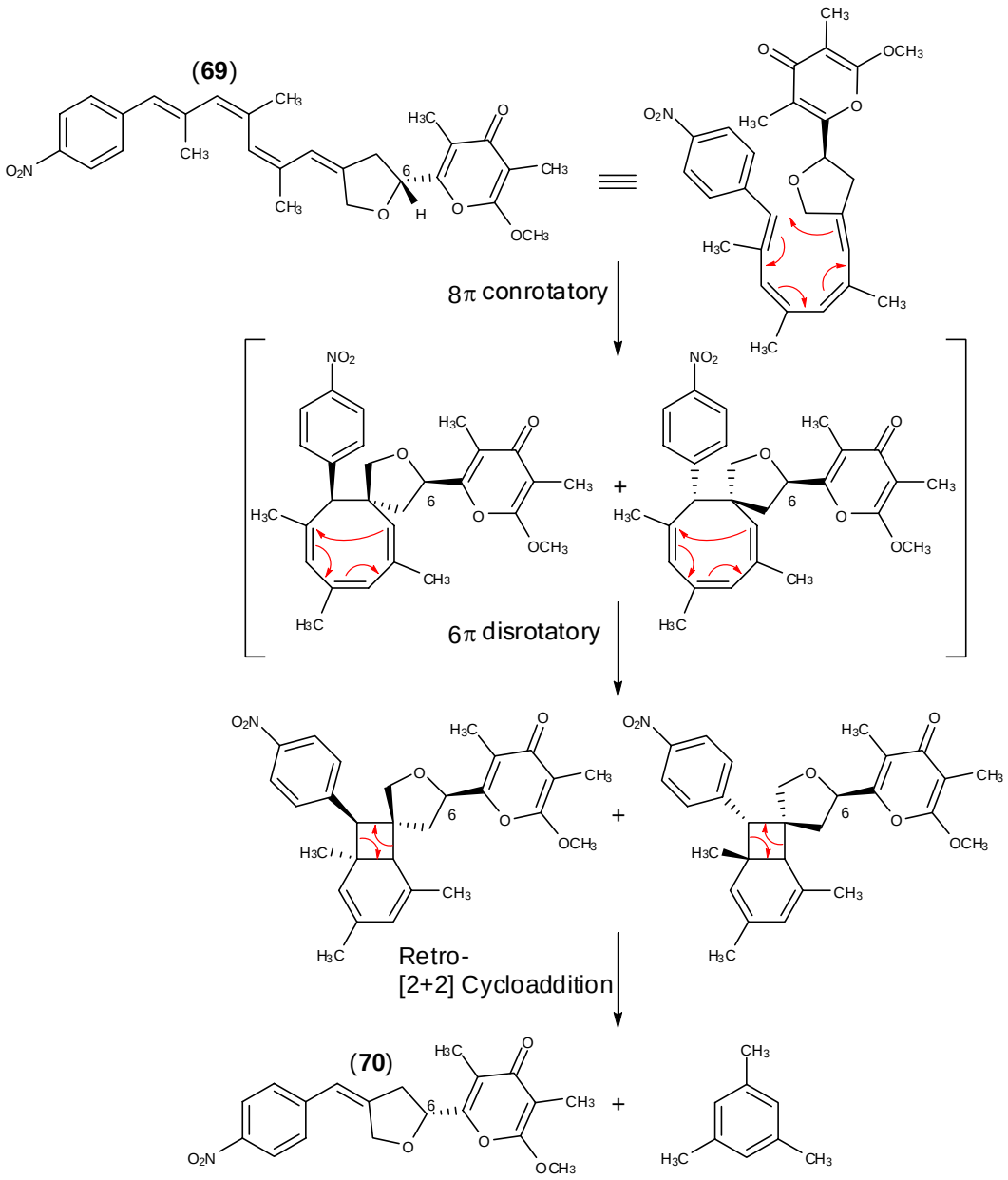

Figure IV.11. Photoinduced Electrocyclic Rearrangement Cascade Neoaureothin (69)

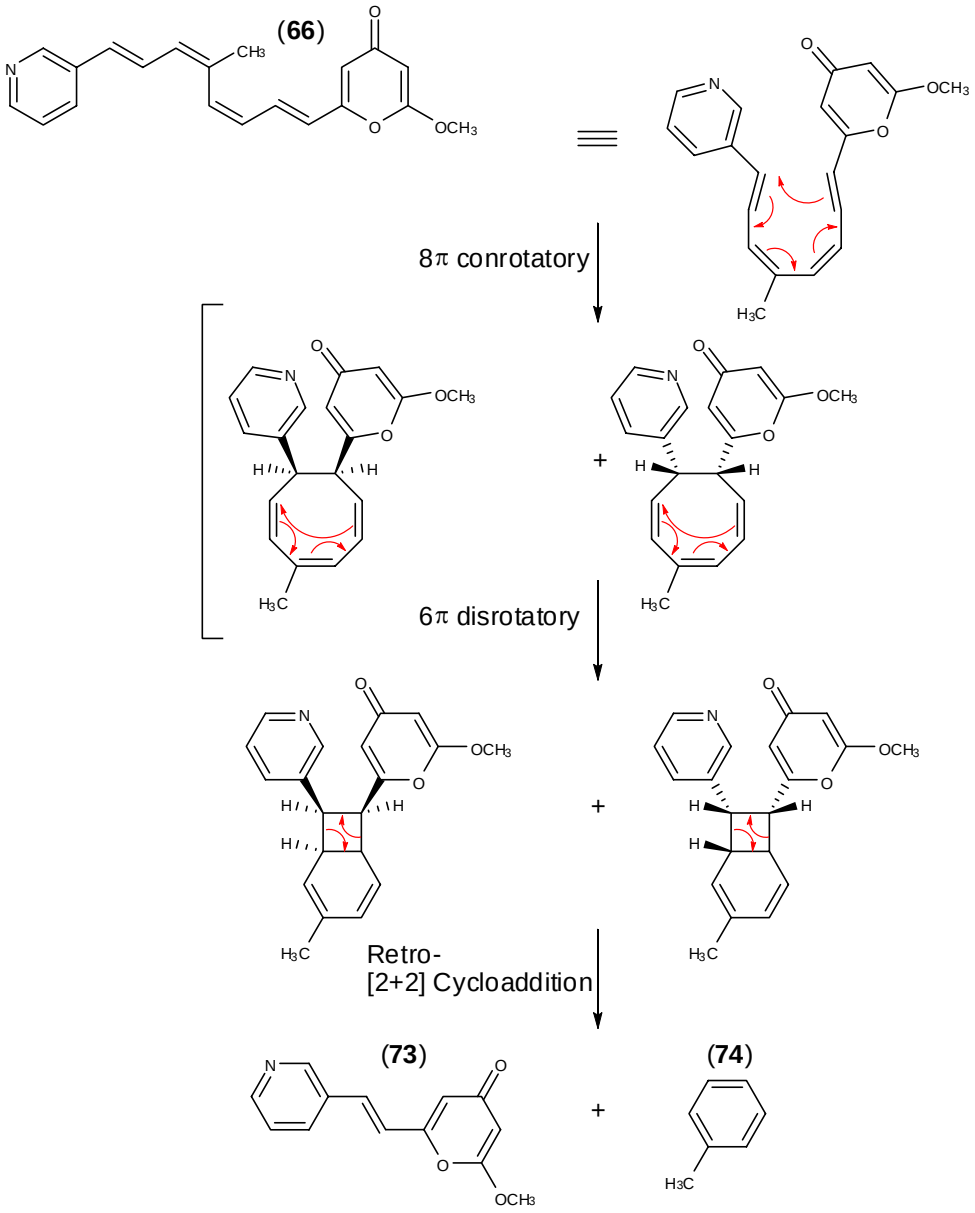

Figure IV.12. Hypothetical Photoinduced Electrocyclic Rearrangement Cascade for Pyrdinopyrone A (66)

The potential of photoinduced rearrangement to generate novel carbon skeletons derived from the pyridinopyrone B (**66**), was first examined by placing a small amount

of **66** (5.0mg/mL, CH_3CN) into a borosilicate glass tube and exposing it to daylight. The reaction was monitored via LCMS with UV detection at 210 and 254nm the results of which are shown in Figure IV.13. Although some apparently photoinduced degradation appears to have occurred (Figure IV.13), a significant amount starting material remained in the reaction mixture even after the 20day incubation period. Further, following intense scrutiny of the mass spectrum, no peak with a mass corresponding to what would be expected from the endpoint of the photochemical rearrangement cascade shown in figure IV.10 could be identified (e.g. (**73**) $[M+H]^+$ m/z = 230, [M+Na] m/z = 252), (e.g. (**74**) $[M+H]^+$ m/z = 93, [M+Na] m/z = 115). However, it is interesting to note that the UV spectrum of many of the peaks contained within the reaction mixture exhibited a λ_{max} that was hypsochromically shifted from that of the starting material (λ_{max} = 394nm) possibly indicating the loss of some degree of conjugation as would be expected in a photoinduced cyclization (Figure IV.14). It is also interesting to note that in several instances [e.g. peaks (4)-(8)], masses larger than that that of the starting material were observed [i.e. (4) = 355, (5-8) = 353] indicating that some other atoms had been incorporated into the structure of the starting material during the photochemical rearrangement.

In an attempt to increase the yield and shorten reaction time, a second experiment was undertaken wherein a sample of **66** (5.0mg/mL, CH_3CN) was placed in another borosilicate glass tube and exposed directly to UV light (350nm). Following a 12hr incubation period, LCMS analysis revealed the starting material had been completely consumed and the resulting mixture contained multiple new products (Figure IV.15).

The LCMS elution profile of the second reaction is shown in Figure IV.15 and the UV profiles of selected peaks contained within the products of the reaction are shown in figure IV.16. It is noteworthy that both photochemical reactions produced peaks with identical retention times and UV profiles [e.g. Figure IV.14 (**1**), (**2**), (**3**); Figure IV.16. (**1**), (**2**), (**3**)] and that the same increase in mass was also observed in selected products from both reactions.

At the time of writing, complete structural characterization of the products by spectral methods has been initiated. Hopefully these studies will able to provide insight into the overall photo-reactivity of the pyridinopyrones to fully understand the photochemical reactivity of this interesting new class of compounds.

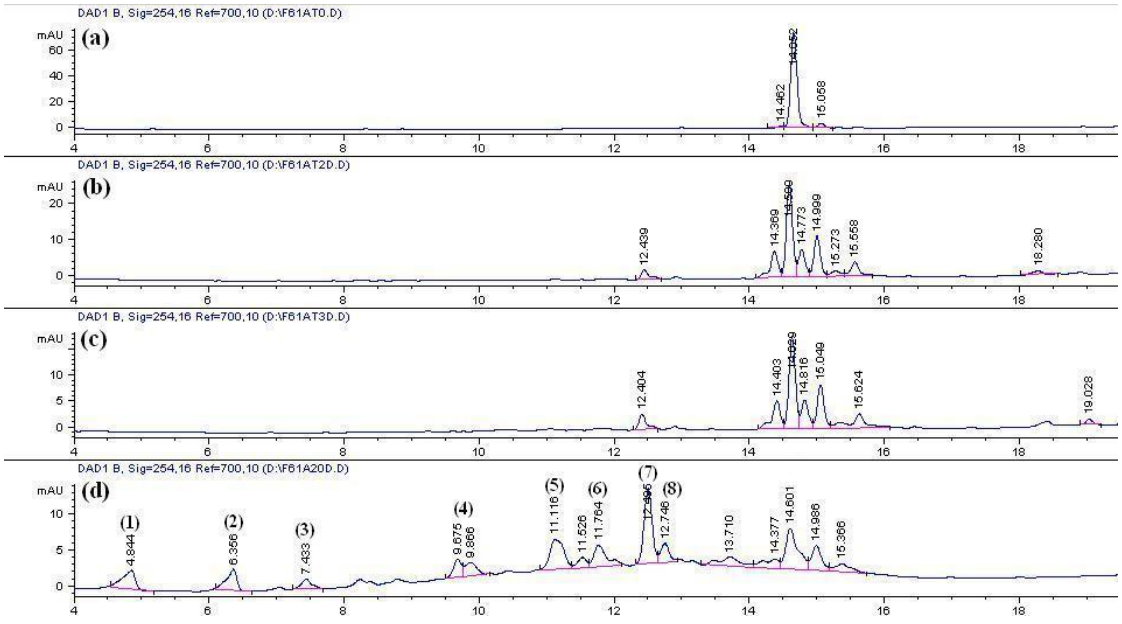

Figure IV.13. LCMS Elution Profile of Products from Ambient Light Photoinduced Rearrangement Experiment

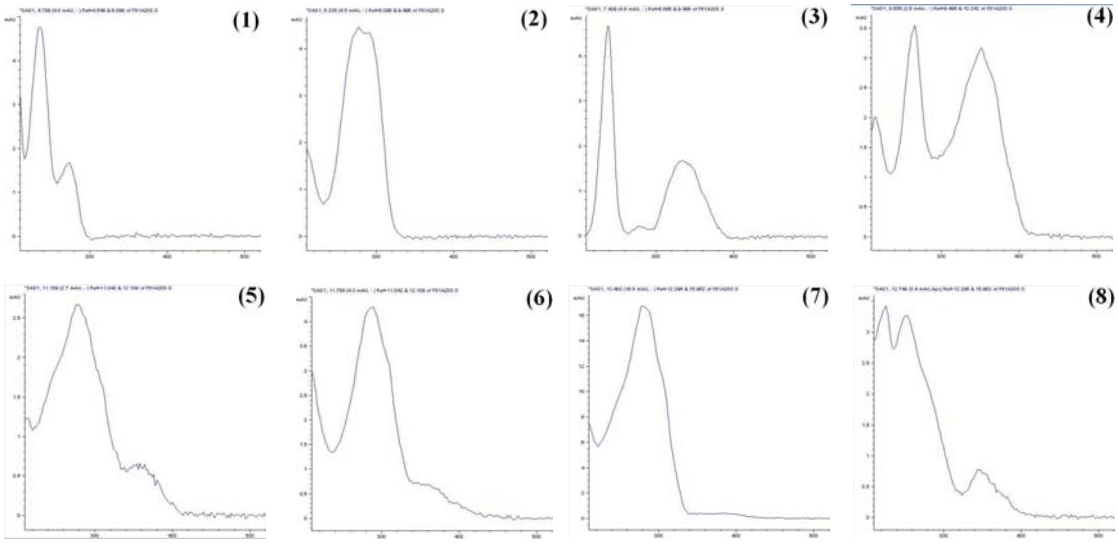

Figure IV.14. UV Profiles of Selected Products From Ambient Light Photo-induced Rearrangement Experiment

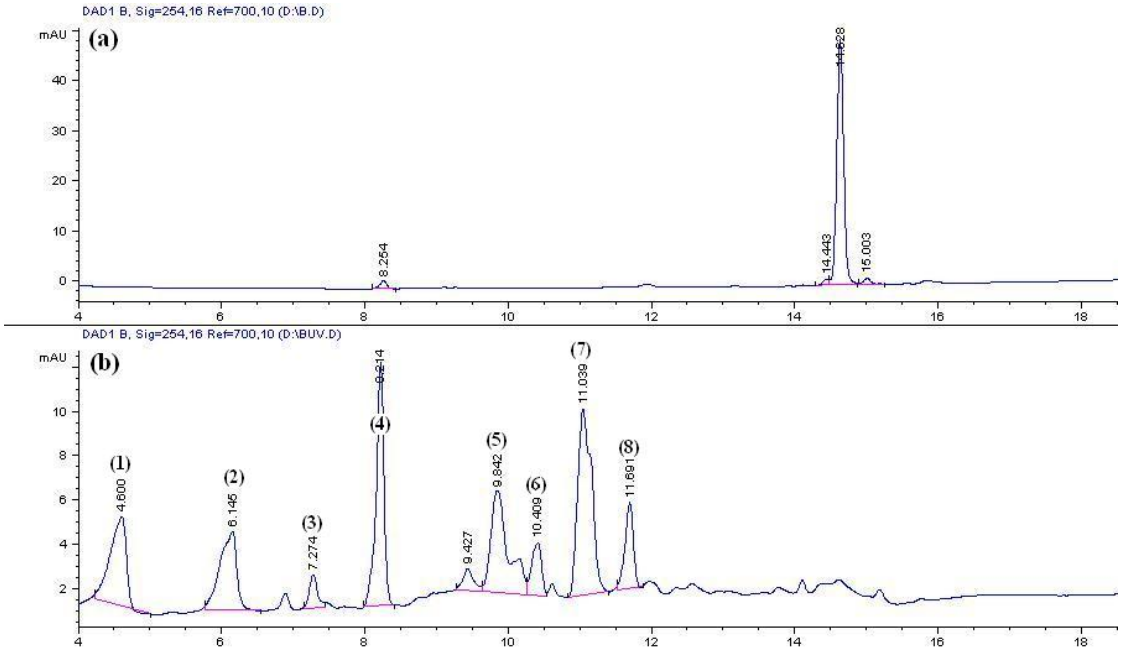

Figure IV.15. LCMS Elution Profile of Product of UV Light (350 nm) Photo-induced Rearrangement Experiment

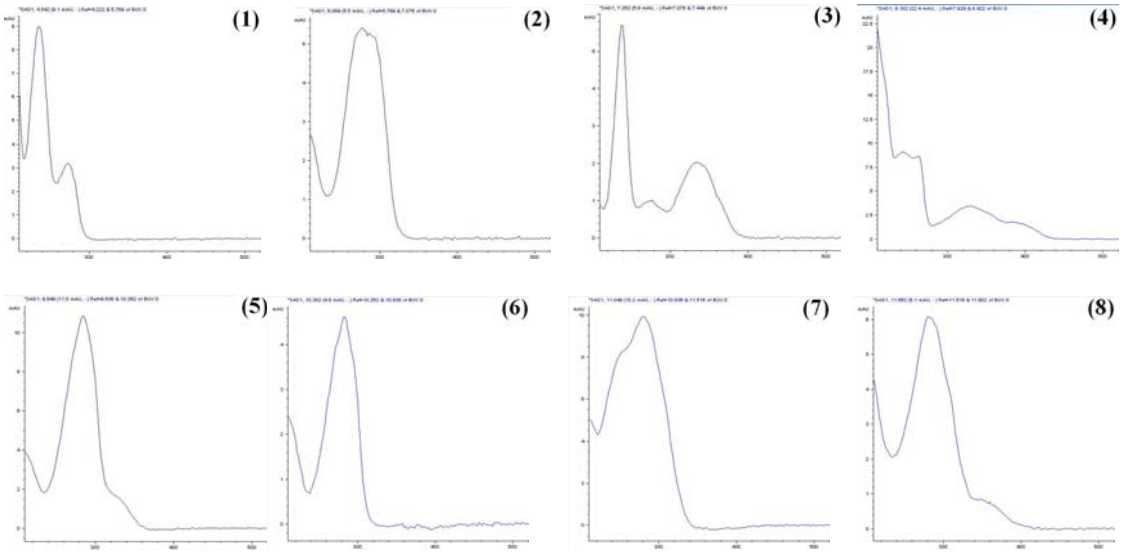

Figure IV.16. UV Profiles of Selected Products UV Light (350 nm) Photo-induced Rearrangement Experiment

IV.4. Formulation of a Hypothetical Biosynthetic Pathway to the Pyridinopyrones

It is interesting to note that 3-tetraenylpyridines of strikingly similar structure to those reported here have been previously isolated from the Opisthobranch molluscs *Navanax inermis* [e.g. navenone A (**75**)][241,242] and *Haminoea navicula* [e.g. haminol A (**76**)].[228] In these reports, elegant examinations of the ecological roles of the compounds were performed leading the authors conclude that both **75** and **76** are produced by the organism as an apparent mechanism of species preservation following "great molestation". In the case of *Navanax*, when greatly molested, it secretes a yellow hydrophobic substance directly into its slime trail (navenone A). This

secretion emanates from a small, specialized gland located beneath and near the anus of the animal. When this is encountered by a trail-following *Navanax*, an immediate alarm and avoidance response is induced, which terminates trail following behavior and generates a deviation in direction of greater than 90°.[242] The ecological role of haminol A has also been suggested to be that of an alarm pheromone and it too elicits rapid deviation from a previously produced slime trail.[244] It is further interesting to note that the same substituted γ-pyrone moiety observed in the pyridinopyrones has also been isolated from a marine ascoglossan, *Cyerce cristallina* [e.g. cyercene B (**77**)]. The ecological role of cyercene B has been postulated to be that of a defensive molecule due to its extreme level of toxicity to the mosquito fish *Gambusia affinis*.[244]

Although to suggest a microbial origin for the alarm pheromones navenone A and haminol A and the defensive molecule cyercene B is extremely presumptuous, it is well known that shell-less gastropods such as nudibranchs, ascoglossans and sea hares sequester metabolites from their prey and use them for chemical defense.[228, 245-248] This assertion in conjunction with the knowledge that these organisms thrive in murky mud flats rich in microbial life makes microbial-mollusc interactions likely. However, the exact interactions and specifically, the biosynthetic origin of the active molecules will remain purely speculative without appropriate experimentation. Nonetheless, the structural similarities between navenone A (**75**), haminol A (**76**), cyercene B (**77**), (See Figure IV.17) and pyridinopyrone A and B (**65**-**66**) suggest that they share a common biosynthetic route that is likely polyketide in nature.

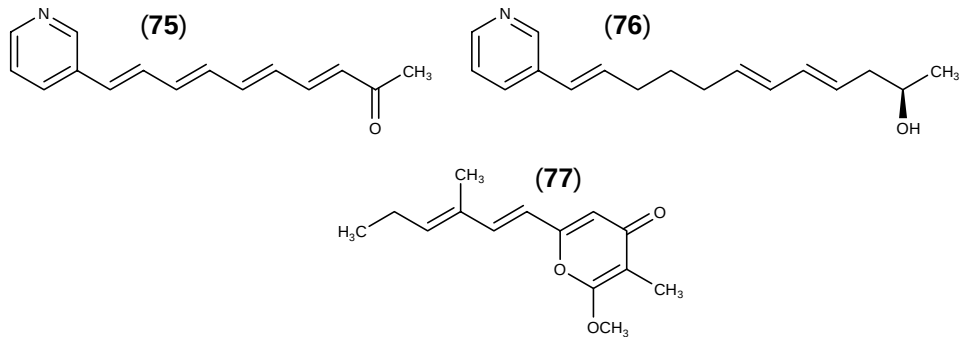

Figure IV.17. Secondary Metabolites Isolated From Nudibranchs

The polyketide origin of the 3-alkylpyridines has been examined in detail in the case of haminol A by *in vivo* incorporation studies using [1,2-$^{13}C_2$ acetate] and labeled nicotinic acid.[249,250] Importantly, these experiments indicated that the 3-alkylpyridine in haminol A was derived from nicotinic acid with the unsaturated chain being formed by subsequent elongation via acetate or malonate units.[251] Further, the biosynthesis of the substituted γ-pyrone in cyercene B has also been suggested to be polyketide in nature following incorporation studies using labeled acetate and propionate units.[251]

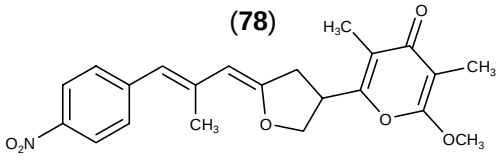

Figure IV.18. Chemical Structure of Aureothin

Additional studies concerning the biosynthesis of the *streptomyces* derived molecule aureothin (**78**), that also contains a substituted γ-pyrone moiety were

conducted by Müller et al.[252] In these studies, the biosynthetic gene cluster for aureothin (**78**) was cloned and sequenced from *S. thioletus* and the researchers found that **78** is too synthesized by an aberrant, iterative modular polyketide synthase (PKS). Upon assembly of the polyketide backbone, a tailoring reaction occurs that induces methylation of the pyrone ring to furnish the final product.[252] These studies by Müller et al. also indicated that the tailoring reaction is achieved via a regiospecific γ-pyrone methyltransferase (Aurl) that contains a conserved domain characteristic for the *S*-adenosylmethionine (SAM) binding transferases. This finding is in accordance with previous research indicating that the pyrone methoxyl group is derived from methionine.[253] Extrapolating the information gleaned from the biosynthetic pathways proposed for haminol A, cyercene B and aureothin to the structure of pyridinopyrone A, allows for a hypothetical biosynthetic pathway for pyridinopyrone A to be proposed as shown in Figure IV.19.

In conclusion, from a biomedical standpoint, the pyridinopyrones represent a new class of naturally derived molecules that may be useful in the treatment of cancer through their inhibition of the enzyme aromatase. In addition, the relatively simple chemical scaffold of the pyridinopyrones makes these molecules attractive substrates for synthetic chemical manipulation and SAR studies. Previous SAR studies initiated with molecules of similar structure have identified several key aspects of the inherent pyridinopyrone structure that may serve as logical starting points for these manipulations.

Finally, although the pyridinopyrones are structurally novel chemical entities, it is interesting to note that several examples exist where similar compounds have been isolated from marine organisms of vastly different taxonomic classification (e.g. nudibranchs). The proposal of a microbial origin for the molecules isolated from nudibranchs is an attractive theory that is supported by the fact that microbial interactions with numerous other species are well known. However, this theory could be easily disputed by the fact that evolution will often select for the most potent secondary metabolites regardless of taxonomic classification. Hopefully future study that is focused toward understanding the ecological role of the pyridinopyrones will answer some of these important questions.

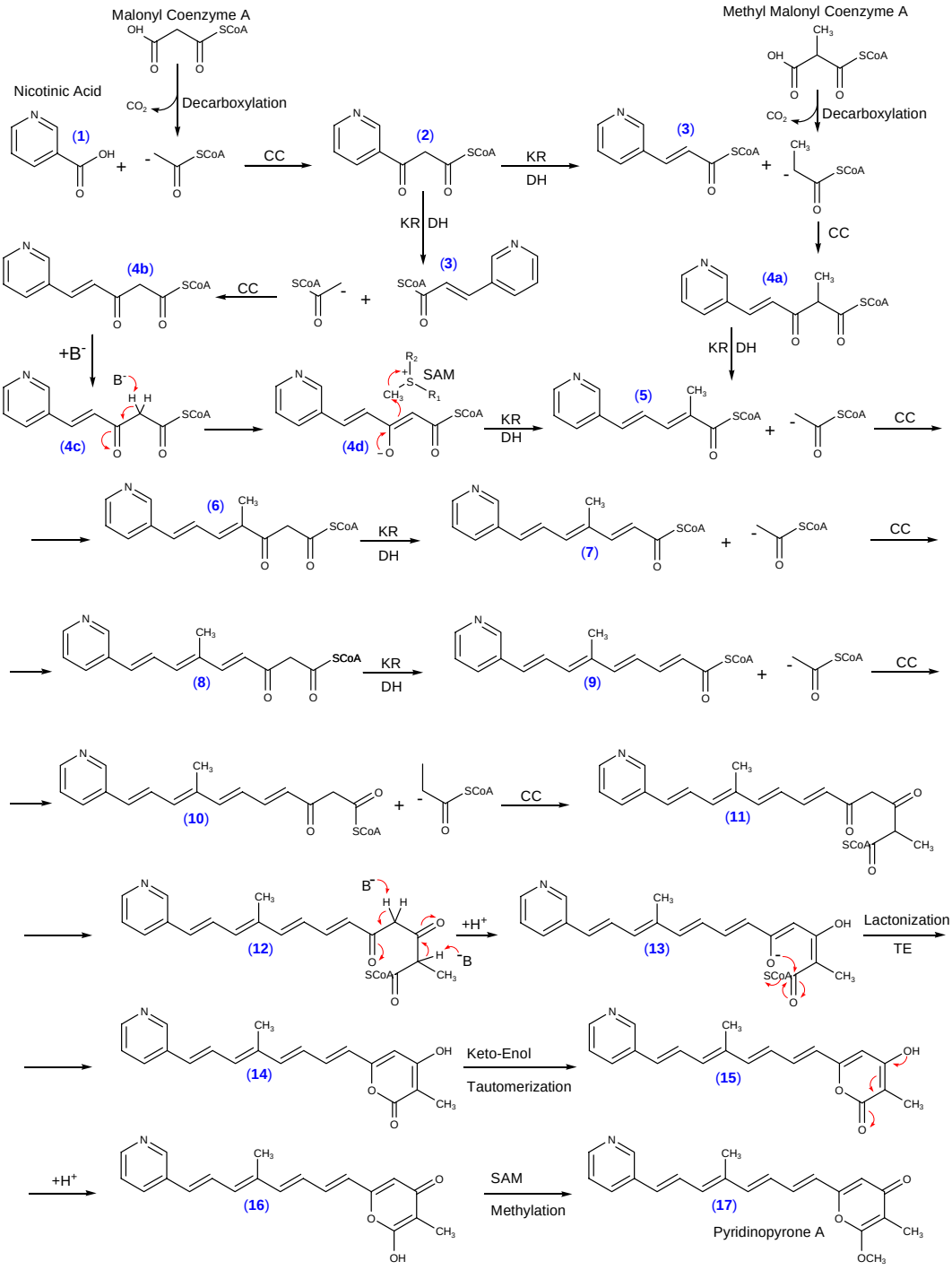

Figure IV.19. Hypothetical Biosynthetic Pathway to the Pyridinopyrones [(CC) = Claisen Condensation, (KR) = Keto Reductase, (DH) = Dehydratase, (SAM) = *S*-adenosylmethionine, (TE) = Thioesterase, (B) = Base]

References

(190) Brueggemeier, R.W.; Hackett, J.C.; Diaz-Cruz, E.S. *Endocrine Reviews* **2005**, *26*, 331-345

(191) Serrano, D.; Perego, E.; Costa, A.; Decensi, A. *Critical Reviews in Oncology/Hematology* **2004**, *49*, 109-17.

(192) James, V.; McNeill, J.; Lai, L.; Newton, C.; Ghilchik, M.; Reed, M. *Steroids* **1988**, *50*, 269-79

(193) Miller, W.; O'Neill, J. *Steroids* **1987**, *50*, 537-48

(194) Reed, M.; Owen, A.; Lai, L.; Coldham, N.; Ghilchik, M.; Shaikh, N.; James, V.; *International Journal of Cancer* **1989**, *44*, 233-237

(195) Bulun,S.; Price, T.; Aitken, J.; Mahendroo, M.; Simpson, E. *Journal of Clinical Endocrinology and Metabolism* **1993**, *77*, 1622-1628

(196) Simpson, E.; Mahendroo, M.; Means, G.; Kilgore, M.; Hinshelwood, M.; Graham-Lorence, S.; Amarneh, B.; Ito, Y.; Fisher, C. *Endocrine Reviews* **1994**, *15*, 342-355

(197) Simpson, E.; Mahendroo, M.; Means, G.; Kilgore, M.; Corbin, C.; Mendelson, C. *Journal of Steroid Biochemistry and Molecular Biology* **1993**, *44*, 321-330

(198) Kellis, J.; Vickery, L. *Journal of Biological Chemistry* **1987**, *262*, 4413-4420

(199) Johnston, J.; Metcalf, B. in Sunkara, *Novel Approaches to Cancer Chemotherapy* **1984** 307-328 in: Prasad, S. (ed) *Novel Approaches to Cancer Chemotherapy* Publisher: Academic, Orlando, Fla

(200) Banting, L.; Smith, H.; James, M.; Jones, G.; Nazareth, W.; Nicholls, P.; Hewlins, M.; Rowlands, M. *Journal of Enzyme Inhibition* **1988**, *2*, 215-229

(201) Banting, L.; Nicholls, P.; Shaw, M.; Smith, H. *Progress in Medicinal Chemistry* **1989**, *26*, 253-298

(202) Covey, D. *Sterol*. *Biosynth*. *Inhib*. **1988**, 534-571

(203) Brueggemeier, R.; *Journal of Enzyme Inhibition* **1990**, *4*, 101-111

(204) Brueggemeier,R. *Breast Cancer Research and Treatment* **1994**, *30*, 31-42

(205) Cole, P.; Robinson, C. *J*. *Med*. *Chem*. **1990**, 33, 2933-2942

(206) Gao, X-P.; Liu, F. *Curr. Opin. Obstetrics and Gynecology*. **2007**, *19*, 68-74

(207) Brueggemeier, R.; Floyd, E.; Counsell, R. *J*. *Med*. *Chem*. **1978**, *21*, 1007-1011

(208) Henderson, D.; Norbisrath, G.; Kerb, U. *Journal of Steroid Biochemistry* **1986**, *24*, 303-306

(209) Brueggemeier, R.; Katlic, N. *Cancer Research* **1987**, *47*, 4548-4551

(210) Brueggemeier, R.; Katlic, N.; Kenreigh, C.; Li, P. *Journal of Steroid Biochemistry and Molecular Biology* **1992**, *41*, 85-90

(211) Brueggemeier, R.; Li, P. *Cancer Research* **1988**, *48*, 6808-6810

(212) Li, P.; Brueggemeier, R. *J*. *Med*. *Chem*. **1990**, *33*, 101-105

(213) Kellis, J.; Childers, W.; Robinson, C.; Vickery, L. *Journal of Biological Chemistry* **1987**, *262*, 4421-4426

(214) Childers, W.; Shih, M.; Furth, P.; Robinson, C. *Steroids* **1988**, *50*, 121-134

(215) Shih, M.; Carrell, M.; Carrell, H.; Wright, C.; Johnston, J.; Robinson, C. *Journal of the Chemical Society, Chemical Communications* **1987**, *3*, 213-214

(216) Bednarski, P.; Porubek, D.; Nelson, S. *J. Med. Chem.* **1985**, *28*, 775-779

(217) Wright, J.; Calder, M.; Akhtar, M. *Journal of the Chemical Society, Chemical Communications* **1985**, *23*, 1733-1735

(218) Peet, N.; Burkhart, J.; Wright, C.; Johnston, J. *J. Med. Chem.* **1992**, 35, 3303-3306

(219) Peet, N.; Johnston, J.; Burkhart, J.; Wright, C. *Journal of Steroid Biochemistry and Molecular Biology* **1993**, *44*, 409-420

(220) Johnston, J.; Wright, C.; Burkhart, J.; Peet, N. *Journal of Steroid Biochemistry and Molecular Biology* **1993**, *44*, 623-631

(221) Balunas, M.J.; Su, B.; Landini, S.; Brueggemeier, R.W.; Kinghorn, A.D. *J. Nat. Prod.* **2006**, *69*, 700-703

(222) Oohata, N.; Kawamura, I.; Lacey, E.; Nishigaki, F.; Matsumoto, S.; Tsujimoto, S.; Naoe, Y.; Manda, T.; Shimomura, K. *Journal of Antibiotics* **1995**, *48*, 763-767

(223) Oohata, N.; Hori, Y.; Yamagishi, Y.; Fujita, T.; Takase, S.; Yamashita, M.; Terano, H.; Okuhara, M. *Journal of Antibiotics* **1995**, *48*, 757-762

(224) Ohmori, K.; Mori, K.; Ishikawa, Y.; Tsuruta, H.; Kuwahara, S.; Harada, N.; Suzuki, K. *Angew. Chem. Int. Ed.* **2004**, *43*, 3167-3171

(225) Larsen, D.; O'Shea, M. *J. Org. Chem.* **1996**, *61*, 5681-5683

(226) Kanamaru, T.; Nozaki, Y.; Muroi, M. *Jpn. Kokai. Tokkyo. Koho*. **1990**

(227) See Experimental Section (Assay for Inhibition of Aromatase Activityin) in Lee, D.; Bhat, K.; Fong, H.; Farnsworth, N.; Pezzuto, J.; Kinghorn, D. *J. Nat. Prod*. **2001**, *64*, 1286-1293

(228) Rousis, V.; Pawlik, J.; Hay, M.E.; Fenical, W. *Experientia*. **1990**, *46*, 327-329

(229) Dukes, M.; Edwards, P.N.; large, M.; Smith, I.K.; Boyle, T. *J. Steroid. Biochem. Molec. Biol*. **1996**, *58*, 439-445

(230) Ibrahim, A.R.; Abul-Hajj, Y.J. *J. Steroid. Mol. Biol*. **1990**, *37*, 257-260

(231) Pouget, C.; fagnere, C.; Basly, J-P.; Habrioux, G.; Chuila, A. *Bioorganic & Medicinal Chemistry Letters* **2002**, *12*, 2859-2861

(232) Brueggemeier, R. *American Journal of Therapeutics* **2001**, *8*, 333-334

(233) Kim, Y-W.; Hackett, J.C.; Brueggemeier, R.W. *J. Med. Chem*. **2004**, *47*, 4032-4040

(234) Osawa, Y.; Tochigi, B.; Tochigi, M.; Ohnishi, S.; Wantanabe, Y.; Bullion, K.; Osawa, G.; Nakabayashi, Y.; Yarborough, C.; *Journal of Enzyme Inhibition*. **1990**, *4*, 187-200

(235) Takahashi, N.; Tamagawa, K.; Kubo, Y.; Fukui, T.; Wakabayashi, H.; Honda, T. *Bioorganic & Medicinal Chemistry* **2003**, *11*, 3255-3260

(236) Decensi, A.; Serrano, D.; Bonanni, B.; Cazzaniga, M.; Guerrieri-Gonzaga, A. *J. Mammary Gland Bio. Neo*. **2003**, *8*, 19-29

(237) Ciolino, H.; Wang, T.; Sathyamoorthy, N. *British Journal of Cancer*. **2000**, *83*, 333-337

(238) Müller, M.; Kusenbach, B.; Liang, G.; Beaudry, C.M.; Trauner, D.; Hertweck, C. *Angew. Chem. Int. Ed.* **2006**, *45*, 7835-7838

(239) Beaudry, C.M.; Malerich, J.P.; Trauner, D. *Chem. Rev.* **2005**, *105*, 4757

(240) Miller, A.K.; Trauner, D. *Synlett* **2006**, *14*, 229

(241) Sleeper, H.L.; Fenical, W. *J. Am. Chem. Soc.* **1977**, *99*, 2367-2368

(242) Sleeper, H.L.; Paul, V.J.; Fenical, W. *Journal of Chemical Ecology* **1980**, *6*, 57-70

(243) Cimino, G.; Passeggio, A.; Sodano, G.; Spinella, A.; Villani, G. *Experientia.* **1991**, *47*, 61-63

(244) Vardaro, R.R.; Di Marzo, V.; Crispino, A.; Cimino, G. *Tetrahedron* **1991**, *47*, 5569-5576

(245) Faulkner, D.J.; Ghiselin, M.T. *Mar. Ecol. Prog. Ser.* **1983**, *13*, 295

(246) Faulkner, D.J. *Nat. Prod. Rep.* **1984**, *1*, 251

(247) Carefoot, T.H. *Mar. Biol. Ann. Rev.* **1987**, *25*, 167

(248) Norris, J.N.; Fenical, W. *Smithsonian Contrib. Mar. Sci.* **1982**, *12*, 417

(249) Cutignano, A.; Tramice, A.; De Caro, S.; Villani, G.; Cimino, G.; Fontana, A. *Angew. Chem. Int. Ed.* **2003**, *42*, 2633-2636

(250) Cutignano, A.; Cimino, G.; Giordano, A.; d'Ippolito, G.; Fontana, A. *Tetrahedron Letters* **2004**, *45*, 2627-2629

(251) Di Marzo, V.; Vardaro, R.R.; De Petrocellis, L.; Villani, G.; Minei, R.; Cimino, G. *Experentia* **1991**, *47*, 1221-1227

(252) Müller, M.; He, J.;Hertweck, C. *Chembiochem* **2006**, *7*, 37-39

(253) Yamazaki, M.; Maebayashi, Y.; Katoh, H.; Ohishi, J.-L.; Koyama, Y. *Chem. Pharm. Bull*. **1975**, *23*, 569

V

Conclusions from Thesis Research

V.1. Conclusions

This thesis sought to examine the potential of using marine sediment-derived actinomycetes as a source for novel molecules that were effective in the treatment and prevention of cancer. The research reported herein culminated in the isolation of several molecules, representing two distinct biosynthetic classes all of which exhibited some form of anticancer activity.

The first project to be undertaken yielded the piperazimycins, a new class of cyclic hexadepsipeptides comprised of exclusively unusual amino acid residues that were isolated from a marine-derived *Streptomyces sp*. While potently cytotoxic, the piperazimycins exhibited little selectivity in the NCI 60 cell-line panel and therefore their development as anticancer agents is unlikely. However, the piperazimycins also exhibited potent activity against ornithine decarboxylase (ODC), an important cancer chemoprevention target. Although the inherent cytotoxicity of the piperazimycins may preclude their development as chemopreventative agents, due to their potency in the ODC system, they may still be able to serve as biological tools to further elucidate as yet undetermined details of the ODC pathway. Ongoing investigations will hopefully provide additional insight into the ODC inhibitory activities of the piperazimycins.

The second project led to the isolation of another interesting suite of molecules, the arenicolides. The arenicolides differed from the piperazimycins in that they were polyketide-derived and exhibited only moderate cytotoxicity. However, the complexity of their chemical structure and the fact that they were isolated from the marine actinomycete *Salinispora arenicola* made for an interesting project and full

structural characterization of the arenicolides was pursued with great vigor. The approaches used to solve the planar structures and stereochemistry of the arenicolides resulted in an excellent publication in which several new methods for structure elucidation were applied and tested. Further, due to the profound biological activity that is often associated with macrocyclic polyketides such as the arenicolides and the novelty of their chemical structure, the NCI has recently agreed to reinvestigate these molecules in the 60 cell-line panel. Further testing in enzyme-based assays will serve to evaluate the potential of the arenicolides as mechanism based anti-cancer agents as well.

Unlike the first two projects that sought to discover cytotoxic molecules to treat established cancers, the final thesis related endeavor attempted to identify molecules that could prevent the initiation or progression of cancer. This approach yielded another novel class of compounds, the pyridinopyrones that displayed effective inhibitory activity toward the enzyme aromatase. The relative structural simplicity of the pyridinopyrones makes them attractive molecules for both chemical syntheses and structure activity relationship studies. Ongoing experimentation with the goal of increasing the efficacy of the pyridinopyrones will surely lead to a better understanding of their aromatase inhibitory activity and possibly generate more potent molecules that are based on the natural product's chemical scaffold.

In conclusion, the research presented in this thesis showed that marine sediment-derived actinomycetes are prolific sources for new molecules that are effective in the treatment and prevention of cancer. When the structures of the piperazimycins, arenicolides and pyridinopyrones are viewed together the diversity of chemical

structures produced by marine sediment-derived actinomycetes is realized. On one hand, large structurally complex molecules containing multiple chiral centers (e.g piperazimycins A-C, arenicolides A-C) have been isolated while on the other hand structurally simple planar molecules (e.g. pyridinopyrones A and B) have been identified. When one considers that each of these molecules exhibit some utility in the treatment of cancer the outlook for the discovery of new anti-cancer drugs from marine sediment-derived actinomycetes becomes very promising.

Finally, given the profound effect that terrestrial actinomycetes have had on drug discovery and the realization that the oceans represent an essentially untapped resource for novel actinomycetes, it is hypothesized that the future will without question see clinically approved drugs that are derived from marine microbes. The early clinical success of salinosporamide A for the treatment of multiple myeloma serves to support this hypothesis. Further, the continuing quest to isolate novel genera of microbes and the desire to improve fermentation techniques will open up an even wider array of possibilities for drug discovery. If advances in these areas are coupled with the utilization of state of the art cancer relevant assays, the chances of discovering potential drugs becomes even more likely.

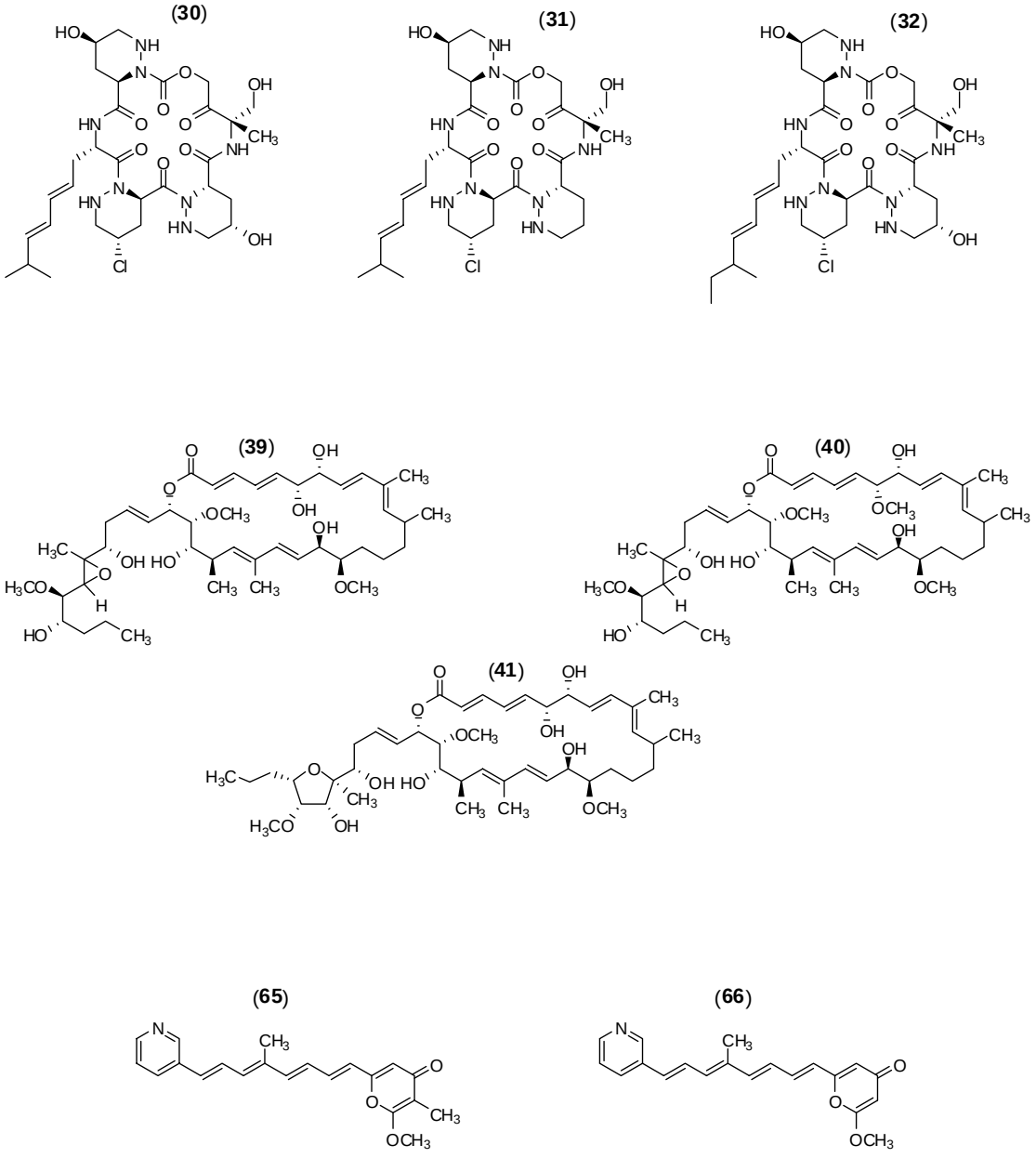

Figure V.1. Summary of New Cancer Relevant Molecules Isolated as a Result of Thesis Research